UNIVERSITY OF WISCONSIN
DEPARTMENT OF METEOROLOGY
MADISON, NOVEMBER 1963

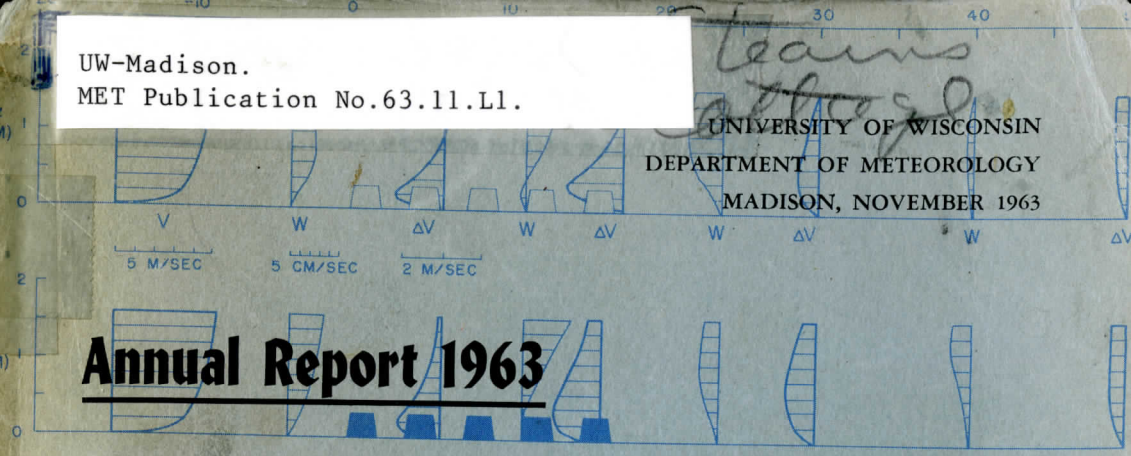

Annual Report 1963

STUDIES OF THE EFFECTS OF VARIATIONS IN BOUNDARY CONDITIONS ON THE ATMOSPHERIC BOUNDARY LAYER

Heinz H. Lettau
Project Supervisor

Contributions by
Raymond J. Deland
John P. Kearns
Ernest C. Kung
Larry S. Slotta
Charles R. Stearns

Contract DA-36-039-AMC-00878
DA-Task 1-A-0-11001-B-021-08

Sponsored by Department of Meteorology
U. S. Army Electronics Research and Development Activity
Fort Huachuca, Arizona

University of Wisconsin
Department of Meteorology
Madison, November 1963

ANNUAL REPORT 1963

STUDIES OF THE EFFECTS OF VARIATIONS IN BOUNDARY CONDITIONS ON THE ATMOSPHERIC BOUNDARY LAYER

Heinz H. Lettau
Project Supervisor

Contributions by

Raymond J. Deland
John P. Kearns
Ernest C. Kung
Larry S. Slotta
Charles R. Stearns

Contract DA-36-039-AMC-00878
DA Task 1-A-0-11001-B-021-08

Sponsored by Department of Meteorology
U. S. Army Electronics Research and Development Activity
Fort Huachuca, Arizona

Scanner's note:

This page is blank.

General Introduction

In this first Annual Report, results are summarized which concern four phases of the work specified in the objectives of the contract. These include (1) A critical study of the significance of Karman's constant in boundary layer profiles, (2) A detailed survey of the natural boundary structure on Northern hemispheric continents coupled with an approach to a climatology of energy dissipation in the atmospheric boundary layer, (3) Controlled experiments in airflow over the ice of Lake Mendota devoted (3a) to the effect of an artificial roughness field on the variance spectra of air temperature, (3b) the momentum budget over an artificial forest of conifer saplings, and (3c) the effect of obstacle albedo and solar heating on momentum transfer, and (4) a theoretical approach to a closed solution of diabatic, steady-state profile structure for the special micrometeorological problem of katabatic flow.

Each of the five individual papers of this report is accompanied by an abstract which summarizes the problems under discussion, and the results, in detail.

Heinz H. Lettau
Madison, Wisconsin

November 1963

Scanner's note:

This page is blank.

Table of Contents

Page

General Introduction — Heinz H. Lettau iii

List of Illustrations vi

1. A Critical Investigation of the Universality of Karman's Constant in Turbulent Flow — Larry S. Slotta 1

2. Climatology of Aerodynamic Roughness Parameter and Energy Dissipation in the Planetary Boundary Layer of the Northern Hemisphere — Ernest C. Kung. 37

3. The Modification of Temperature Variance Spectra in Airflow over Artificially Controlled Surface Roughness — John P. Kearns and Raymond J. Deland. 97

4. Report on Two Wind-Profile Modification Experiments in Airflow over the Ice of Lake Mendota — Charles R. Stearns and Heinz H. Lettau 115

5. Preliminary Note on the Theory of Steady Katabatic Flow for Height-Dependent Eddy Diffusivity — Heinz H. Lettau . . 139

Index of Distribution 151

List of Illustrations

Section 1

		Page
Fig. 1	Boundary-layer velocity profiles in terms of the wall law and the velocity defect law. Data from NASA TR R-26, skin friction measurements in incompressible flow, Figures 15, 16. Smith and Walker, 1959.	6
Fig. 2	Schematic representation of shearing stress profiles and velocity distributions for duct flow, boundary layer flow on a flat plate, and atmospheric flow . . .	8
Fig. 3.	Reanalysis of NACA 1030 data. $u^*/((du/U)/d\ell ny)$ Plotted Versus y/δ^*	22
Fig. 4	NACA 1030 Reanalysis. $u^*/((du/U)/d\ell n_e y)$ Family as dependent on y/δ^* and Re_{δ^*}	24
Fig. 5	NASA TR R-26 Reanalysis $\sqrt{.5 C_\tau}/((\Delta u/U)/\Delta \ell n_e Y)$ Plotted Versus $Yave/\delta^*$	28
Fig. 6	NASA TR R-26 Reanalysis $\sqrt{.5 C_\tau}/((\Delta u/U)/\Delta \ell n_e Y)$ Plotted vs. $Yave/\delta^*$.	30

Section 2

Fig. 1	Average aerodynamic roughness parameter z_0 (cm) of vegetation 0 to 100 miles radial distance from Drexel, Nebraska.	50
Fig. 2	Meridional profiles of ratio between wind speed at height z and geostrophic wind speed over the North American Continent. Climatologic means derived from Lauscher (1951) (dashed lines) in comparison with computed ratios for z = 4, 8, and 16m.	52
Fig. 3	Area contrast of mean seasonal energy dissipation E over the Northern Hemisphere. (December through February).	70

Fig. 4 Area contrast of mean seasonal energy dissipation E over the Northern Hemisphere (June through August) 71

Fig. 5 Regional contrast of January energy dissipation E over the North American continent 72

Fig. 6 Regional contrast of July energy dissipation over the North American continent 73

Fig. 7 Seasonal mean energy dissipation E over the North American continent 74

Fig. 8 Seasonal mean energy dissipation E over the Northern Hemisphere 75

Fig. 9 Year to year contrast in January energy dissipation E over the North American continent from 1851 to 1955 76

Section 3

Fig. 1 Comparison of spectra for two runs over ice surface at 226 cm 106

Fig. 2 Comparison of spectra: 113 cm above bushel baskets vs 113 cm over ice surface. 107

Fig. 3 Comparison of spectra: 226 cm above bushel baskets vs 113 cm over ice surface. 108

Fig. 4 Comparison of two bushel basket runs: 226 cm vs 113 cm . . . 109

Section 4

Fig. 1 Layout for the "Christmas Tree Experiment" on the ice of Lake Mendota, 21 March, 1963 120

Fig. 2 View of the artificial forest on the ice of Lake Mendota 120

Fig. 3 Dimensions of "black" and "white" field in the layout for the Bushel Basket Experiment on the ice of Lake Mendota, 23 March, 1963 122

Fig. 4 - Fig. 7 Christmas tree experiment, 21 March, 1963; examples of wind profiles at center-point of array (main mast) and at four positions of moving mast (16m upwind, at leading edge, at back edge, and 78m downwind of leading edge) as indicated on upper left corner of individual figures. The log-profile labeled "reference" is approximately representative of upwind conditions over clear ice. . . . 124

Fig. 8 Schematic illustration of wind profile evaluation using the 1963-model. α = profile contour number, φ = diabatic influence function, and Φ = integral-diabatic influence function. 131

Fig. 9 Christmas tree experiment on the ice of Lake Mendota, 21 March, 1963, 13:15 to 17:13 CST.

Fig. 10 Bushel Basket Experiment on the ice of Lake Mendota, 23 March, 1963, 11:17 to 12:45 (white basket field, upper part), 13:32 to 14:45 (black basket field, lower part). V = profile of undisturbed velocity; W = profile of computed vertical motion; ΔV = profiles of velocity-defect (disturbance). 135

Fig. 11 Bushel Basket Experiment on the ice of Lake Mendota, 23 March, 1963. Local momentum budget constituents for four air volumes along trajectories across the white and black fields. Symbols are explained in caption for Fig. 9. 135

A Critical Investigation of the Universality of Karman's Constant in Turbulent Flow*

Larry S. Slotta

Department of Civil Engineering
University of Wisconsin

Abstract: The aim of this study was a basic examination of von Karman's constant. A literature review revealed essentially three methods of determination for this semi-empirical value: (1) that sought by the statistician on the basis of decay of turbulent energy, (2) that found by the slope of the logarithmic plot of nominal height versus dimensionless velocity (thus assuming a logarithmic velocity distribution), (3) that determined from approach of a limiting wall condition for an explicit function described by the structure of the flow.

The third method was used by Lettau (1961) in a reanalysis of "classical" pipe flow data to show independently that, if a universal velocity profile exists, the Karman constant is universal only for flow in rough pipes. In the present study, this method was employed to investigate data from two "classical" flat plate boundary layer experiments incorporating over 75 velocity profiles. The Karman constant was again found not to be universal but to vary with Reynolds numbers. The average k values from these reanalyses were 0.52 ± 0.02 for NACA 1030, and $k = 0.47 \pm 0.02$ for NASA R-26 (as compared with 0.46 by the author's assumption of logarithmic slope). Utilizing the NACA 1030 boundary layer data, whose

---

*This work is part of a thesis submitted to the University of Wisconsin in partial fulfillment of the requirements for the Ph. D. degree, written under the supervision of Professor H. Lettau, Department of Meteorology and Department of Civil Engineering.

pattern of F-functions was in accord with theoretical considerations, the dimensional similarity constant of Lettau's extended linear law was found to be $m = \frac{1}{2}$.

List of Contents

1.0 List of Symbols

1.1 Introduction

1.2 Physical Considerations

1.3 Review of Literature on Karman's Constant
- 1.3.1 Introductory Remarks
- 1.3.2 Specific Investigations
- 1.3.3 Summary of Values

1.4 Reanalysis of Flat-Plate Boundary Layer Data
- 1.4.1 Introductory Remarks
- 1.4.2 NACA Report 1030
- 1.4.3 NASA TR R 26

1.5 Comments and Comparisons of the Two Reanalyses
- 1.5.1 Comments
- 1.5.2 Conclusions

1.6 References

1.0 List of Symbols

Subscripts and Mathematical Symbols

$\bar{}$ = bar, denoting average

$_0$ = subscript, denoting value of quantity at boundary

$'$ = prime, indicating turbulent fluctuations

Δ = delta, increment of values

Fluid Properties and Boundary Characteristics

ρ = fluid density

ν = kinematic viscosity of fluid

$2R$ = lateral diameter of duct

Dimensional Variables and Flow Parameters

y = nominal height or lateral distance from boundary

u = $u(y)$ mean velocity profile; horizontal wind component

v = lateral velocity component

w = vertical velocity component

U = maximum mean velocity, or free-stream velocity

δ = boundary layer thickness

$\delta^* = \int_0^\infty (1 - u/U)\, dy$ = displacement thickness of boundary layer

p = pressure

τ = $\tau(y)$ = shearing stress profile

$u^* = (\tau/\rho)^{\frac{1}{2}} = u^*(y)$ = friction velocity profile

u_0^* = wall friction velocity

$L = u^*/(du/dy) = L(y)$ = profile of characteristic length scale of turbulence

Dimensionless Boundary Characteristics, Variables and Flow Parameters

$\underline{Re}_x = xu/\nu$ = Reynolds number based on distance from leading edge

$\underline{Re}^* = \delta^* U/\nu$ = Reynolds number based on boundary layer displacement thickness

X = $1 - r/R$ dimensionless lateral distance from the wall of a duct

y/δ = dimensionless lateral distance from the surface considered in boundary layer studies

ζ = correction term function

$\eta = (U - u)/u_0^* = \eta(y)$ = dimensionless velocity defect

$\bar{\eta} = (U - \bar{u})/u_0^*$ = average dimensionless velocity defect

k = Karman's numerical constant

$F = L/y = f(y/\delta)$ = dimensionless length scale of turbulence

m = numerical constant used in dimensional similarity discussion

c_τ = stress or drag coefficient

1.1 Introduction

In an effort to determine a generalized mathematical model of turbulent flow near a boundary, preliminary literature investigations revealed divergent values for the Karman constant. The von Karman constant is a semi-empirical value used especially in concepts concerning technical application of boundary layer theory.

This study was undertaken with the aim of examining the physical basis of von Karman's constant and thence of establishing its values from fundamental considerations. The effects of flow geometry as well as generation and decay of eddy energy were to be considered.

1.2 Physical Considerations

To illustrate or theoretically express the manner in which the velocity of a fluid varies for flow over a boundary has long been the aim of many investigators. Their results are dependently represented, in either Eulerian or Lagrangian fashion, on the basis of measured quantities. At present our knowledge of the mechanism of turbulence and its processes is still inadequate as a basis for a theory. Theoreticians' endeavors to provide a complete solution of the transport problem have been restricted because of lack of complete knowledge of statistical functions describing the detail of turbulent motion. Klebanoff (1955) relates that any attempt to investigate the mechanism of turbulence is hampered by the lack of an experimental technique for the exact measurement of pressure fluctuations. Even so, investigators have been able to include spectral measurements of turbulent energy, shear stress, turbulent dissipation, probability densities of velocity fluctuations in the direction of flow. Attempts to correlate the results of these studies to those of phenomenological theories are acknowledged in the review of literature. Considering the formidable difficulties associated with turbulent shear flow, at this time the solutions offered by statistical analysis of the transport problem are at best approximate.

Deductive methods for analyzing flow data taken for the Eulerian case usually attempt to express the mean velocity as a function of boundary distance in terms of other measured parameters, notably the wall friction velocity u_0*. These phenomenological theories continue to be most useful for description of the turbulent transport process.

In turbulent flow, the proximity of the rigid boundary or wall has a direct bearing on the turbulence. For a smooth wall this effect

occurs through the action of viscous stresses, for a rough wall through the action of more complicated forces resulting from the flow around the individual roughness elements.

It follows from the equation of motion, that the relations which are determined by the flow structure and boundary conditions can be expressed by two functions. These are:

the dimensionless equation for the shear stress profile

$$\tau/\tau_0 = (u^*/u_0^*)^2 \equiv \varphi(y/\delta), \qquad (1)$$

and, knowing $u = \int_0^y (du/dy)\,dy$ and $U = \int_0^\delta (du/dy)\,dy$,

the dimensionless velocity-defect equation,

$$\eta \equiv (U-u)/u_0^* = \int_y^\delta (u^*/u_0^*)\,u^{*-1}(du/dy)\,dy = \int_y^\delta \varphi^{\frac{1}{2}} L^{-1}\,dy \qquad (2)$$

Here, $L = u^*/(du/dy)$ identifies the profile of a characteristic length scale of turbulence. The problem of describing the flow requires that $L(y)$ be known. Karman's constant may be defined as:

$$k = \lim_{y \to 0} (L/y) = \text{universal constant} \qquad (3)$$

In terms of the discussion above, for the "inner region" (i.e., at $y \ll \delta$) where φ must be sufficiently close to unity, one may arrive at an expression for the "law of the wall,"

$$u = \int_0^y (du/dy)\,dy = u_0^* \int_0^y L^{-1}\,dy \qquad (4)$$

Many investigators have determined the value of k for experimental flow data, as the slope for the linear portion of the curve of a nominal height plotted logarithmically versus the normalized experimental velocity found at that height (See Figure 1). This method assumes a logarithmic velocity profile of the form $u/u_0^* = 1/k \ln(y/y_0) + \text{Const.}$ This standard or reference distribution requires that $\varphi^{\frac{1}{2}}/L \approx u^*/L = k/y$ which can be valid for either $\varphi = 1$, or $\varphi = \varphi(y/\delta)$ only when $L(y/\delta)$ is properly adjusted; see Lettau (1961) concerning Prandtl's modified law. To find the Karman constant from flow data in a region where the velocity distribution becomes quasi-logarithmic (for a profile in which the shearing stress is assumed constant), may thus be questioned in light of determining the constant as the limiting condition of approaching the boundary.

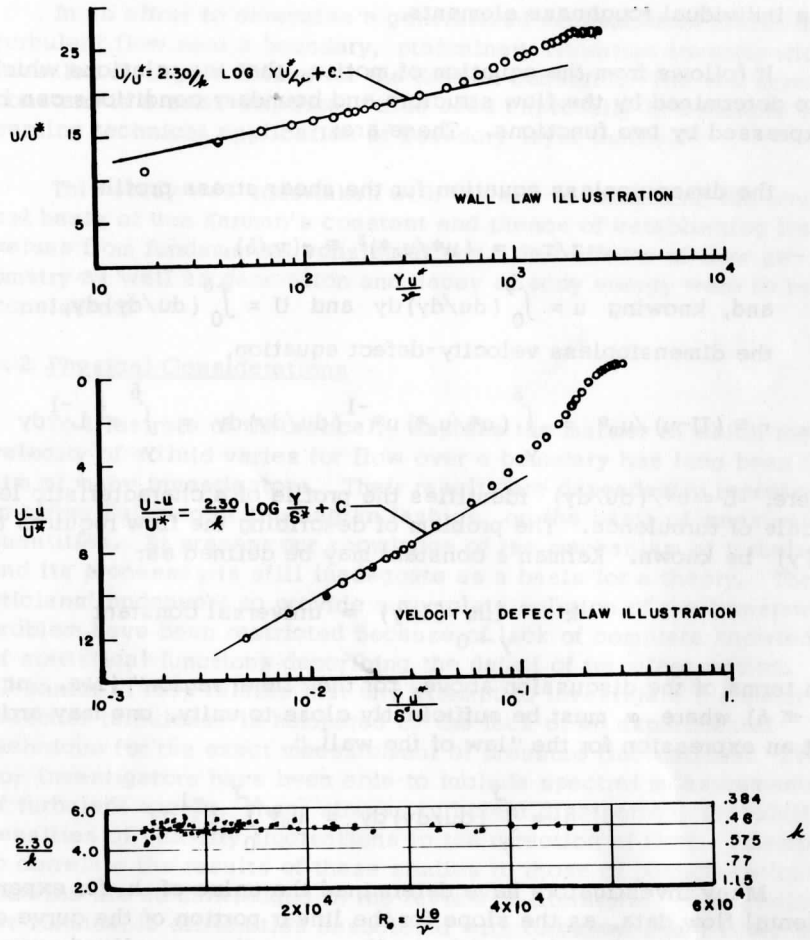

Fig. 1. Boundary-layer velocity profiles in terms of the wall law and the velocity defect law. Data from NASA TR R-26, skin friction measurements in incompressible flow, Figures 15, 16. Smith and Walker, 1959.

It is instructive at this point to discuss a few basic types of shearing stress distributions, their dependence on boundary geometry, and to indicate their importance in the determination of k as defined.

The velocity distribution and shearing stress distribution for fully developed steady duct flow, where the equation of motion reduces to $\partial p/\partial x = \partial \tau/\partial y$ is shown graphically in Figure 2.

The stress configuration for fluctuating turbulent velocity components in the boundary layer on a flat plate at zero incidence is also sketched in Figure 2, as measured by Klebanoff (1954). The condition that for this flow type the shear stress distribution curve is relatively constant at the boundary, although not linear, will be used in a later section. Note that at the boundary, $y = 0$, the gradient $(\partial \tau/\partial y)$, is normal to the boundary and approaches asymptotically zero as y approaches δ.

Lettau (1960-61) in describing the shear profile for atmospheric flow has shown that atmospheric flow is more akin to duct flow than to boundary layer flow. This is illustrated on Figure 2 for both the distribution of velocity and of shearing stress. The gradient of the atmospheric shearing stress $\partial \tau/\partial y$ at $y = 0$ is relatively the same as for pipe flow, even though it departs from the linear case. The height y at which $y/\delta = 1$ for the atmosphere is of the order of several hundred meters, whereas for duct flow y/δ is equivalent to the pipe radius. Considering the atmosphere's macro-scale, one may neglect the shearing stress variation within the first few meters above the surface. This, coupled with an assumed proportional linearity between the length scale of turbulence and the distance from the boundary, permits one to utilize the "standard" logarithmic model to study turbulent flow near the surface in the atmosphere.

1.3 Review of Literature

1.3.1 Introductory Remarks

A considerable amount of research concerning turbulent flow has been conducted since Prandtl's introduction in 1932 of a method to obtain a universal law of velocity distribution in smooth pipes, and Nikuradse's flow measurements published in 1933. Many of the following studies have either relied on the value of von Karman's constant, as given by Nikuradse, without questioning its universality or merely have reported their results in a comparative manner. Few investigators have conducted their studies specifically to determine

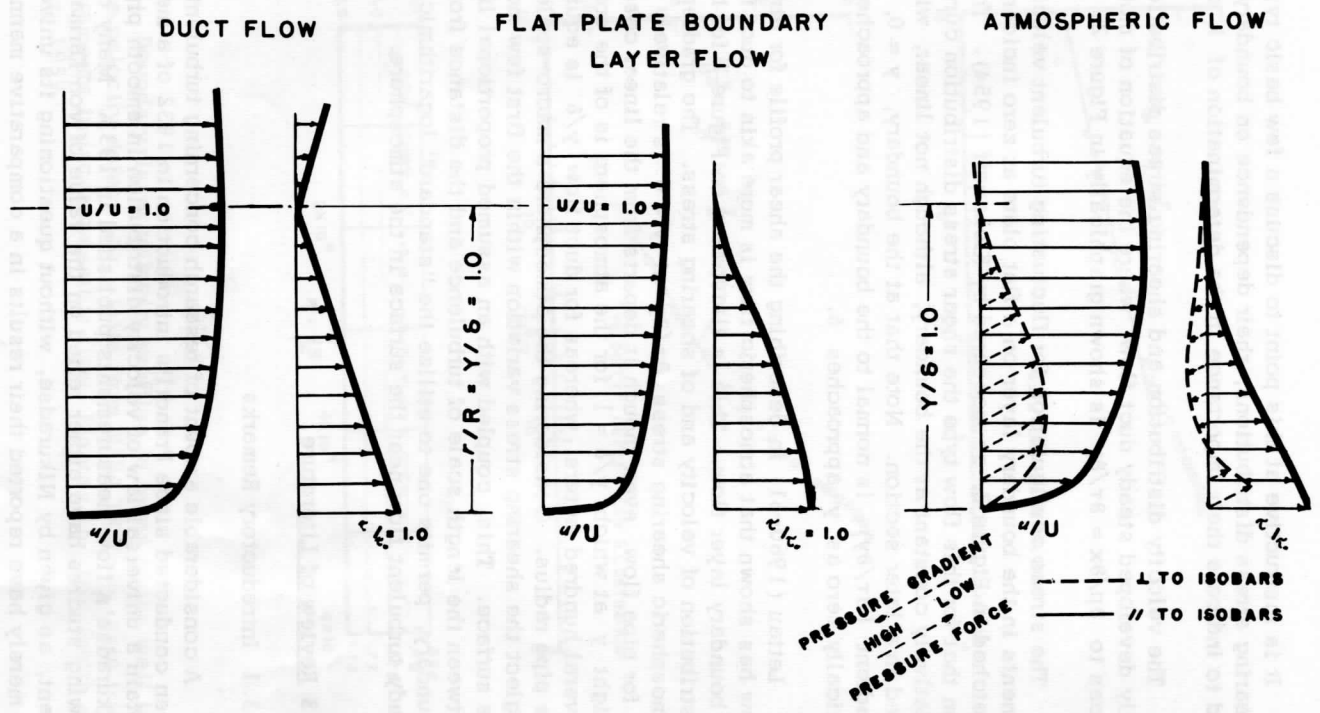

Fig. 2. Schematic representation of shearing stress profiles and velocity distributions for duct flow, boundary layer flow on a flat plate, and atmospheric flow

the Karman constant. In view of the divergent values reported for the Karman "constant" and considering the important role of this semi-empirical value in current concepts of a universal velocity profile in turbulent flow, it seemed that a thorough review of previous data and analyses was desirable.

During the course of this study, Lettau made a contribution bearing on the universality of von Karman's constant. Duct flow data was reanalyzed to show that a universal velocity profile for fully developed flow exists, independent of k, and that Karman's constant is not of universal nature.

Data for flat plate studies in the boundary layer are reanalyzed in Section 1.4. The results of this investigation are also shown in the summary in this section.

1.3.2 Specific Investigations

(1937) A large body of available data was collected by Goldstein to investigate the Karman constant. His determinations were based on the velocity defect law and he found k was independent of boundary shape or roughness. For the scatter of plotted data, the value of $k = 0.40$ was used for comparison and considered satisfactory.

(1938) Millikan stated in his critical discussion of turbulent flows that it would be undesirable to attempt to improve the agreement between existing theories and experiment by a change in k based on the action of viscosity. Millikan's justification was that viscosity seems to have no effect outside the viscous sublayer, that is, for $(y\, u^*/\nu) \geq 30$.

(1947) In the paper "Generalization for mixing length" Montgomery pointed out that the value obtained for von Karman's constant "experimentally depends ... on the particular form of the general theory employed." Upon examining Prandtl's form of the general theory ($k = 0.40$) and von Karman's velocity defect form ($k = 0.31$), both forms were found unsatisfactory because their expressions gave "finite shear at the axis, which is physically impossible." Montgomery presented a new hypothesis for the mixing length based upon a cylindrical model where the mixing length depended on the distance to the cylinder's wall in all directions on the cross sectional plane. His model, satisfying zero shear at the axis, gave 0.45 as the universal constant.

(1947) Sheppard's shear stress determinations with a floating element were effectively the first measured in the lower atmosphere, coupled with wind profiles, to provide a value of von Karman's constant. He gave evidence for considerable variation in k dependent on conditions of atmospheric stability. Assuming a strictly logarithmic wind profile, his determination of k produced values from 0.44 to 0.49 with an average of 0.46 for moderately unstable atmospheric stratification.

(1948) Heisenberg related that k "must be exactly determined by the hydrodynamic equations; it has the same numerical value in all cases where one may speak of statistical isotropic turbulence, and does not depend in any way on the geometry of the flow." The theoretical determination of von Karman's constant was attempted while qualitatively mathematically representing the processes on which energy dissipation is based. A crude estimate of k (determined in the study, k = 0.98) which Heisenberg pointed out could differ as much as by a factor of two.

(1953, 1954) Twelve values of von Karman's constant, determined by investigators from 1932 to 1951 and including a reanalysis of Nikuradse's data, were averaged by Ross (1953) to give k = 0.415. Similarly, Clauser (1954) compiled data from a number of turbulent boundary layer studies with and without pressure gradients. His result, k = 0.412, is used frequently in the present literature.

(1953, 1955) Suspended material in the flow systematically influences the k value, as reported by Vanoni (1953) and Bender (1955). Bender noted that k decreases with increase in suspended sediment and that k varies with sediment size. Also shown in his open channel studies was that side or wall effects, as well as bed roughness affected k.

(1956) Spatial variations and spectral structure of steady state turbulent shear flow in channels were investigated by Malkus without introducing empirical parameters. He outlined a variational approach designed to find the momentum transport spectrum and mean velocity profile which leads to a marginally stable mean field of maximum dissipation rate. A first approximation to the spectrum was found, showing that "... all known gross qualitative features of turbulent flow in smooth channels ... (are manifested) ... from an optimization of the dissipation rate subject to the mean stability constraints." A quantitative comparison was made between his theoretical statistical organization of turbulents fields with observations; here, Malkus determined k = 0.332.

(1961) Lettau presented the "extended linear law" as a generalized mathematical model of the mean-velocity distribution in fully developed turbulent flow in terms of an explicit L/R function. Existing phenomenological expressions for the mean velocity profile were critically reviewed in similar fashion. Lettau's approach was a discrete separation of two problems: (1) the question whether a universal velocity profile exists and (2) whether the Karman constant is a universal constant.

To compare the success of the theoretical forms a "normalized correction term function," independent of the Karman constant, was utilized to describe the correlation of observed data and theoretically predicted distributions. This normalized correction term function ζ expresses the difference of the ratio $k\eta/k\bar{\eta} = (U-u)/(U-\bar{u})$ from a "standard" logarithmic velocity-defect distribution. Agreement between the experimental data (in air by Laufer, 1954; in water by Nikuradse, 1932, 1933) and theoretical distributions was met satisfactorily by Lettau's "extended linear law" for all sections of the data. The other theoretical distributions show marked dissimilarity from the experimental results. Thus, a manifestation of his study is that a universal velocity distribution exists that applies to turbulent flow in smooth as well as rough ducts.

The existence of a universal velocity distribution implies that $k\bar{\eta}$ is a universal constant. Thus k will be a universal constant only when the average dimensionless velocity defect is independent of flow conditions. For fully developed rough boundary flow the velocity defect does not vary with wall roughness or Reynolds number. However, a reanalysis of Laufer's and Nikuradse's experiments for turbulent flow in smooth pipes by Lettau showed that the average dimensionless velocity-defect varies with Reynolds number. Thus for smooth duct turbulence, the Karman constant is not a universal constant. k is shown to be dependent on the particular theoretical form of model that is assumed and fitted to experimental data.

1.3.3 Summary of Values

Work done by many others warrants recognition. Excellent reviews of experimental studies for incompressible boundary layer flow have been presented by Ross (1953) in his Ph.D. thesis and by Coles in his 1953 Ph.D. thesis and his recent 1961 report. Their efforts were an aid in the literature search made in this study.

Studies reporting k merely as a result of experimental agreement rather than as a specific aim of the investigation are contained in the summary that follows. The value of von Karman's constant from more than 46 investigations have been tabulated in Table 1 to facilitate comparison and reference.

TABLE 1

SUMMARY OF STUDIES REPORTING THE KARMAN CONSTANT

INVESTIGATOR	MODEL	COMMENTS	KARMAN CONSTANT
Ashkenas, H. I. (1958)	yawed plate	follows Cole's treatment of law of the wall; used slope of log plot to determine k .	0. 40
Bender, D. L. (1955)	open channel	used slope of log plot of depth vs. velocity to get k; k decreases with increase in suspended sediment; k varies with sediment size; side or wall affects k as well as bed roughness.	0. 546 ave. (18) 0. 73 to 0. 37
Cermak, J. E. and Koloseus, H. J. (1953)	wind tunnel	k of 0. 4 questioned but accepted.	0. 40
Chanda, B. (1958)	wind tunnel	value of k from Clauser and Hama	0. 412
Clauser, F. H. (1954)	other's data	compilation of data obtained from turbulent boundary layers with and without pressure gradients.	0. 412
Coles, D. E. (1953, 1956, 1961)	wind tunnel and data of others	value of k from straight line fitted to data in the logarithmic region	0. 39 to 0. 41 0. 41 used

TABLE 1 (Continued)

Corrsin, S. (1957)	divergent channel	J. H. U.'s data, ; Laufer, Ludwieg and Tillman, Klebanoff and Diehl's data	0. 393
Deacon, E. L. (1954)	atmosphere	k when $\underline{Ri} = 0$.	0. 379
Dhawan, S. (1953)	wind tunnel	floating element for shear.	0. 33
Elata, C. and Ippen, A. T. (1961)	open channel	k varied for no sediment suspension as 0. 387 to 0. 248 for 26% suspended material; 0. 371 was average for no suspended material.	0. 371 ave.
Fenter, F. W. and Stalmach, C. J., Jr. (1958)	wind tunnel	accepted "experimental evidence" of others that k is constant.	0. 40
Goldstein, S. (1948)	collected data		0. 40, 0. 417
Hama, F. R. (1954)		Hama's investigations:	0. 472
		Clauser	0. 412
		Squire and Young	0. 391
		Prandtl and Schlichting	0. 40
		Landweber	0. 393
		Schultz-Grunow	0. 365
		Schoenherr and Granville	0. 393
		Hughes	0. 42
		Colebrook formula	0. 407

TABLE 1 (Continued)

Heisenberg, W. (1948)		theoretical determination of k provided by mathematical representation on which energy dissipation is considered. k may differ by a factor of two from 0.98	
Hinze (1959)		value used in text	0.41
Klebanoff, P.S. and Diehl, Z.W. (1952)	boundary layer zero pressure gradient	k found from slope of log region	0.40
Kutzbach, J.E. (1961)	atmosphere	wind profiles modified by artificial roughness.	0.41 ± .07
Landweber, L. and Siso, T.T. (1958)	flat plate	slope of inner and outer region gave the Karman constant.	0.423
Lettau, H.H. (1961)	pipe data. atmosphere	reanalysis of Nikuradse and Laufer's data. Lettau shows that k depends on the model law chosen to describe boundary layer. k = 0.40 only when logarithmic distribution is valid. k = 0.428 for extended linear law.	0.428

TABLE 1 (Continued)

Malaika, J. (1961)	open channel reanalysis	checked Schlichting's data, disregard points at boundary and proximity of central region. Resulting k for sparce distribution of roughness was 0.35 and for dense distribution k = 0.38. Malaika received similar trend in magnitude and direction in his study.	0.38
Malkus, W.V.R. (1956)		k determined from theoretical statistical organization of turbulent fields.	0.332
Matting, F.W., et al. (1961)	wind tunnel	skin friction at high Mach numbers in air and helium.	0.40
Meter, D.M. and Bird, R.B. (1961)	annulus flow	application of the Prandtl mixing length model k = 0.407 for limiting case of parallel plates.	0.407
Mickley, H.S. and Davis, R.S. (1957)	flat plate	from velocity profile: from C_f vs. R. from C_f vs. R_x the value of k increases with increased blowing through porous plate. Average k value = 0.451.	0.412 0.400 0.352 0.392
Millikan, C.B. (1938)	pipe flow	compiled and analysed duct flow data. k found by log slope.	0.40

TABLE 1 (Continued)

Montgomery, R. B. (1947)	pipe flow	introduced a mixing length based on a cylindrical model with zero-shear at axis of flow	0. 45
Moore, G. K. and Laird, A. D. K. (1957)	wind tunnel	direct shear stresses on mechanical wave boundary. k = 0. 393 used as by Schlichting k = 0. 43 for flat surface and k = 0. 37 for standing waves.	0. 40
Nikuradse, J. (1933)	pipe flow	see note under Lettau	0. 40
Reichardt (1951)	channel flow	variation of k cleared only through research	0. 40
Robertson, J. M. (1957)	pipe flow	from Ross's reanalysis of Nikuradse's data	0. 412
Roberson, J. A. (1961)	roughness elements	value of constant used, not determined.	0. 40
Ross, D. R. (1953)		average of values of k = 0. 415 for the following reviewed investigations:	0. 415
		Nikuradse (1932)	0. 40
		Millikan (1938)	0. 412
		Diessler (1950)	0. 383
		Fage (1936)	0. 368
		Donch (1926)	0. 403
		Reichardt (1940)	0. 426

TABLE 1 (Continued)

		Laufer (1950)	0. 390
		Skinner (1951)	0. 390
		Schultz-Grunow (1940)	0. 397
		Klebanoff and Diehl (1951)	0. 426
		Ludwieg, and Tillman (1949)	0. 442
		Fage and Falkner (1930)	0. 415
Rotts, J. (1950)		Schultz-Grunow and W. Tillman's velocity profiles	0. 40
Rubesin, M. W. (1954)	compressible boundary layer	values evaluated from Coles' figures:	
		velocity profiles:	0. 40
		C_f vs. $\underline{Re}$	0. 352
		C_f vs. $\underline{Re_x}$	0. 392
		Mickley and Davis	0. 392
Sayre, W. W. and Albertson, M. L. (1959, 1961)	open channel	roughness pattern rather than degree of roughness caused variation in k. k found to be between 0. 34 to 2. 77. k in final analysis taken as 0. 38.	0. 38
Schlichting, H.	flat plate	Karman constant found from velocity distribution above rough plates.	0. 40
Schubauer, G. B. and Klebanoff, P. S. (1951)	flat plate	Slotta's analysis of 20 cases of x distance from leading edge of plate; k was found to lie between 0. 35 and 0. 75	0. 52 ± . 02

TABLE 1 (Continued)

Sheppard, P. (1947)	atmosphere	floating element to determine shear	0.46 (ave.) 0.44 to 0.49
Smith, D.W. and Walker, J.H. (1959)	wind tunnel	floating element data; reduced by machine computation (Slotta). Smith and Walker's data gave k between 0.39 and 0.55 with average of 0.46; found by slope of wall law and velocity defect curves in similarity region. Slotta's reanalysis agrees, $k = 0.47 \pm .02$.	0.46 $0.47 \pm .02$
Stevenson, M. (1959)	plate with wire roughness	9 profiles	0.41
Szablewski, W. (1951)		$k = 0.388$ for flat plate $k = 0.417$ for pipe flow	
Taylor, G.I. (1937)	Parallel planes and pipes	for Prandtl's momentum transport theory $k = 0.27$ by Goldstein; 0.23 by Taylor for parallel planes; $k = 0.17$ Goldstein, 0.2 Taylor for pipes. For Karman's vorticity theory $k = 0.165$ Goldstein, 0.23 Taylor for parallel planes and $k = 0.128$ Goldstein, 0.19 Taylor for pipes. Taylor gave $k = 0.4$ for both planes and pipes as	0.4

TABLE 1 (Continued)

		limiting value at the wall for momentum transport theory.	
Tracy, H. J. and Lester, C. M. (1959)	open channel	each u/u_0* vs log ($y\ u*/\nu$) defines a straight line represented by equation of slope intercept form. The lines of 20 profiles do not have common slope. Limiting value of $k = 0.40$ is approached at smaller depths.	0.40
Vanoni, V. A. (1953)	open channels	study of suspended sediment $k \neq$ constant; but influenced by suspended-sediment concentration, secondary circulation and perhaps boundary roughness.	0.4
Vehrencamp (1954)	atmosphere	k varied from 0.18 to 0.5, floating element used to determine τ	0.38
Wieghardt, K. and Tillman, W. (1944)	boundary layer	cases of rising pressure $k = 1.1$ to 2.0 Nikuradse, pipe, $k = 0.40$ Schultz-Grunow, plate, $k = 0.43$.	0.43

1.4 Reanalysis of Flat-Plate Boundary Layer Data

1.4.1 Introductory Remarks

Published data from reliable experimental studies which completely investigate boundary layer flow are limited in quantity. An appeal is made for experimenters to report their results more completely, both in tabular and graphical form, for the benefit of future studies.

The aim of boundary layer investigations is to present the relations determined by boundary conditions and the structure of the flow; generally by examining velocity profiles and measured surface drag. Few techniques have been simultaneously employed to gather data in the most refined manner possible. Often, one facet of a study is obtained at the expense of other sought parameters, e.g. studies reporting improved velocity profiles frequently have not obtained the boundary stress value nor its gradient from the boundary. Complementary and complete investigations continue to be sought in this day of "refined" instrumentation.

Accounts for observed anomalies in boundary layer flow have been discussed by Coles (1961). Influencing factors such as: external stream turbulence; effects of pressure gradients; sensor or probe interference with the flow; three dimensionality of the flow; secular ambient conditions, density and viscosity changes; and facility organization have caused discrepancies from normal flow.

A review of instruments presently used to measure turbulent flow (mean and fluctuating) is given by Hinze (1959). Of the sensor type instruments (including: the pitot tube with a sensitive pressure transducer; the electric corona-discharge anemometer; and the method of electromagnetic induction) the hot-wire anomometer is to date the most successful instrument for measuring flow, intensities, correlations, integral and micro scales, etc.

Efforts to measure the shearing stress have involved the use of elaborate floating skin friction balances (cf., Schultz-Grunow (1940), Dhawan (1951), Coles (1953), and Smith and Walker (1959)). In addition, a calibrated surface stagnation tube has been employed to determine the coefficient of surface shearing stress (cf., Dutton (1955), Preston (1953), Landweber and Sizo (1958), Coles (1961), and Smith and Walker (1959)). Attempts to obtain the gradient of turbulent shearing stress have been reported by Schubauer and Klebanoff (1951) in which crossed hot wire anemometers (also cf., Ashkenas (1952), Spengos (1956)) were used. The anemoclinometer reportedly

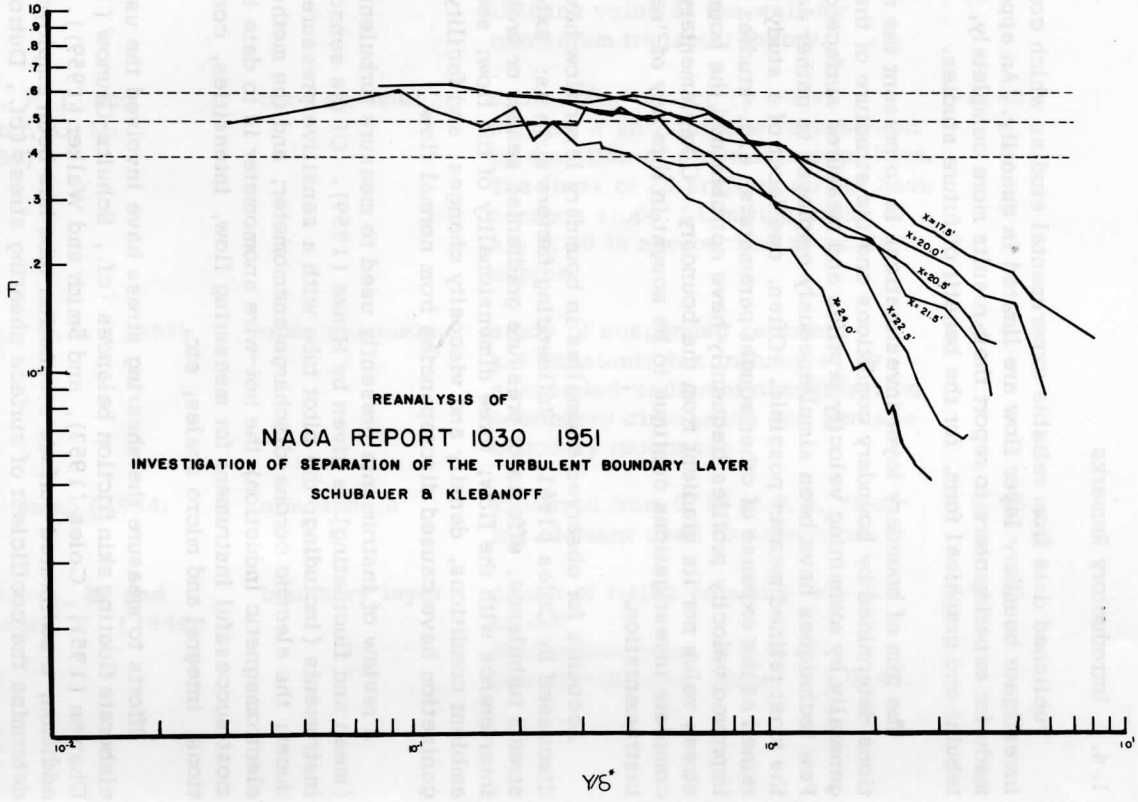

Fig. 3. Reanalysis of NACA 1030 data. $u^*/((du/U)/d\,\ell n\, y)$ Plotted Versus y/δ^*

measures $\overline{\rho u'w'}$ as given by the potential solution for flow about a sphere (cf. Frenkiel, 1952).

1.4.2 NACA Report 1030

The first data reanalyzed in this study was that provided by Schubauer and Klebanoff in NACA Report 1030 (1951). The reduction of this data is discussed below. The desired result of this analysis was to obtain a measure of Karman's constant for boundary layer data. k had not previously been determined from this NACA report.

In Schubauer and Klebanoff's report the shearing stress profile was given in terms of a stress coefficient $c_\tau = \overline{2u'v'}/U^2$. The mean velocity profile was listed as u/U at height y. The Reynolds number for the entire series of measurements was kept constant. The displacement thickness δ^* was reported for each station located at distance x from the leading edge of the surface. It was necessary to algebraically transform their data to solve for the dimensionless length scale of turbulence function as follows:

$$F = (\tau/\rho)^{\frac{1}{2}}/(du/d \log_e y) = (c_\tau/2)^{\frac{1}{2}}/d(u/U)/d \log_e y$$
$$= 1.628(c_\tau)^{\frac{1}{2}}/d(u/U)/d \log_{10} y \qquad (5)$$

Observed k values found in the initial analysis in which the velocity gradient was graphically determined, were between 0.35 and 0.8. Considering the uneven behavior of the computed function near the boundary, another analysis was made utilizing a smoothed velocity gradient. The F-function data for this analysis are shown in Figure 3, plotted logarithmically versus $\log (y/\delta^*)$.

A dependence of the function on station location is noted in the plot and k values are seen to lie between 0.38 and 0.64 as y/δ^* becomes small.

The function F was also noted to depend on the Reynolds number based on the displacement thickness, $\underline{Re}^*$. (For the NACA-1030 data δ^*U/ν was found from $\underline{Re}_x = 14.3 \times 10^6$; $U/\nu = 10^6/\text{ft.}$) The plot of data in Figure 4 was gained by considering the intercept of a desired value of the function with a line connecting the previously plotted computed function data (Figure 3) for flow measurements made at a particular station x along the flat plate. Thus for that station the known displacement thickness was used in determining $\underline{Re}^*$ and the intercept gave the respective value y/δ^*.

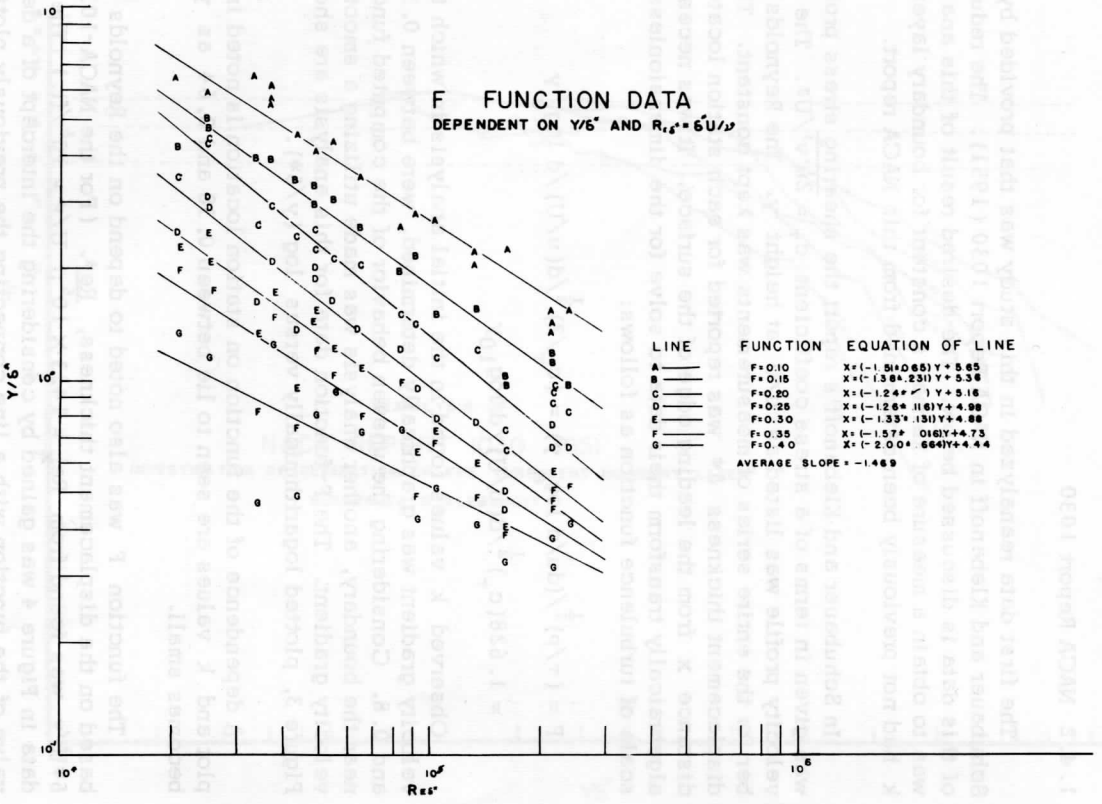

Fig. 4. NACA 1030 Reanalysis. $u^*/((du/U)/d\ell n_D\ y)$ Family as dependent on y/δ^* and

A regression analysis of the data plotted in Figure 4 showed that the functions were a family of curves having common slope, within experimental error. The importance of the related functions and their common slope is revealed in a discussion of a universal similarity principle relating flows by their geometry or dimensionality by Lettau (1961, see pg. 129). Lettau's (1961) "extended linear law," previously mentioned in the review of literature, satisfactorily agreed with observed duct data. It was shown to be a universal velocity distribution utilizing a form of the dimensionless length-scale of turbulence given as:

$$F = L/R = kX/(1 + m^{-1}X^{1+m}) \qquad (6)$$

where: $X = 1 - r/R = y/\delta$. The law contains but one number in addition to the Karman constant. This parameter m, appears to be determined by the flow structure. Observations suggest that $m = 1/2$ for duct flow (one dimensional flow) and $m = 1/4$ for atmospheric (two dimensional)flow.

From Figure 4, the average slope $1.469 \approx 1.50$ represents the term $1 + m$ such that $m = 1/2$ for flat plate flow. Thus boundary layer flow is similar to duct flow being that both flows are one-dimensional and $m = 1/2$.

1.4.3 NASA TR R-26

Work completed for NASA recently by Smith and Walker (1959) reported a wind tunnel investigation giving detailed velocity profiles and measured surface drag on a small, smooth flat plate. The shearing stress results were determined by using a floating skin friction balance and also a calibrated Preston pitot shear tube. The reanalysis study was conducted by using the reported wall shear coefficient throughout the boundary layer since the gradient of shearing stress was lacking. The success of using smoothed velocity gradients in the previous analysis prompted data reduction and the function evaluation by electronic computer in a manner outlined in the following flow chart.

FLOW CHART FOR COMPUTATION OF

$$\frac{\bar{Y}AVE}{\delta^*} \text{ VS } F = \frac{\sqrt{\frac{1}{2} C_\tau}}{\frac{\Delta u/U}{\Delta LNy}}$$

Read-In Published Data

1. Station Location, Mach Number, Reynolds Number
2. Coefficient of Friction
3. N = Number of Operands; M = N - 2

A. Read $yi \rightarrow N$, $(u/U)i \rightarrow N$

B. Compute $(LN\,y)\,i \rightarrow N$

C. Compute $(LN\,\bar{Y}AVE)\,i \rightarrow M = \left[\frac{(LN\,yi + LN\,(yi+2)}{2}\right]_{i \rightarrow M}$

D. Compute $\bar{Y}AVE\ i \rightarrow M = e^{(LN\,\bar{Y}AVE)\,i \rightarrow M}$

E. Compute $(\bar{Y}AVE/\delta^*)\,i \rightarrow M$

F. Compute $F_N = \frac{(\frac{1}{2} C_\tau)^{\frac{1}{2}}}{[(U_{(i+2)} - U_i)/(LN\,y_{(i+2)} - LN\,y_i))]_{i \rightarrow M}}$

Print:

1. Station location and identifying data
2. $(\bar{Y}AVE/\delta^*)\,i \rightarrow M$
3. $(FN) = \frac{(\frac{1}{2} C_\tau)^{\frac{1}{2}}}{\left[\frac{\Delta u/U}{\Delta LN\,y}\right]_{i \rightarrow M}}$

Representative results for data having equivalent Mach numbers are plotted linearly in Figure 5 and logarithmically in Figure 6; indicating again k as the limiting value of the function approaching the boundary. The logarithmic plot produces a smoother curve but may give a first impression of not approaching the boundary. The Karman constant value for this data varies between 0.38 and 0.55, compared to $k = 0.46$ as reported by Smith and Walker; see Figure 1.

The data plotted in Figures 5 and 6 is representative of the narrow confine of data scatter. The dependence of F on station location (x) and similarly for Reynolds number $\underline{Re}_x$ is evident for $y/\delta^* > 1.0$. Increase in Reynolds numbers yields larger F-functions. This dependence effect is opposite to that noted in the reanalysis of NACA 1030 as shown in Figures 3 and 4. No explanation of this difference can be postulated at this time.

1.5 Comments and Comparisons of the Two Reanalyses

1.5.1 Comments

In NASA TR R-26 the shearing stress was assumed constant from the boundary. The effect of this assumption on the computed values can be cleared by use of an expression fit to measured flat plate boundary layer shear stress profiles. Lettau (1960-61) has suggested a simple fourth-order parabola; $\tau/\tau_0 = (1 - (y/\delta)^2)^2$ which satisfactorily describes the variation of shear stress shown as illustrated on page 491 of Hinze's (1959) text. It checks also with profiles measured by Ashkenas (1958). For $y/\delta = 0.1$, τ/τ_0 would change about 2% from the boundary value. Thus for $y/\delta = 0.2$, $\delta^* \approx 0.5\delta$ for an assumed linear velocity distribution, or y/δ^* is greater than 0.4; in this case τ/τ_0 would have decreased by approximately 8%. On the plots, Figure 5 and 6, less than 1% change of τ/τ_0 has taken place at $y/\delta^* = 0.1$. This should be tolerable for computation of the limiting value of the F function. The peak F values arise at about $Yave/\delta^* = 0.5$ and correspond closely to the values of k obtained in the NASA R-26 analysis. Perhaps the peak values describe the Karman constant for logarithmic profiles.

The initial value near $y/\delta^* = 0$ in Figure 6 tends toward zero, which is an anomalous behaviour, for one would expect F to become large as shown in Figure 3 for the NACA 1030 reanalysis. Considering for this case $F = (1/2\, C\tau)^{\frac{1}{2}} / ((\Delta u/U)/\Delta \ell n Y)$, $\Delta u/U$ becomes small, $\Delta \ell n\, y (= \ell n\, Yi + 2 - \ell n\, Yi)$ becomes large as $y \to 0$. Thus F should increase as rapidly as $\Delta u/U$ is found near the wall. The extreme

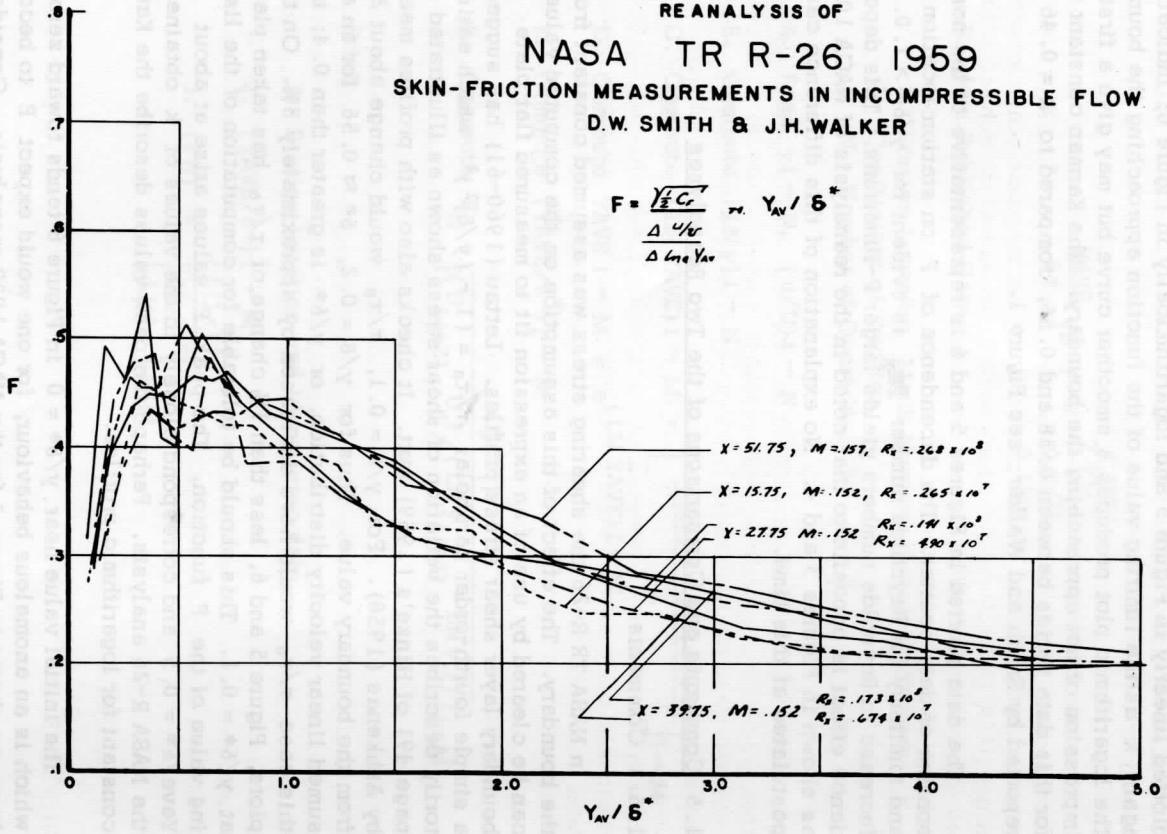

Fig. 5. NASA TR R-26 Reanalysis $\sqrt{.5 C_T}/((\Delta u/U)/\Delta \ell n_e Y)$ Plotted Versus Yave/δ*

region close to the wall must, of course, be neglected both because of instrument sensor limitations, and because F should approach infinity at the wall.

The two experiments were markedly different considering model dimensions. The first and last stations position for the NACA 1030 study were at 14.0 and 25.0 ft. for studying transition phenomenon whereas in the NASA TR R-26 the positions were at 15 and 51.5 inches. Coles relates that comparative results are sometimes limited by difference in boundary layer structure produced by different tripping devices or even by the tunnel facilities themselves.

1.5.2 Conclusions

Values of the von Karman constant for two separate analyses vary from 0.3 to 0.8. The following method was used to obtain an average k for each study. In the NACA 1030 reanalysis, where the F function approaches the wall in a manner parallel to theoretical expectations, the final and generally the largest two F values near the wall for over 20 studies were averaged to give $k_{ave} = 0.52 \pm 0.02$. Because of sizable fluctuations of the computed function for Smith and Walker's data, three values of each profile were considered in the averaging process. The functions immediately preceding, following, and the largest computed F value were averaged for more than 58 profiles for the value $k = 0.47 \pm 0.02$. This result agrees favorably with the 0.46 reported by the authors of NASA TR R-26, as found from fitting their data to a logarithmic velocity distribution.

The Karman constant is not universal for flat plate boundary layer flow as it is shown to vary with Reynolds numbers. Comparing both studies, it is apparent that the determining function for k was dependent on station position. The NACA 1030 data follow a pattern compatible with theory and are shown to contribute to similarity or dimensional characterization of turbulent flows. The constant in Lettau's extended linear law is $m = 1/2$ for flat plate boundary layer flow.

1.6 References

ASHKENAS, H.I., Turbulent Shearing Stress in the Boundary Layer of Yawed Flat Plates. NACA T.N. 4140 (1958) See also NACA T.N. 3383 (1955)

BAINES, W.D., 1951, A Literature Survey of Boundary-Layer Developments on Smooth and Rough Surfaces at Zero Pressure Gradient.

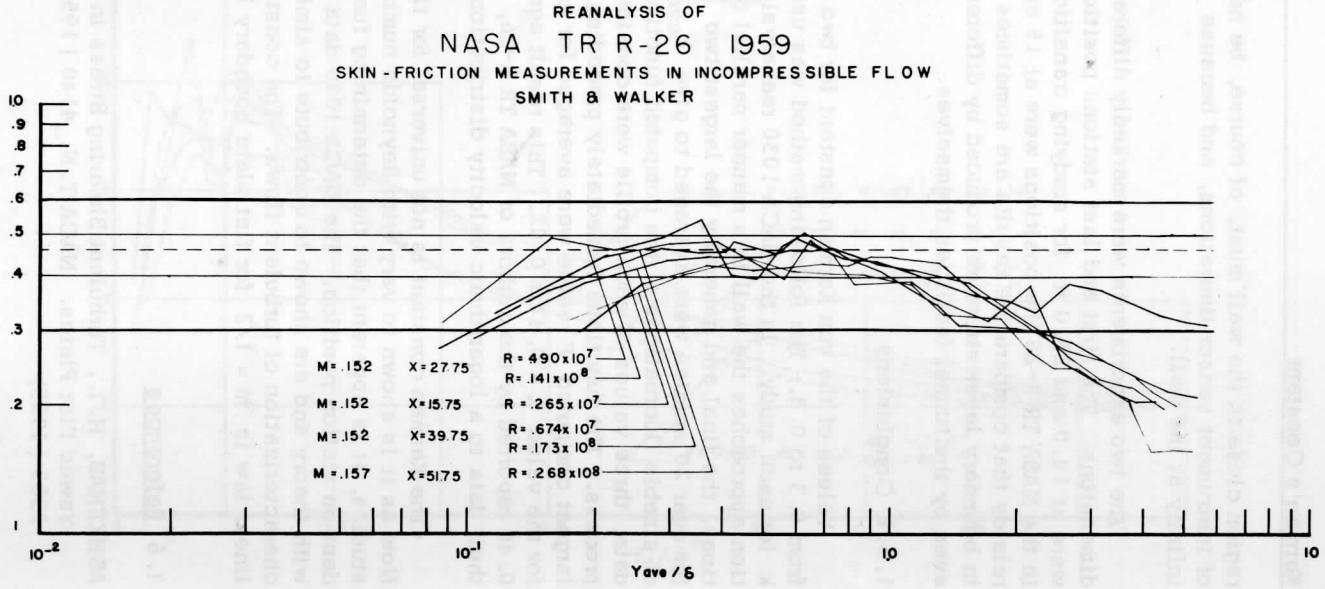

Fig. 6. NASA TR R-26 Reanalysis $\sqrt{.5\,C_\tau}/((\Delta u/U)/\Delta \ell n_e Y)$ Plotted vs. Yave/δ*

Iowa Institute of Hydraulic Research. State University of Iowa, Iowa City 1951.

BENDER, D. L., 1955, Suspended Sediment Transport in Alluvial Irrigation Channels. M. S. -Thesis Colorado A and M, Fort Collins, Colorado 1955.

CERMAK, J. E. and KOLOSEUS, H. J. 1953. Lake Hefner Model Studies of Wind Structure and Evaporation. Final Report Part I Colorado A and M Report No. 54 JEC 20.

CHANDA, B., 1958. Turbulent Boundary Layer over Heated and Unheated, Plane, Rough Surfaces. Scientific Report No. 1 Contract AF 19 (604)-1706 Colorado State University 1958 CER 58 BC 21.

CLAUSER, F. H., 1954, 1956. Turbulent Boundary Layers in Adverse Pressure Gradients. J. Aero. Sci., Vol. 21, No. 2, pp. 91-108 Feb. 1954 Advances in Applied Mechanics, IV. N. Y. Academic Press, Inc.

COLES, D. E., 1953, 1956, 1961. Measurements in the Boundary Layer on a Smooth Plate in Super-Sonic Flow. Ph. D. Thesis Calif. Institute Tech., Pasadena 1953.

_____, The Law of the Wake in the Turbulent Boundary Layer, Jour. Fluid Mech. Vol. 1, pt. 2, July 1956, pp. 191-226.

_____, The Turbulent Boundary Layer in a Compressible Fluid, P-2417, Aug. 1961. The RAND Corporation.

CORRSIN, S., 1957. Some Current Problems in Turbulent Shear Flows. Naval Hydrodynamics Publication 515 National Academy of Sciences, National Research Council (1957).

CORRSIN, S. and RUETENIK, J. R., 1955. 50 Jahre Grenzschichtforschung, edited by Gortler and Tollmien. 1955 Braunschweig.

DEACON, E. L., 1954. A Study of Turbulent Transfer in the Layers of Air near the Ground. Division of Meteorological Physics, 1961 Commonwealth Scientific and Industrial Research Organization, Melbourne.

DHAWAN, S., 1953. Direct Measurements of Skin Friction. NACA TN 2567, NACA Report 1121 Cal. Tech. 1953.

DRYDEN, H. L., 1955. Fifty Years of Boundary-Layer Theory and Experiment. Science Mar. 18, 1955, pp. 375-380.

DUTTON, R. A., The Velocity Distribution in a Turbulent Boundary Layer on a Flat Plate. C. P. No. 453 (19, 576 A. R. C. Tech. Report (1959).

ELATA, C. and IPPEN, A. T., 1961. The Dynamics of Open Channel Flow with Suspensions of Neutrally Buoyant Particles. M. I. T. Hydrodynamics Laboratory Tech. Report No. 45, Jan. 1961.

FENTER, F. W. and Stalmach, C. J. JR., 1958. Measurement of Turbulent Boundary Layer Shear Stress by Means of Surface Impact Pressure Probes. Aero/Space Sci. 25: 793-4 Dec. 1958. Also see: U. of Texas, Defense Research Laboratory Report 392.

FRENKIEL, F. N., et. al., 1952. The IMFL Anemoclinometer — An Instrument for the Investigation of a Fluctuating Velocity Vector. The Review of Scientific Instruments, Vol. 23, No. 12, pp. 661-666, Dec. 1952.

GOLDSTEIN, S. The Similarity Theory of Turbulence, and Flow between parallel planes and through pipes. Proc. Roy. Soc. of London, 4899, Vol. 159, pp. 473-496. 1937.

HAMA, F. R., 1954. Boundary Layer Characteristics for Smooth and Rough Surfaces. Soc. Naval Arch. and Marine Engineers, Nov. 1954.

HEISENBERG, W., 1948. On the Statistical Theory of Turbulence. (1948). Translation, NACA Tech Memo 1431 Jan. 1958.

HINZE, J. O., 1959. TURBULENCE, McGraw-Hill Book Company, Inc.

HSU, E. Y. The Measurement of Local Turbulent Skin Friction by Means of Surface Pitot Tubes. Report 957 David Taylor Model Basin, Washington D C, 1955.

KLEBANOFF, P. S. and DIEHL, Z. W., 1952. Some Features of Artificially Thickened Fully Developed Turbulent Boundary Layers with Zero Pressure Gradient. NACA Report 1110 1952.

_____, 1954, NACA Tech. Note 3178, 1954.

_____, SCHUBAUER, G. B., and TIDSTROM, K. D. Measurements of the Effect of Two-Dimensional and Three-Dimensional Roughness Elements on Boundary Layer Transition. J. Aero Sci. Nor. 1955 pp. 803-804.

KUTZBACH, J. E., 1961. Investigations of the Modification of Wind Profiles by Artificially Controlled Surface Roughness M. S. Thesis, U. of Wisconsin 1961. Also see, "Studies of the Three Dimensional Structure of the Planetary Boundary Layer," with H. H. Lettau 1961. Contract DA-36-039-SC-80282, Madison, Wisconsin, 1961.

LANDWEBER, L. and SIAO, T. T., 1958. Comparison of two Analyses of Boundary-Layer Data on a Flat Plate from Mar. 1958, Journal of Ship Research.

_____, Reanalysis of Boundary Layer Data on a Flat Plate. Ninth International Towing Tank Conference, Paris (1960).

LAUFER, 1954. The Structure of Turbulence in Fully Developed Pipe Flow, NACA, Tech. Rep. No. 1174, 1954.

LETTAU, H. H., 1961. A Generalized Mathematical Model of the Mean Velocity Distribution in Fully Turbulent Duct Flow. Studies of the Three-Dimensional Structure of the Planetary Boundary Layer. Dept. of Meteorology, University of Wisconsin, Contract DA-36-049-Sc-80282, 1961.

LETTAU, H. H. and DAVIDSON, B. (editors) (1957, Vol. I, II) Exploring the Atmosphere's First Mile. Press Inc. London and New York, 1957, PERGAMON.

LETTAU, H. H., 1959, 1960, 1961. Class Notes, Department of Civil Engineering and Meteorology.

MALAIKA, J., 1961. Discussion of "Roughness Spacing in Rigid Open Channels," by Sayre and Albertson, 1961. Journal of Hydraulics Division, Proceedings of A. S. C. E. Vol. 87, No. HY 6, No. 1961, part 1, pg. 249-251.

MALKUS, W. V. R., Outline of a Theory of Turbulent Shear Flow. Journal of Fluid Mechanics, Vol. 1, 1959, pp. 521-539.

MATTING, F. W., CHAPMAN, D. R., NYHOLM, J. R. and THOMAS, A. G. 1961. Turbulent Skin Friction at High Mach Numbers and Reynolds Numbers in Air and Helium. NASA Tech. Report R-82. 1961.

METER, D. M., and BIRD, R. B. 1961. Turbulent Newton Flow in Annuli. University of Wisconsin, Engineering Experiment Station, Reprint 435; AICHE, Journal I, 41-45, 1961.

MICKLEY, H. S. and DAVIS, R. S. 1957. Momentum Transfer for Flow over a Flat Plate with Blowing. NACA TN 4017, Nov. 1957.

MILLIKAN, C. B. 1938. A Critical Discussion of Turbulent Flow in Channels and Circular Tubes. Proceedings of Fifth International Congress of Applied Mechanics 1938, pp. 386-392.

MONTGOMERY, R. B. 1947. On The Velocity Distribution of Turbulent Flow in Pipes and Channels of Constant Cross Section. Mechanical Engineering, Vol. 69, 1947, pg. 950.

_____, Generalization for Cylinders of Prandtl's Linear Assumption for Mixing Length. Annals of the New York Academy of Sciences, Vol. 44, Act. 1, "Boundary-Layer Problems in the Atmosphere and Ocean," May 29, 1943, pp. 89-103.

MOORE, G. K. and LAIRD, A. D. K. 1957. Direct Shear Stresses and Air Velocity Profiles on a Mechanical Wave Boundary. Vol. 38, No. 5, Transactions, American Geophysical Union, Oct. 1957.

NIKURADSE, J., 1933. Laws of Flow in Rough Pipes. Translation, NACA Tech. Memo 1292, Nov 1950.

PASQUILL, 1950. The Aerodynamic Drag of Grassland. Proc. Royal Soc., London, 202, Series A, 1950.

POPPENDIEK, H. J. and VEHRENCAMP, J. E. Investigation of Atmospheric Diffusion Processes by Means of Experimental, Analytical and Numerical Methods. U. of Calif., Dept. of Engineering, Contract N6-ONR-275, May 1950.

PRANDTL, L. Text: Essentials of Fluid Dynamics. Hafner Publishing Co., N. Y. 1952.

PRESTON, 1953. The Determination of Turbulent Skin Friction by Means of Pitot Tubes. J. Roy Ae. S. Vol. 58, No. 110, Feb. 54.

_____, The Minimum Reynolds Number for a Turbulent Boundary Layer and the Selection of a Transition Device 1958, Jour. Fluid Mech. 3, 373-384.

REICHARDT, H. 1951. Vollstandige Darstellung der turbulenten Geschwindigkeitsverteilung in glatten Leitungen (Velocity Distribution for Turbulent Pipe Flow). Zeitschrift fur angewandte Mathematik und Mechanik, Vol. 31, 1951.

RIDER, N.E. 1954. Eddy Diffusion of Momentum, Water Vapour, and Heat Near the Ground. Phil. Trans. Royal Soc. London, 246, Series A, 1954.

ROBERSON, J.A. 1961. Surface Resistance as a Function of the Concentration and Size of Roughness Elements. Ph.D. Thesis, State U. of Iowa, 1961 (Hydraulic Engineering).

ROBERTSON, J.M. 1957. The Turbulent Velocity Distribution in a Rough Pipe. Fifth Midwestern Conference on Fluid Mechanics, 1957.

ROSS, D.R., 1953. A Study of Incompressible Turbulent Boundary Layers, Ph.D. Thesis (Physics), Harvard University, 1953.

ROTTA, J., 1950. On The Theory of the Turbulent Boundary Layer, 1950. Translation, NACA Tech. Memo 1344, 1953.

RUBESIN, M.W., 1954. An Analytical Estimation of the Effect of Transpiration Cooling on the Heat Transfer and Skin Friction Characteristics of a Compressible Boundary Layer. NACA Technical Note 3341, 1954.

SAYRE, W.W. and ALBERTSON, M.L., 1959, 1961. The Effect of Roughness Spacing in Rigid Open Channels. Dept. of Civil Engineering, Colorado State University, Fort Collins, Oct. 1959, CER WWS 31. Also see, Proceedings of ASCE, May, 1961.

SCHLICHTING, H., Experimental Investigation of the Problem of Surface Roughness. Translation, NACA TN. 823.

_____, Text BOUNDARY LAYER THEORY, McGraw-Hill Book Co., Inc. 1960.

SCHUBAUER, G.B., and KLEBANOFF, P.S., 1951. Investigation of Separation of the Turbulent Boundary Layer, NACA Report 1030, 1951.

_____, and KLEBANOFF, P.S., 1955. Contributions on the Mechanics of Boundary Layer Transition. NACA TN 3489 (Sept. 1955).

SCHULTZ-GRUNOW, 1940. New Frictional Resistance Law for Smooth Plates (1940). Translation NACA Tech. Memo 986. 1941.

SHEPPARD, P., 1947. The Aerodynamic Drag of the Earth's Surface and the Value of von Karman's Constant in the Lower Atmosphere. Proc. Royal Soc. A, 188, 208-222.

SMITH, D. W. and WALKER, J. H., 1959. Skin Friction Measurements in Incompressible Flow. NASA TR R-26. 1959.

STEVENSON, M., 1959. Roughness Effect and Correlation of Two-Dimensional Wire Roughness in Turbulent Shear Flow. Tech. Note BN 181 Dec. 1959, The Institute for Fluid Dynamics and Applied Mathematics, University of Maryland, College Park, Md.

SZABLEWSKI, 1951. Berechung der turbulenten Stromung im Rohr auf der Grundlage der Mischungsweghypothese. Zeitschrift fur angewandte Matematik und Mechanik, Vol. 31, 1951.

TAYLOR, G. I., 1937. Flow in Pipes and Between Parallel Planes. Proc. Roy Soc. Series A, Vol. 159, 1937, pp. 496-506.

TILLMAN, W. Investigations of Some Particulars of Turbulent Boundary Layers on Plates. Translation by Armed Services Technical Information Agency, ATI 35833, Arlington, Va.

TRACY, H. J. and LESTER, C. M., 1959. Resistance Coefficients and Velocity Distribution in a Smooth Rectangular Channel. Geological Survey Water Supply Paper 1592-A.

VANONI, V. A., 1953. Some Effects of Suspended Sediment on Flow Characteristics. Proc., Fifth Hydr. Conf., State Univ. of Iowa, Studies in Engineering Bulletin 34, 1953, pp. 137-138.

VEHRENCAMP, J. E., 1954. "Studies of Transfer Processes in the Lower Atmosphere," Univ. of Calif., Dept. of Engineering, Los Angeles. Tech. Rep. No. 54-28, Prepared under Contract No. NG-ONR-275, 1954. See also: Lettau and Davidson, 1957, Exploring the Atmosphere's First Mile, Vol. 1, pp. 99-113.

WIEGHARDT, K. and TILLMAN, W., 1944. On the Turbulent Friction Layer for Rising Pressure, 1944. Translation, NACA Tech. Memo 1314.

2

Climatology of Aerodynamic Roughness Parameter and Energy Dissipation in the Planetary Boundary Layer over the Northern Hemisphere*

Ernest Chen-Tsun Kung

Department of Meteorology
University of Wisconsin

Abstract: This investigation is an attempt to obtain direct information on the climatological pattern of mechanical energy dissipation in the lower atmosphere over the Northern Hemisphere, utilizing a theoretical model of the atmospheric boundary layer, and a survey of aerodynamic roughness of natural ground. With the aid of an empirical numerical relationship between vegetation height and aerodynamic roughness length z_0, and the results of a land-use survey, meridional profiles of z_0 for all continents, and regional-seasonal variations over the North American Continent were derived between latitudes 25° and 70°N. The representativeness of the derived z_0 values was tested using climatological data on the ratio of wind speed at anemometer level to geostrophic speed.

Geostrophic speeds at the 1000-mb surface for 360 gridpoints over the hemisphere were computed from daily pressure data for the ten-year period 1945 to 1955. Utilizing the concept of the geostrophic drag coefficient and its dependency on the surface-Rossby number, basically micrometeorological parameterization was applied to the large-scale problem of computing energy dissipation in the planetary boundary layer.

---

*This work is part of a thesis submitted to the University of Wisconsin in partial fulfillment of the requirements for the Ph. D. degree, written under the supervision of Professor H. Lettau, Department of Meteorology.

The results are presented in detailed tables. Seasonal hemispheric means of energy dissipation for winter, spring, summer, and fall conditions in the planetary boundary layer were obtained as 1.94, 1.33, 0.70, and 1.40 watts/m^2, respectively.

List of Contents

2.0 Introduction
- 2.0.1 General Remarks
- 2.0.2 Roughness Parameter Related to Vegetation Height and Land Use

2.1 Evaluation of Horizontal and Seasonal Variations of Continental Roughness Parameter from Vegetation Cover
- 2.1.1 Method and Data
- 2.1.2 Meridional Distribution of Continental Roughness Parameters over the Northern Hemisphere and Regional Distribution over the North American Continent
- 2.1.3 Testings Using Ratio of Windspeed at Anemometer Level to Geostrophic Speed

2.2 Distribution and Seasonal Variations of Geostrophic Drag Coefficients and Energy Dissipation
- 2.2.1 Method and Data
- 2.2.2 Hemispheric Distributions and Seasonal Variations of Geostrophic Drag Coefficients and Energy Dissipation
- 2.2.3 Regional Distribution and Seasonal Variation of Energy Dissipation over the North American Continent
  - 2.2.3.1 Estimates Based on Geostrophic Drag Coefficients
  - 2.2.3.2 Comparison with Results Using Cressman's Skin-Drag Coefficient

2.3 Discussion of Results

2.4 References

2.0 Introduction

2.0.1 General Remarks

Dissipation of mechanical energy is one of the major processes of the atmospheric energy cycle. The mechanical energy which is generated from the conversion of available potential energy is eventually dissipated and changed into internal energy through frictional processes which are generally irreversible. The maintenance of the large-scale general circulation against the frictional dissipation is one focus of interest in current theories. Likewise, the rate of energy dissipation also has synoptic importance since it affects the generation and decay of weather disturbances. It is thus highly desirable to investigate climatological patterns of the process of mechanical energy dissipation, as a basis both for the development of theoretical meteorology and practical applications. Since the energy dissipation in the atmospheric boundary layer represents the major portion of the continuous decay of the energy of all large-scale atmospheric motions, this part of the energy dissipation is of primary concern.

Previous approaches to evaluation of the energy dissipation may be separated into two categories. One approach is to obtain estimates of the energy dissipation indirectly from the balance requirement using conventional energy equations. Another direct approach is to use boundary layer equations with the dynamical degrees of freedom reduced in extreme, i.e., over-simplified models of boundary layer structure and external conditions are assumed. These investigations were also limited in the spatial extent of the samples or periods of sampling. References can be made to Brunt (1941), Jensen (1961), Lettau (1954, 1959, 1961b), White and Saltzman (1956), and others. Those approaches, of course, have their merits in discussions of local and regional aspects of the process of energy dissipation or in the schematical discussions of particular cases, but the results are restricted when we wish to study climatological and synoptic aspects of the energy dissipation in terms of multi-annual hemispheric averages.

Lettau's (1961) theoretical model of atmospheric boundary layer structure permits us to determine certain boundary layer characteristics such as the geostrophic drag coefficient C, the surface stress τ_0, and the angle α_0 formed by surface stress and geostrophic wind at surface level, as unique-valued functions of the surface-Rossby number $Ro_0 = V_{g.0}/(z_0 f)$, where ρ = air density, $V_{g.0}$ = geostrophic wind speed at surface level, f = Coriolis parameter, and z_0 = aerodynamic roughness parameter. This set of values permits us also to compute the total energy dissipation in the boundary layer. A necessary and

sufficient prerequisite is that three external parameters $V_{g,0}$, f, and z_0 are specified. The objective of this study are (1) to develop a technique to determine representative regional values of the aerodynamic roughness parameter for the earth-air interface from vegetation covers of the land surfaces and wind profile analysis over the ocean surface, (2) to compute geostrophic wind speed at the 1000 mb surface, and (3) to derive geostrophic drag coefficients and values of energy dissipation in the lower atmosphere over the entire Northern Hemisphere from 25°N to 70°N. Essentially, this is an attempt to apply micrometeorological parameterization to large-scale problems, utilizing the concept of the geostrophic drag coefficient.

2.0.2 Roughness Parameter Related to Vegetation Height and Land Use

With the aid of an analysis of wind profile data over tall vegetation, reported in the literature, Kung (1961) has extended Deacon's (1953) tabulation of roughness parameters for natural surfaces. The relation between z_0 and plant height has resulted in the following regression line,

$$\log z_0 = -1.24 + 1.19 \log h, \qquad (1)$$

where z_0 and plant height h are both expressed in cm.

It is interesting to study the ratio $N = h/z_0$ which we will refer to as Nikuradse's roughness ratio. It indicates the effectiveness of obstacles as roughness elements; the smaller the N-value of a certain kind of obstacle, the larger the z_0-value in proportion to height. Using equation (1), the resulting values of z_0 and N for a typical range of h are shown in Table 1.

TABLE 1. Roughness length z_0 versus obstacle height h

h(cm)	Type of obstacles	z_0(cm)	$N = h/z_0$
1000	Forest trees	214.0	4.7
100	Tall grasses	13.8	7.2
10	Low grasses	0.80	11.2
1	Bare soils	0.0576	17.4
0.1	Sands	0.00363	26.9

Using the assumption of a logarithmic velocity distribution and the universal Karman constant of k = 0.4, Nikuradse (1933) found N = 30 in his duct flow experiments through circular pipes coated with sands grains. Lettau (1961a) pointed out that according to his new mathematical model of the universal velocity distribution law for fully turbulent flow in rough ducts, Nikuradse's experiments give k = 0.428 and N = 23.9. Paeschke (1937) obtained N = 7.35 for his wind measurements over grassland and a beet field. These values compare well with the values listed in Table 1. Tall obstacles as represented by forest trees, are highly effective roughness elements compared with obstacles of the lower height.

Kutzbach (1961), in his wind profile modification experiments on the ice of Lake Mendota, used bushel baskets as roughness elements. He showed that z_0 is a function of obstacle density as well as obstacle height. Since equation (1) is established by the analysis of wind data above dense uniform vegetation, saturation obstacle-density (i.e., the obstacle density which gives the maximum z_0-value) is assumed in applying this equation. Kutzbach (1961) also raised this point, comparing equation (1) with his and Schlichting's experimental data.

Assuming that morphological differences among plant species and the response of z_0 to wind speed (induced by the response of plant shape to changing wind speed) are negligible, vegetation height can be treated as the major factor in causing aerodynamic roughness for dense uniform vegetation sites. This assumption is valid since z_0, as a function of h, can vary over several powers of ten while the neglected factors affect z_0 within less than one power of ten in the natural geophysical environment. It is also expected that over an area of $10^4 km^2$ or larger the errors induced by this assumption may tend to cancel within the region.

In order to obtain the representative z_0 for a large region, in contrast to those of a defined micrometeorological site, data on land use (i.e., horizontal distribution of vegetation cover) and phenological variation of vegetations must be combined with the numerical relationship between z_0 and h. The logarithm of the surface-Rossby number, which is inversely proportional to z_0, determines the geostrophic drag coefficient. In view of this, it is concluded that the representative area-mean of roughness parameters can be computed as the area-weighted average of log z_0-values for various vegetation types in the region rather than the corresponding arithmetic mean of z_0-values.

2.1 Evaluation of Horizontal and Seasonal Variations of Continental Roughness Parameter From Vegetation Cover

2.1.1 Method and Data

The evaluation of the aerodynamic roughness of a selected continental region involves the following four steps:

(1) Classification of the vegetation into major types and determination of the area-percentage of each type (i.e., the "land use").
(2) Estimation of representative heights for each vegetation type with a break-down by season.
(3) On the basis of (2) assignment of a roughness parameter to each vegetation type.
(4) Computation of the regional means of the logarithm of the roughness parameters, employing the percentage area of each vegetation type as a weighing factor, with a break-down by season.

The following eight classes of continental vegetation cover were distinguished: (1) Crops - (2) Woodland and tree crops - (3) Meadow and pasture - (4) Forest - (5) Natural vegetations - (6) Tundra - (7) Desert - and, (8) Built-on and waste land.

The data on land use were obtained from various sources. For the United States and Canada the main sources of information were official statistics by the United States Department of Agriculture (1958a, 1958b) and the Dominion Bureau of Statistics (1958). The data for China and India were obtained from Shen (1951) and the Times of India (1956 to 1960) respectively, together with a survey of existing maps (Hammond, Van Royan, 1954; and others). The 1957 FAO Yearbook (1958) was used for all other areas. Atlases such as the Oxford Regional Economic Atlas (1956) and other miscellaneous information (Balchin, 1955; Klages, 1942; and others) were also used for bridging gaps, and to make slight adjustments in a few cases where the statistical data were insufficient or incomplete.

Phenological data and estimates of plant heights were obtained from various sources (Klages, 1942; Kung, 1959; Curtis, 1959; Packard, 1957; Wilson, 1955) and also as the result of discussion with staff members of the Departments of Agronomy and Botany at the University of Wisconsin. For the estimate of roughness parameter on the basis of plant height, the numerical relationship presented in 2.0.2 was used.

2.1.2 Meridional Distribution of Continental Roughness Parameters over the Northern Hemisphere and Regional Distribution over the North American Continent

The land area of the Northern Hemisphere was studied separately for: (1) North America, (2) Europe-Africa, (3) and Asia (including the USSR). The first region was subdivided into Western, Central, and Eastern North America. However, the longitudinal areas studied for those three subsections on the North American Continent are not in perfect consistency with each other and with (1); longitudinal limits were slightly adjusted for convenient data treatment. A latitudinal breakdown by 10-degree zones, and 5-degree zones between 30° and 50°N in North America was used. Table 2 indicates the longitudinal areas considered in each continental section of the Northern Hemisphere.

For each of these latitudinal zones, roughness parameters were computed following the procedures described in Section 2.1.1. Values of $z_0 = 0.03$ cm for desert, and $z_0 = 0.1$ cm for snow cover were adopted from the study of Deacon (1953). On the basis of computed zonal roughness parameter, the latitudinal profiles of roughness parameter were derived for 5-degree intervals from 25°N to 70°N. If a specified latitude were within one of the zones described in Table 2, the computed roughness parameter of the zone was taken. If the specified latitude fell between two latitudinal zones, the average of the log z_0-values was taken. Meridional profiles of roughness parameters thus estimated are summarized in Table 3 for the four seasons. These values will be regarded as representative z_0-values of 5-degree latitudinal zones centered at specified latitudes. For corresponding data on the Southern Hemisphere, reference is made to Kung and Lettau (1961).

To facilitate a more detailed investigation of geostrophic drag coefficients and energy dissipation over the North American Continent, the horizontal distribution and seasonal variation of roughness parameters were estimated over this continent. The computed zonal roughness parameters of Western, Central and Eastern North America were adjusted by using more detailed data of the original land use survey to assign roughness parameters for all sections of 5-degree in latitude by 10-degree in longitude. The results are summarized in Table 4.

The meridional profiles of roughness parameter in Table 3 reflect the characteristic vegetation cover over the continents. In general, the meridional sequence of vegetation types ranges from tropical forests with high z_0-values (see Kung and Lettau, 1961) to low natural vegetation

TABLE 2. Longitudinal limits (all in deg West of Greenwich, 0 to 360) at specified latitudes Φ (deg) for indicated continental sections of the Northern Hemisphere.

Φ	Western North America	Central North America	Eastern North America	North Atlantic	Europe-Africa	Asia	North Pacific
70°N	140-160	70-140	-----	340-25	330-340	185-330	160-185
65	140-165	70-140	-----	350-40	330-350	180-330	165-180
60	140-165	95-140	70-80	355-65	330-355	190-330	165-190
55	100-130	85-100	60-80	10-60	335-350	225-335	130-195
50	100-125	80-100	65-80	5-55	335-0	215-335	125-215
45	105-125	75-105	65-75	0-65	330-0	225-320	125-215
40	100-125	80-100	75-80	10-75	0-10	230-335	125-220
35	105-120	85-100	75-85	5-75	350-5	220-325	120-220
30	105-115	90-95	80-90	10-80	325-10	240-325	115-240
25	100-110	-----	80-85	15-80	325-15	240-325	110-240

TABLE 3. Estimated values of aerodynamic roughness parameter z_0 (cm) for indicated regions and seasons, as a function of geographic latitude Φ (deg)

Φ Dec-Feb	Western North America	Central North America	Eastern North America	North America	Europe-Africa	Asia (including USSR)
70°N	1.7	1.2	---	1.4	3.9	9.3
65	1.7	1.2	---	1.4	3.9	9.3
60	1.7	7.3	31	6.9	1.4	4.2
55	46	25	31	35	0.51	1.9
50	9.2	3.85	31	12	1.2	0.63
45	1.9	0.55	19	2.3	2.9	0.21
40	5.0	2.0	25	4.1	2.3	0.76
35	13	22	65	17	1.8	2.7
30	13	58	90	16	0.27	3.1
25	12	---	106	12	0.04	3.4
Mar-May						
70°N	4.2	1.2	---	1.9	4.7	11
65	4.2	1.2	---	1.9	4.7	11
60	4.2	8.4	34	8.9	3.2	7.3
55	59	29	34	42	2.2	5.0
50	25	12	34	27	4.0	1.8
45	12	5.2	34	13	7.5	0.67
40	14	7.6	47	13	4.1	1.5
35	16	29	81	22	2.2	3.5
30	18	77	111	21	0.30	3.8
25	15	---	124	15	0.041	4.1
Jun-Aug						
70°N	19	5.5	---	8.7	17	30
65	19	5.5	---	8.7	17	30
60	19	30	136	35	18	30
55	162	123	136	141	18	29
50	77	67	136	87	22	7.6
45	37	32	100	41	26	2.0
40	32	24	86	32	8.5	3.5
35	22	53	118	34	2.8	6.1
30	18	99	133	24	0.34	5.6
25	17	---	132	17	0.042	5.1

TABLE 3 (Continued)

Φ Sep-Nov	Western North America	Central North America	Eastern North America	North America	Europe-Africa	Asia (including USSR)
70°N	5.2	1.2	---	2.1	12	11
65	5.2	1.2	---	2.1	12	11
60	5.2	11	82	13	7.3	9.8
55	109	71	82	87	4.5	8.6
50	40	25	82	47	7.0	3.0
45	15	12	69	22	11	1.1
40	17	15	65	20	5.0	2.3
35	18	32	84	24	2.3	4.9
30	18	75	103	21	0.31	4.3
25	15	---	121	15	0.041	3.7

and crops at about 20 to 30°N with relatively small z_0-values, then to the woodland and coniferous forests of the temperate zone accompanied by relatively high z_0-values. Farther north the z_0-values decrease again, especially in America, due to lower vegetation and extended tundra regions.

In the Northern Hemisphere, there are significant differences in the latitudinal distribution of z_0 for the continental sections studied. In the low and middle latitudes of Europe and North Africa, extremely small z_0-values are due to extended low vegetation and desert areas, while lush vegetation in the same latitudes of North America and Asia causes relatively high z_0-values. At highest latitudes of Europe and Asia the roughness parameter is significantly larger than in North America owing to the differences in northern extent of coniferous and other forests.

The data in Table 4 demonstrate that there are significant regional contrasts between Western, Central, and Eastern North America, due to differences in characteristic vegetation types. The small z_0-values in the middle latitude of Central North America are the consequence of heavy crop acreage and low natural vegetation, while in the other parts of this continent forest acreage and other types of natural vegetation produce relatively high roughness parameters. These contrasts, however, become less in summer because of the luxuriance of crops in

TABLE 4. Regional distribution of estimated aerodynamic roughness parameter z_0 (cm) for indicated geographic latitude, longitude, and season over the North American continent.

Latitude	70°N	65	60	55	50	45	40	35	30	25
Longitude										
Dec-Feb										
65°W			31	31						
75	1.2	1.2	31	31	31	19	12			
85	1.2	1.2		25	25	2.5	2.0	56	106	
95	1.2	1.2	5.4	27	3.8	0.53	8.2	22	58	
105	1.2	1.2	7.3	37	5.9	1.0	13	10	12	12
115	1.2	1.2	7.3	46	9.2	1.0	13	13	12	
125	1.2	1.2	7.3	46	9.2					
135		1.2	7.4							
145	1.7	1.4								
155	1.7	1.7	1.7							
Mar-May										
65			34	34						
75	1.2	1.2	34	34	34	34	34			
85	1.2	1.2		29	29	13	7.3	71	124	
95	1.2	1.2	5.8	32	12	5.3	11	29	77	
105	1.2	1.2	8.4	45	17	7.9	15	14	15	15
115	1.2	1.2	8.4	59	25	12	15	16	15	
125	1.2	1.2	8.4	59	25					
135		1.2	8.4							
145	4.2	2.2								
155	4.2	4.2	4.2							
Jun-Aug										
65			136	136						
75	5.5	5.5	136	136	136	98	71			
85	5.5	5.5		123	123	44	28	102	132	
95	5.5	5.5	26	127	67	29	28	53	99	
105	5.5	5.5	30	146	72	34	28	22	17	17
115	5.5	5.5	30	162	77	37	28	22	17	
125	5.5	5.5	30	162	77					
135		5.5	30							
145	19	10								
155	19	19	19							

TABLE 4 (Continued)

	70°N	65	60	55	50	45	40	35	30	25
Sep-Nov										
65°W			82	82						
75	1.2	1.2	82	82	82	70	59			
85	1.2	1.2		71	71	31	15	73	121	
95	1.2	1.2	9.2	75	25	14	14	32	75	
105	1.2	1.2	11	93	32	13	18	16	15	15
115	1.2	1.2	11	109	40	16	18	18	15	
125	1.2	1.2	11	109	40					
135		1.2	11							
145	5.2	2.5								
155	5.2	5.2	52							

general, and especially that of the dominant crop of this continent, which is corn.

The seasonal trends of the computed roughness parameters reflect the phenological cycle. There is little seasonal change in and near tropical regions. However, crop growth and phenological sequences of vegetation height in middle and high latitudes cause roughness maxima in summer and minima in winter. The autumn-wilting of low-type vegetations, and winter snow covering them significantly affect the seasonal changes in roughness parameter.

2.1.3 Testings using Ratio of Wind Speed at Anemometer Level to Geostrophic Wind Speed

Before the above derived z_0-values are utilized for the computations of geostrophic drag coefficients and energy dissipation, it is desirable to demonstrate that the concept of estimating the effective aerodynamic roughness of land surfaces from vegetation cover is physically sound. This can be demonstrated with the aid of results obtained by Johnson (1962) concerning an "atmospheric boundary layer climatology," and also by computation of the ratio of wind speed at a given height above the ground to geostrophic wind speed at surface level. Lettau (1959) has shown that this ratio is a relatively direct measure of surface smoothness. Comparison between computed and observed wind data will provide a simple testing of the derived regional z_0-values in terms of climatological averages. Correspondingly, the angle α_0 formed by the surface wind and isobars is a simple measure of surface friction.

Johnson (1962), in an attempt to compare theoretical with observed wind spiral parameters, made an analysis of aerological kite data at four stations in the United States. In a special investigation Kung (1959) computed z_0-values for each of eight 45-degree segments at 0- to 100-mile radial distance from Drexel, Nebraska by the method described in Section 2.1.1, utilizing agricultural yearbooks of Nebraska and Iowa. The results are illustrated in Figure 1. Drexel, Nebraska was one of the sections analyzed by Johnson (1962). The z_0-values for the three other stations were directly interpolated from Table 4. Though it could hardly be expected that z_0-values, which were estimated on a large-scale basis, will satisfactorily apply to the analysis of single station data, tolerable agreement was found between the theoretical and derived values of the wind spiral parameters. Especially noteworthy is the following statement by Johnson (1962): "The topography of the land surrounding each site was examined in an attempt to discover any dependence of α_0 upon surface-wind direction, but no clear-cut relationship was discovered. For example, it was found that the Drexel station was located near the edge of a plateau, about a mile east of a rather steep drop-off to the Platte River Valley. However, no unusual behavior of the derived values of α_0 for westerly surface-wind at Drexel is evident." This is interesting, because it was also found that the aerodynamic roughness estimated from vegetation cover did not show an unusual behavior for westerly azimuths at Drexel; see Figure 1. It can be concluded that vegetation cover, rather than topography, represents the most efficient roughness structure on land areas.

Climatological means of the ratio V_A/V_g of wind speed at anemometer level V_A to geostrophic wind speed V_g can be used as a relatively direct and readily available measure of actual frictional effects. In combination with the computed ratio V_z/V_g, of wind speed V_z at any level z in the surface layer, to V_g, the ratio V_A/V_g will be used to test the validity of the continental roughness derived in the preceding section.

Meridional profiles of monthly means (for January and July) of wind speed at anemometer levels were derived from a study by Lauscher (1951) for the North American Continent, where a relatively dense and uniform network of climatological stations promised to produce relatively reliable and representative estimates. Utilizing computed continental values of 1000 mb geostrophic wind speed V_g (see Sections 2.2.1 and 2.2.2) a meridional profile of "observed" mean ratio V_A/V_g was obtained. This was compared with "computed" V_z/V_g ratios given by the conventional logarithmic wind profile

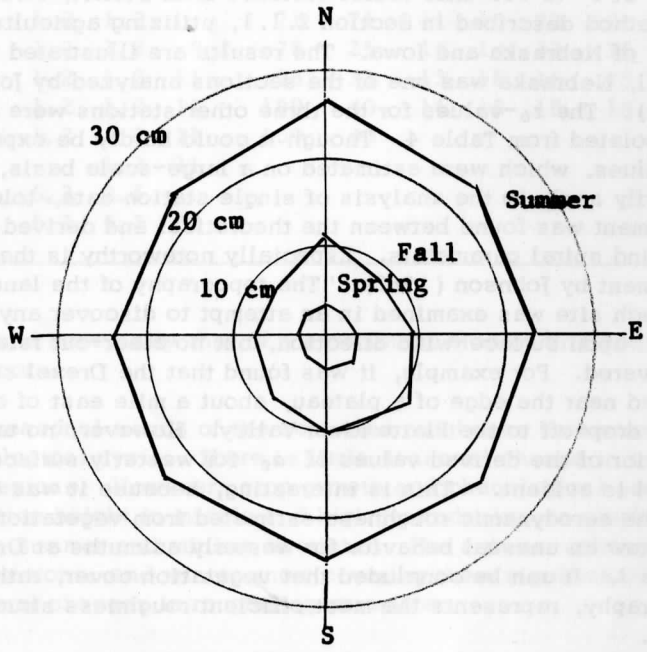

Fig. 1. Average aerodynamic roughness parameter z_0 (cm) of vegetation 0 to 100 miles radial distance from Drexel, Nebraska.

equation and the geostrophic drag coefficient C, of corresponding seasons and latitudes, i.e.,

$$V_z/V_g = 2.5\ C \log_e(1 + z/z_0) \qquad (2)$$

Because the actual anemometer level will vary from station to station, z was taken to be 400, 800, and 1600 cm to enclose its most probable range. The results are listed in Table 5 and illustrated in Fig. 2, as functions of geographic latitude. In view of the fact that Lauscher's (1951) climatological data are a synthesis of changing synoptic patterns at different weather stations and include diabatic effects, the comparison should be restricted to the average of January and July values. Then the agreement between ratios V_A/V_g and V_z/V_g is satisfactory and appears to support the representativeness of the continental roughness parameters. We notice that the ratios V_A/V_g tend to be lower in January and higher in July than corresponding ratios V_z/V_g, while these seasonal trends are fairly well eliminated in the averages of January and July values. This appears to reflect the seasonal variations of thermal stability in the surface layer. We also notice that these departures are more pronounced for latitudes of lower z_0-values and less for the latitudes of higher z_0-values. This may be related, at least to a certain extent, to differences in heat budget of the different vegetation cover. For example, Lenschow's (1962) airborne bolometer measurement of surface temperature over southern Wisconsin indicates that during daytime the surface temperature was highest over farm land, and lower over hilly woods. However, more experimental work is necessary to clarify the relationship between thermal stability and surface temperature variations.

While on land the thermal effects tend to be neutralized in the climatological mean values due to pronounced diurnal and annual cycles, persistent heating and cooling belts or regions exist over the oceans. Lettau (1959) pointed out that over the oceans the dependency of observed V_A/V_g ratios on geographic latitude will primarily reflect diabatic effects at the ocean/air interface.

The ratios V_A/V_g, (observed) and V_z/V_g (computed) were derived for the North Atlantic and Pacific Oceans, also using V_A-values from Lauscher (1951) and assuming for the oceans $z_0 = 0.1$ cm. This value was selected as a compromise figure after studying a fair amount of papers in the literature on oceanic roughness parameters. The references include Brocks (1959), Bryson (1962), Deacon (1953, 1962), Frost (1948), Haines and Bryson (1961), Munk (1941), Rossby (1936), Schooley (1961).

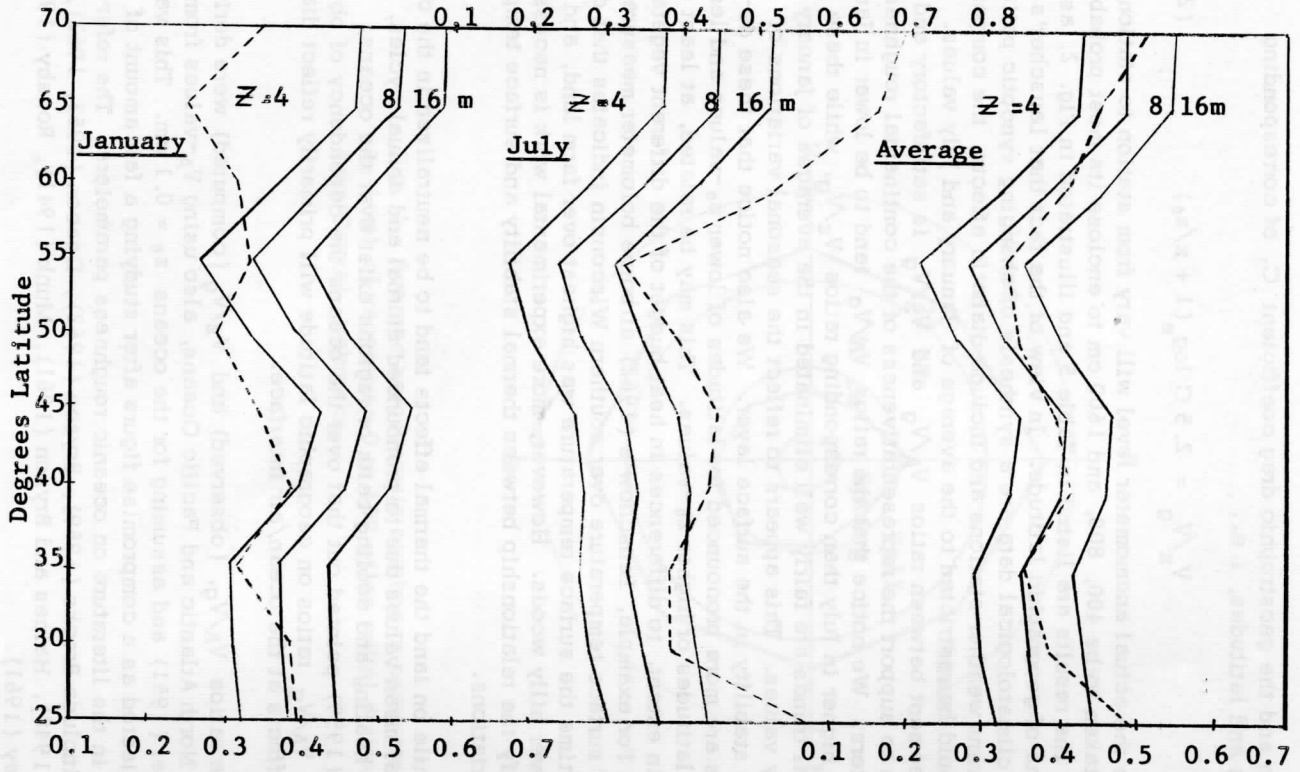

FIG. 2. Meridional profiles of ratio between wind speed at height z and geostrophic wind speed over the North American Continent. Climatologic means derived from Lauscher (1951) (dashed lines) in comparison with computed ratios for z = 4, 8, and 16m.

TABLE 5. Ratios of observed wind speed at anemometer level to 1000 mb geostrophic wind speed (V_A/V_g) using Lauscher's (1951) V_A-values, and computed ratios V_z/V_g at three levels z = 4m, 8m, and 16m over the North American Continent, as functions of geographic latitude Φ (deg).

	Φ	V_A/V_g	V_4/V_g	V_8/V_g	V_{16}/V_g
January	70°N	.369	.474	.532	.590
	65	.253	.470	.528	.585
	60	.317	.374	.437	.500
	55	.338	.263	.332	.402
	50	.291	.331	.394	.458
	45	.341	.427	.484	.541
	40	.384	.400	.460	.520
	35	.316	.308	.372	.437
	30	.386	.311	.375	.441
	25	.398	.323	.386	.449
July	70	.689	.379	.446	.514
	65	.655	.377	.444	.511
	60	.523	.275	.347	.420
	55	.325	.168	.237	.314
	50	.396	.198	.267	.341
	45	.447	.255	.325	.397
	40	.437	.273	.342	.412
	35	.387	.265	.334	.404
	30	.385	.287	.353	.421
	25	.568	.307	.371	.436
Average	70	.529	.427	.489	.552
	65	.454	.424	.486	.548
	60	.420	.325	.392	.460
	55	.332	.216	.285	.358
	50	.344	.265	.331	.400
	45	.394	.341	.405	.469
	40	.411	.337	.401	.466
	35	.352	.287	.353	.421
	30	.386	.299	.364	.431
	25	.483	.315	.379	.443

TABLE 6. Ratios of observed wind speed at anemometer level to 1000 mb geostrophic wind speed V/V_g using Lauscher's (1951) V_A-values, and computed ratios V_z/V_g at three anemometer levels z = 4m, 8m, and 16m over the North Atlantic and Pacific Oceans, as functions of geographic latitude Φ (deg). Averaged for January and July.

	Φ	V_A/V_g	V_4/V_g	V_8/V_g	V_{16}/V_g
North Atlantic	70°N	.582	.581	.630	.678
	65	.575	.578	.626	.675
	60	.605	.574	.622	.670
	55	.630	.568	.615	.663
	50	.543	.563	.610	.657
	45	.523	.562	.609	.661
	40	.692	.570	.617	.665
	35	.623	.565	.612	.659
	30	.806	.570	.618	.665
	25	.620	.559	.605	.652
North Pacific	70°N	----	.587	.636	.685
	65	----	.583	.632	.681
	60	----	.574	.622	.670
	55	.598	.576	.624	.673
	50	.444	.564	.611	.658
	45	.482	.563	.610	.657
	40	.618	.568	.616	.664
	35	.538	.561	.608	.655
	30	.651	.566	.613	.660
	25	.545	.558	.604	.651

Average values of observed and computed wind ratios for January and July are listed in Table 6, as functions of geographic latitude. The V_A, V_g ratios by Gordon (see Lettau, 1959) show a trend which is similar to that in Table 6 but with more pronounced deviations from V_z/V_g around 35°N. Due to the lack of a theory of diabatic boundary layer structure it is difficult to explain the pronounced departure of V_A/V_g from V_z/V_g at the lower-middle latitudes as effects of thermal stability. Furthermore, the tentative constant of $z_0 = 0.1$ for the ocean is uncertain. Only the order of magnitude of z_0 seems to be correct.

Notwithstanding the more complicated structure of the land surface and limitations imposed by available experimental information and statistical data in deriving continental roughness parameters as a function of phenological height of vegetation cover, the above derived results seem to indicate that these area-weighted mean log z_0-values are more realistic than the tentative constant assumed for oceanic z_0. Even so, all z_0-values presented in Tables 3 and 4 must be considered tentative.

2.2 Distributions and Seasonal Variations of Geostrophic Drag Coefficients and Energy Dissipation

2.2.1 Method and Data

Utilizing Lettau's (1961b) analytical tabulation of various parameters and coefficients of theoretical wind and stress spirals as unique-valued functions of the surface-Rossby number $\underline{Ro}_0 = V_{g,0}/z_0 f$, regression equations were established between log $\underline{Ro}_0$, the geostrophic drag coefficient C, and the angle formed by surface stress and surface geostrophic wind α_0 (in degrees):

$$C = 0.205/(\log_{10}\underline{Ro}_0 - 0.556) \qquad \pm 0.0004, \qquad (3)$$

and

$$\alpha_0 = -3.03 + 173.58/\log_{10}\underline{Ro}_0 \qquad \pm 0.19. \qquad (4)$$

These regression equations give satisfactory interpolations of C and α_0 in the range of log $\underline{Ro}_0$ from 4.5 to 9.5; the standard deviations for interpolation of C and α_0 are ± 0.0004 and ± 0.19 degrees, respectively. Lettau's (1961) energy dissipation equation

$$E = V_g \tau_0 \cos\alpha_0 = \rho C^2 V_g^3 \cos\alpha_0 \qquad (5)$$

was used to obtain the total energy dissipation rate in the boundary layer.

Daily data on the height of the 1000 mb isobaric surface during the eleven years from 1945 to 1955 over the Northern Hemisphere were used for the computations of V_g. The data were originally supplied by the United States Weather Bureau, and a card deck is in possession of the University of Wisconsin Department of Meteorology. The data was examined and months of suspicious data were eliminated. Seven to nine years' data were available for each month after the elimination of questionable cases. Monthly values of 1000 mb surface geostrophic

wind V_g, as averages of daily values, were computed for 360 points using a diamond-grid determined by the intersections of longitudes ending in 0 degrees, with latitudes ending in 5 degrees for the hemispheric belt extending from 25° to 70°N. The 1000 mb surface geostrophic wind, which is regarded as the geostrophic wind at the earth/air interface, is assumed to be independent of height in the entire boundary layer.

Continental and regional values of z_0 for each season are listed in Tables 3 and 4. The Coriolis parameter f is specified for particular latitudes. Monthly mean temperatures for latitudinal circles (5-degrees apart) over the Northern Hemisphere were adopted from Gentilli's (1958) tabulation to compute air density ρ for the different months and latitudes. Combining this information with the monthly values of 1000 mb surface geostrophic wind speed, the values of $\underline{Ro}_0$, C, α_0, and E were computed with the above regression equations and the energy dissipation equation.

All computations were performed by the CDC 1604 electronic computer of the University of Wisconsin Numerical Analysis Laboratory. A program by Hutchins (1960) was utilized for the computation of 1000-mb surface geostrophic wind speed. All other computations were programmed by the author.

2.2.2 Hemispheric Distributions and Seasonal Variations of Geostrophic Drag Coefficients and Energy Dissipation

Monthly values of 1000 mb surface geostrophic wind speed, geostrophic drag coefficient, and energy dissipation were written out by the CDC 1604 computer in detail for all available individual months during the period of 1945 to 1955 for five sections of the Northerm Hemisphere: (1) North America, (2) North Atlantic, (3) Europe-Africa, (4) Asia, including USSR, and (5) North Pacific. As indicated in Table 2, the first section was subdivided into Western, Central, and Eastern North America. The computer also computed the monthly means of those quantities and the standard deviation of monthly energy dissipation values.

"Monthly mean," hereafter, refers to the average of monthly values of all available years during the period of 1945 to 1955 for a particular month. The standard deviation is a measure of the year-to-year differences of the monthly value.

Monthly means of 1000 mb geostrophic wind speed and of geostrophic drag coefficient are listed for each month in Table 7, and monthly

means of energy dissipation and their standard deviations in Table 8. Those two tables illustrate the meridional profiles and the seasonal variation of the results over the North American Continent.

Seasonal means of V_g, C, E, and standard deviation of E for all eight area sections of the Northern Hemisphere were obtained by averaging the monthly means, for: (1) December through February (winter), (2) March through May (spring), (3) June through August (summer), and (4) September through November (fall). The resulting meridional profiles of V_g and C are listed in Tables 9 through 12, those of E and their standard deviations are shown in Tables 13 through 16.

Utilizing seasonal means of E and their standard deviations for area sections of the Northern Hemisphere, seasonal and annual zonal means for the whole Northern Hemisphere were calculated from 25°N to 70°N; see Table 17. In calculating zonal means, supplementary data were used which covered the areas between the sections specified in Table 2. In the supplementary computation, a roughness value of $z_0 = 0.014$ cm (as obtained for the antartic continent by Dalrymple, Lettau, and Wallaston (1963)) was tentatively used for Greenland. The values for the whole North American Continent were used in calculating zonal means, instead of values for western, central, and eastern parts of this continent.

In the discussion of the results presented in Tables 7 through 16, it should be remembered that the latitudinal distribution of the geostrophic drag coefficient is determined by that of the surface-Rossby number which in turn depends on the three external parameters V_g, z_0, and f. The parameter f is a mathematical function of geographic latitude; small f-value in lower latitudes tends to produce small C-values, and the large f-value in higher latitudes tends to give large C-values. The parameter V_g is generally small at low latitudes, increases at middle latitudes, and again decreases at high latitudes. In the summer, the relatively low V_g-values of middle latitudes obscure this trend in Europe and Asia. A small V_g tends to produce a large C, and vice versa. Over the oceans, where z_0 is assumed to be constant, the latitudinal distribution of C is determined by those of V_g and f. C is relatively large near polar regions in the North Atlantic and Pacific due to small V_g- and large f-values. Over middle and lower latitudes of the oceans, the latitudinal distribution of C shows no significant variation due to roughly parallel trends in V_g and f. Also, the difference between near polar and other oceanic latitudes is very small; C ranges only between 0.0270 and 0.0285. In contrast to conditions over the oceans, it is found that over land z_0 is the decisive factor

TABLE 7. North American Continent: Computed monthly means of geostrophic wind speed at 1000 mb surface V_g (cm/sec) and of geostrophic drag coefficient C (unit of 10^{-4}), as functions of geographic latitude Φ (deg). 1945-1955.

Φ		Dec	Jan	Feb	Mar	Apr	May	Jun	Jul	Aug	Sep	Oct	Nov
70°N	V_g	928	934	904	923	879	787	748	694	734	767	927	1019
	C	334	334	335	342	343	346	391	393	392	349	344	342
65	V_g	950	1017	999	974	931	803	686	708	784	843	943	984
	C	332	331	331	340	341	345	393	392	388	346	343	342
60	V_g	1234	1211	1188	1124	1025	911	821	780	850	1000	1119	1212
	C	367	367	368	377	379	383	435	437	434	393	389	387
55	V_g	1152	1182	1097	1061	972	846	768	769	818	978	1078	1167
	C	420	419	422	430	433	439	500	500	496	464	460	456
50	V_g	1439	1473	1383	1392	1307	1164	1112	1000	1019	1153	1182	1424
	C	374	373	375	402	404	408	456	460	459	428	427	420
45	V_g	1362	1388	1288	1269	1147	1032	955	874	885	1059	1136	1326
	C	330	330	331	379	382	385	427	431	430	401	399	394
40	V_g	1012	1054	1039	1108	1087	993	963	824	765	867	876	1001
	C	349	348	349	378	379	382	414	420	423	401	401	396
35	V_g	1192	1163	1165	1192	1136	1062	968	832	803	946	926	1118
	C	381	382	382	390	392	394	412	418	419	401	401	395
30	V_g	971	980	1019	1113	1106	1054	968	818	790	858	890	976
	C	382	382	381	387	387	388	396	401	403	394	393	390
25	V_g	1023	1006	1081	1136	1154	1063	1039	880	784	916	949	1050
	C	368	368	366	371	370	373	376	381	385	376	375	372

TABLE 8. North American Continent: Computed monthly means and standard deviation of energy dissipation E (watts/m^2), as functions of geographic latitude Φ (deg). 1945-1955.

Φ	Dec	Jan	Feb	Mar	Apr	May	Jun	Jul	Aug	Sep	Oct	Nov
70°N	1.16	1.20	1.08	1.18	1.00	.70	.73	.58	.69	.65	1.15	1.57
	±.23	±.22	±.16	±.18	±.21	±.081	±.14	±.080	±.21	±.098	±.19	±.30
65	1.21	1.50	1.42	1.34	1.15	.72	.56	.60	.81	.83	1.18	1.40
	±.23	±.34	±.34	±.16	±.22	±.068	±.092	±.11	±.19	±.16	±.16	±.38
60	3.09	3.07	2.88	2.47	1.81	1.27	1.13	.98	1.24	1.74	2.43	3.17
	±.37	±1.09	±1.08	±.75	±.33	±.30	±.21	±.29	±.29	±.44	±.29	±.59
55	3.18	3.52	2.76	2.53	1.92	1.25	1.14	1.15	1.37	2.17	2.86	3.73
	±.84	±1.16	±.47	±.46	±.33	±.13	±.17	±.23	±.27	±.65	±.48	±.76
50	4.93	5.41	4.46	5.01	4.07	2.88	2.97	2.19	2.30	3.00	3.29	5.74
	±.80	±1.49	±1.00	±1.01	±.65	±.53	±.57	±.49	±.38	±.50	±.53	±.63
45	3.27	3.54	2.79	3.34	2.47	1.80	1.67	1.28	1.34	2.05	2.56	4.07
	±.53	±1.01	±.38	±.52	±.59	±.40	±.26	±.16	±.25	±.27	±.41	±.57
40	1.47	1.66	1.57	2.18	2.05	1.55	1.61	1.02	.83	1.13	1.17	1.73
	±.33	±.36	±.20	±.35	±.48	±.26	±.20	±.15	±.10	±.25	±.24	±.25
35	2.78	2.61	2.56	2.82	2.45	1.98	1.61	1.03	.94	1.45	1.37	2.36
	±.74	±.73	±.38	±.40	±.52	±.29	±.27	±.13	±.13	±.37	±.29	±.30
30	1.49	1.54	1.69	2.23	2.18	1.87	1.49	.92	.83	1.03	1.15	1.53
	±.45	±.47	±.32	±.36	±.43	±.21	±.21	±.17	±.13	±.18	±.13	±.36
25	1.61	1.58	1.87	2.21	2.32	1.78	1.68	1.05	.77	1.15	1.33	1.78
	±.49	±.66	±.43	±.62	±.79	±.32	±.25	±.23	±.25	±.19	±.51	±.60

TABLE 9. December-through-February-means of geostrophic wind speed at 1000 mb surface V_g (cm/sec) and of geostrophic drag coefficient C (unit of 10^{-4}) for indicated areas, as functions of geographic latitude Φ (deg). 1945-1955.

Φ		Western North America	Central North America	Eastern North America	North America	Atlantic Ocean	Europe-Africa	Asia (including USSR)	Pacific Ocean
70°N	V_g	1011	896	----	922	1294	1038	964	1075
	C	337	331	----	334	276	357	385	279
65	V_g	1167	945	----	988	1342	1276	1074	1213
	C	333	329	----	331	275	351	381	277
60	V_g	1499	1127	1176	1211	1523	1161	1206	1505
	C	327	371	417	367	273	328	353	273
55	V_g	1124	1011	1199	1144	1558	1014	1022	1324
	C	431	412	413	420	271	308	336	274
50	V_g	1445	1387	1610	1432	1771	1260	1174	1765
	C	367	344	401	374	269	320	308	268
45	V_g	1465	1191	1558	1346	1693	1083	1089	1699
	C	324	303	384	330	268	341	287	268
40	V_g	1023	1045	1050	1035	1223	968	865	1349
	C	354	332	403	349	271	336	314	270
35	V_g	1196	1164	1147	1173	1329	878	987	1443
	C	373	390	430	382	268	331	337	267
30	V_g	976	1073	935	990	867	696	868	931
	C	374	423	446	382	273	293	340	272
25	V_g	1037	----	1035	1037	980	735	876	975
	C	367	----	442	367	268	259	338	268

TABLE 10. March-through-May means of geostrophic wind speed at 1000 mb surface V_g (cm/sec) and of geostrophic drag coefficient C (unit of 10^{-4}) for indicated regions, as functions of geographic latitude Φ (deg.) 1945-1955.

Φ		Western North America	Central North America	Eastern North America	North America	Atlantic Ocean	Europe-Africa	Asia (including USSR)	Pacific Ocean
70°N	V_g	956	837	----	863	1055	943	860	947
	C	362	333	----	344	280	366	393	281
65	V_g	918	892	----	903	1145	1059	933	990
	C	363	331	----	342	278	362	389	280
60	V_g	1184	965	1086	1020	1216	945	978	1337
	C	354	380	423	380	276	353	375	275
55	V_g	910	1001	1006	960	1214	776	888	1073
	C	451	418	424	434	275	347	365	277
50	V_g	1241	1367	1318	1288	1491	897	922	1533
	C	403	377	412	405	271	357	337	271
45	V_g	1112	1123	1302	1149	1479	842	980	1536
	C	380	356	409	382	270	374	311	269
40	V_g	1166	1010	880	1063	1088	802	763	1188
	C	380	366	433	380	273	356	332	271
35	V_g	1181	1143	1003	1130	1209	651	848	1208
	C	381	401	445	392	270	342	347	270
30	V_g	1197	1070	900	1031	828	700	772	824
	C	379	434	457	387	274	295	348	273
25	V_g	1118	----	812	1118	829	738	692	947
	C	371	----	459	371	271	259	349	269

TABLE 11. June-through-August-means of geostrophic wind speed at 1000 mb surface V_g (cm/sec) and of geostrophic drag coefficient C (unit of 10^{-4}) for indicated regions, as functions of geographic latitude Φ (deg). 1945-1955.

Φ		Western North America	Central North America	Eastern North America	North America	Atlantic Ocean	Europe-Africa	Asia (including USSR)	Pacific Ocean
70°N	V_g	701	732	----	725	834	758	698	718
	C	420	377	----	392	284	413	438	286
65	V_g	630	746	----	726	825	763	767	738
	C	423	376	----	391	283	411	433	285
60	V_g	929	777	918	817	949	755	697	968
	C	406	431	491	435	280	412	435	280
55	V_g	706	791	871	785	1053	674	660	842
	C	511	491	491	499	277	416	435	281
50	V_g	1118	1014	942	1044	1161	692	686	1151
	C	450	448	484	458	275	419	383	275
45	V_g	925	856	1010	905	1117	604	730	1086
	C	424	421	462	429	274	427	342	275
40	V_g	1053	683	608	851	786	704	717	802
	C	411	416	474	419	278	380	354	278
35	V_g	1071	787	629	868	807	575	753	928
	C	394	437	483	416	276	351	365	274
30	V_g	936	944	625	859	683	744	750	804
	C	388	450	482	400	277	296	359	274
25	V_g	901	----	647	901	781	732	714	884
	C	381	----	472	381	272	259	353	270

TABLE 12. September-through-November-means of geostrophic wind speed at 1000 mb surface V_g (cm/sec) and of geostrophic drag coefficient C (unit of 10^{-4}) for indicated regions, as functions of geographic latitude Φ (deg). 1945-1955.

Φ		Western North America	Central North America	Eastern North America	North America	Atlantic Ocean	Europe-Africa	Asia (including USSR)	Pacific Ocean
70°N	V_g	993	879	----	905	1193	993	900	1019
	C	367	332	----	345	278	393	394	280
65	V_g	935	909	----	924	1216	1142	994	994
	C	368	327	----	344	277	387	389	280
60	V_g	1276	1041	1169	1110	1325	1115	1027	1323
	C	358	386	456	390	275	371	383	274
55	V_g	985	1053	1180	1074	1393	939	972	1183
	C	474	452	453	460	273	361	379	276
50	V_g	1183	1317	1347	1253	1549	1054	963	1540
	C	421	401	445	425	270	368	348	270
45	V_g	1178	1136	1286	1174	1451	887	979	1534
	C	386	379	436	398	270	384	321	269
40	V_g	992	861	802	915	961	785	778	1072
	C	391	392	450	399	275	362	342	273
35	V_g	1041	984	932	996	1038	616	906	1119
	C	388	410	449	399	272	345	355	271
30	V_g	881	1014	855	908	785	626	807	792
	C	388	435	457	392	274	298	350	274
25	V_g	971	----	935	971	867	678	751	885
	C	374	----	451	374	270	260	344	270

TABLE 13. December-through-February-means of energy dissipation E (watts/m^2) and standard deviation of E, as functions of geographic latitude Φ (deg). 1945-1955.

Φ	Western North America	Central North America	Eastern North America	North America	Atlantic Ocean	Europe-Africa	Asia (including) USSR)	Pacific Ocean
70°N	1.62	1.04	----	1.14	2.28	1.96	1.72	1.39
	±.66	±.21	----	±.20	±.70	±.82	±.51	±.66
65	2.40	1.19	----	1.37	2.44	3.31	2.26	1.90
	±.92	±.26	----	±.30	±.57	±.92	±.42	±.81
60	4.17	2.48	3.54	3.01	2.80	2.19	2.76	3.37
	±1.12	±.74	±1.57	±.85	±.66	±.75	±.72	±1.10
55	3.19	2.17	3.58	3.15	3.66	1.37	1.50	2.22
	±1.52	±.65	±1.54	±.82	±1.16	±.75	±.31	±.38
50	4.93	3.92	7.95	4.93	5.05	2.56	1.94	4.96
	±1.35	±1.29	±1.88	±1.10	±1.03	±.76	±.69	±.84
45	4.09	1.92	6.61	3.20	4.34	1.82	1.32	4.32
	±1.11	±.62	±2.18	±.64	±1.15	±.55	±.34	±.76
40	1.57	1.48	2.12	1.57	1.64	1.42	.76	2.15
	±.39	±.34	±.46	±.30	±.41	±.47	±.21	±.41
35	2.71	2.72	3.10	2.65	2.05	.88	1.28	2.56
	±.70	±.78	±.97	±.62	±.70	±.30	±.40	±.64
30	1.46	2.41	1.80	1.57	.59	.34	.86	.70
	±.39	±.67	±.73	±.41	±.26	±.072	±.22	±.16
25	1.68	----	2.37	1.68	.79	.31	.95	.77
	±.53	----	±1.10	±.53	±.25	±.11	±.39	±.19

TABLE 14. March-through-May-means of energy dissipation E (watts/m^2) and standard deviation of E, as functions of geographic latitude Φ (deg). 1945-1955.

Φ	Western North America	Central North America	Eastern North America	North America	Atlantic Ocean	Europe-Africa	Asia (including USSR)	Pacific Ocean
70°N	1.46	.82	----	.96	1.27	1.49	1.21	.91
	±.40	±.12	----	±.15	±.36	±.51	±.20	±.28
65	1.33	.96	----	1.07	1.54	2.09	1.52	1.03
	±.33	±.13	----	±.15	±.34	±.58	±.36	±.35
60	2.61	1.56	2.77	1.85	1.76	1.33	1.70	2.29
	±.88	±.38	±.92	±.46	±.44	±.40	±.58	±.61
55	1.76	1.99	2.14	1.90	1.74	.72	1.12	1.21
	±.45	±.40	±.60	±.31	±.44	±.39	±.18	±.21
50	3.53	4.28	4.74	3.99	3.02	1.12	1.09	3.20
	±.81	±1.26	±1.41	±.73	±.70	±.36	±.21	±.39
45	2.32	2.09	4.29	2.54	2.90	.98	1.09	3.18
	±.69	±.52	±1.08	±.50	±.80	±.17	±.17	±.76
40	2.55	1.59	1.52	1.93	1.17	.80	.57	1.48
	±.62	±.32	±.56	±.36	±.23	±.33	±.12	±.31
35	2.65	2.66	2.28	2.42	1.59	.39	.86	1.52
	±.72	±.75	±.57	±.40	±.50	±.15	±.29	±.30
30	2.68	2.49	1.64	2.09	.53	.35	.62	.50
	±.60	±.80	±.48	±.33	±.18	±.16	±.12	±.16
25	2.10	----	1.18	2.10	.49	.31	.46	.70
	±.58	----	±.26	±.58	±.13	±.074	±.10	±.11

TABLE 15. June-through-August-means of energy dissipation E (watts/m^2) and standard deviation of E, as functions of geographic latitude Φ (deg). 1945-1955

Φ	Western North America	Central North America	Eastern North America	North America	Atlantic Ocean	Europe-Africa	Asia (including USSR)	Pacific Ocean
70°N	.69	.65	----	.67	.58	.85	.72	.38
	±.20	±.17	----	±.14	±.17	±.22	±.18	±.17
65	.52	.66	----	.66	.55	.85	.92	.40
	±.17	±.14	----	±.13	±.17	±.28	±.15	±.14
60	1.50	.94	1.95	1.11	.78	.81	.70	.85
	±.52	±.19	±.53	±.26	±.15	±.22	±.17	±.25
55	.94	1.25	1.66	1.22	1.04	.62	.58	.56
	±.25	±.41	±.41	±.22	±.21	±.30	±.094	±.15
50	3.00	2.20	2.03	2.49	1.36	.65	..53	1.34
	±.63	±.47	±.62	±.48	±.24	±.29	±.15	±.30
45	1.52	1.18	2.30	1.43	1.21	.43	.50	1.11
	±.41	±.26	±.56	±.22	±.29	±.10	±.085	±.19
40	2.11	.61	.54	1.15	.43	.55	.51	.46
	±.27	±.15	±.22	±.15	±.10	±.15	±.11	±.079
35	2.04	.99	.59	1.19	.47	.27	.61	.68
	±.42	±.25	±.18	±.18	±.14	±.14	±.11	±.13
30	1.35	1.76	.60	1.08	.28	.42	.58	.45
	±.27	±.46	±.27	±.17	±.068	±.16	±.11	±.15
25	1.16	----	.63	1.16	.40	.30	.49	.56
	±.24	----	±.27	±.24	±.099	±.098	±.12	±.13

TABLE 16. September-through-November-means of energy dissipation E (watts/m^2) and standard deviation of E, as functions of geographic latitude Φ (deg). 1945-1955.

Φ	Western North America	Central North America	Eastern North America	North America	Atlantic Ocean	Europe-Africa	Asia (including USSR)	Pacific Ocean
70°N	1.73	0.96	----	1.12	1.78	1.96	1.38	1.15
	±.58	±.18	----	±.20	±.61	±.76	±.23	±.35
65	1.43	1.01	----	1.14	1.78	2.82	1.83	1.10
	±.44	±.22	----	±.24	±.24	±1.22	±.49	±.46
60	3.24	1.99	3.76	2.45	2.20	2.36	1.97	2.29
	±.83	±.42	±1.20	±.44	±.52	±.72	±.41	±.96
55	2.40	2.69	3.78	2.92	2.52	1.42	1.56	1.60
	±.51	±.88	±1.03	±.63	±.80	±.78	±.33	±.49
50	3.37	4.25	5.51	4.01	3.33	2.02	1.32	3.28
	±.89	±.96	±1.67	±.56	±.64	±.99	±.27	±.60
45	2.89	2.42	4.51	2.89	2.68	1.26	1.15	3.27
	±.90	±.53	±1.33	±.42	±.52	±.44	±.29	±.98
40	1.65	1.14	1.22	1.34	.83	.80	.64	1.15
	±.45	±.30	±.49	±.25	±.16	±.36	±.16	±.35
35	1.89	1.75	1.82	1.73	1.01	.36	1.08	1.25
	±.38	±.38	±.74	±.32	±.25	±.16	±.29	±.40
30	1.14	2.12	1.40	1.24	.42	.25	.72	.43
	±.35	±.67	±.56	±.22	±.082	±.071	±.17	±.12
25	1.42	----	1.78	1.42	.54	.24	.59	.58
	±.43	----	±.54	±.43	±.11	±.071	±.18	±.083

TABLE 17. Seasonal and annual zonal means of energy dissipation E (watts/m^2) and standard deviation of E, as functions of geographic latitude Φ (deg). 1945-1955.

Φ	Dec - Feb	Mar - May	Jun - Aug	Sep - Nov	Annual Mean
70°N	1.62	1.08	.62	1.32	1.16
	±.47	±.23	±.16	±.31	±.29
65	1.97	1.35	.73	1.58	1.14
	±.45	±.30	±.15	±.45	±.34
60	2.83	1.76	.84	2.18	1.90
	±.78	±.51	±.20	±.50	±.50
55	2.29	1.32	.74	1.90	1.56
	±.70	±.27	±.22	±.50	±.40
50	3.78	2.42	1.18	2.63	2.50
	±.88	±.45	±.27	±.53	±.53
45	3.05	2.19	.94	2.28	2.12
	±.70	±.50	±.18	±.55	±.48
40	1.41	1.10	.54	.87	.98
	±.32	±.23	±.10	±.22	±.22
35	1.89	1.31	.62	1.10	1.23
	±.54	±.32	±.13	±.30	±.32
30	.76	.67	.51	.55	.62
	±.29	±.17	±.13	±.13	±.18
25	.80	.59	.48	.56	.61
	±.26	±.12	±.13	±.13	±.16
*	1.94	1.33	.70	1.40	1.34
	±.51	±.30	±.16	±.34	±.33

*Weighted mean (25° - 70°N). Averaged by cos Φ as weighting factor.

of the C-distribution, since z_0 may vary by several powers of ten. All continental C-values are far greater than oceanic values; they range between 0.030 and 0.050. In general, over land, C has larger values in temperate to high latitudes, and its latitudinal distribution in each continental section responds to the characteristic z_0-distribution which, in turn, reflects the latitudinal sequence of vegetation cover.

Examining the energy dissipation with the aid of equation (5), it is obvious that C and V_g are the major factors which determine the distribution and seasonal variations of E-values. The factors ρ and $\cos \alpha_0$ produce only secondary effects. Due to the combination of large V_g and C, E-values are relatively large for middle latitudes of the continents in comparison to E-values at lower and higher latitudes. Over the oceans, E-values are distinctly large at middle latitudes due to the large V_g. Consequently, the latitudinal distribution of zonal means of E also shows the peak values around 50°N, decreasing both toward the north and south. Figures 3 through 9 illustrate the results; monthly and seasonal E-values of the sections and the whole Northern Hemisphere are plotted as functions of geographic latitude.

While continental C-values are distinctly larger than the oceanic values, there is no corresponding continent-ocean contrast in the E-values. Instead, the North American Continent and the North Atlantic and Pacific Oceans represent one group which is characterized by relatively high E-values, while the Europe-African and the Asian Continents represent one group of lower E-values. The contrast between those two groups is especially striking at middle latitudes. Fig. 3 and 4 illustrate the meridional profiles of E-values for the five sections of the Northern Hemisphere during winter and summer. The large E-values for North America are due to generally large V_g and C on this continent. Noticeably high E-values over the oceans, in contrast to E of the Europe-African and Asian Continents, are due to large V_g over the ocean. A close relation between the E-distributions of the North Atlantic and Pacific areas may be noted.

Regional contrasts of E-values for the Western, Central and Eastern North American sections are also apparent, though the latitudinal trends are similar for all three subdivisions of the continent. The extreme E-value at middle latitude of Eastern North America during the winter (of about 8 watts/m^2) is particularly impressive; it is caused by the combination of large C and V_g. Other regional contrasts are due either to differences in C or V_g, or to combined effect of C and V_g. Fig. 5 and 6 illustrate the regional contrasts of E over North America for January and July.

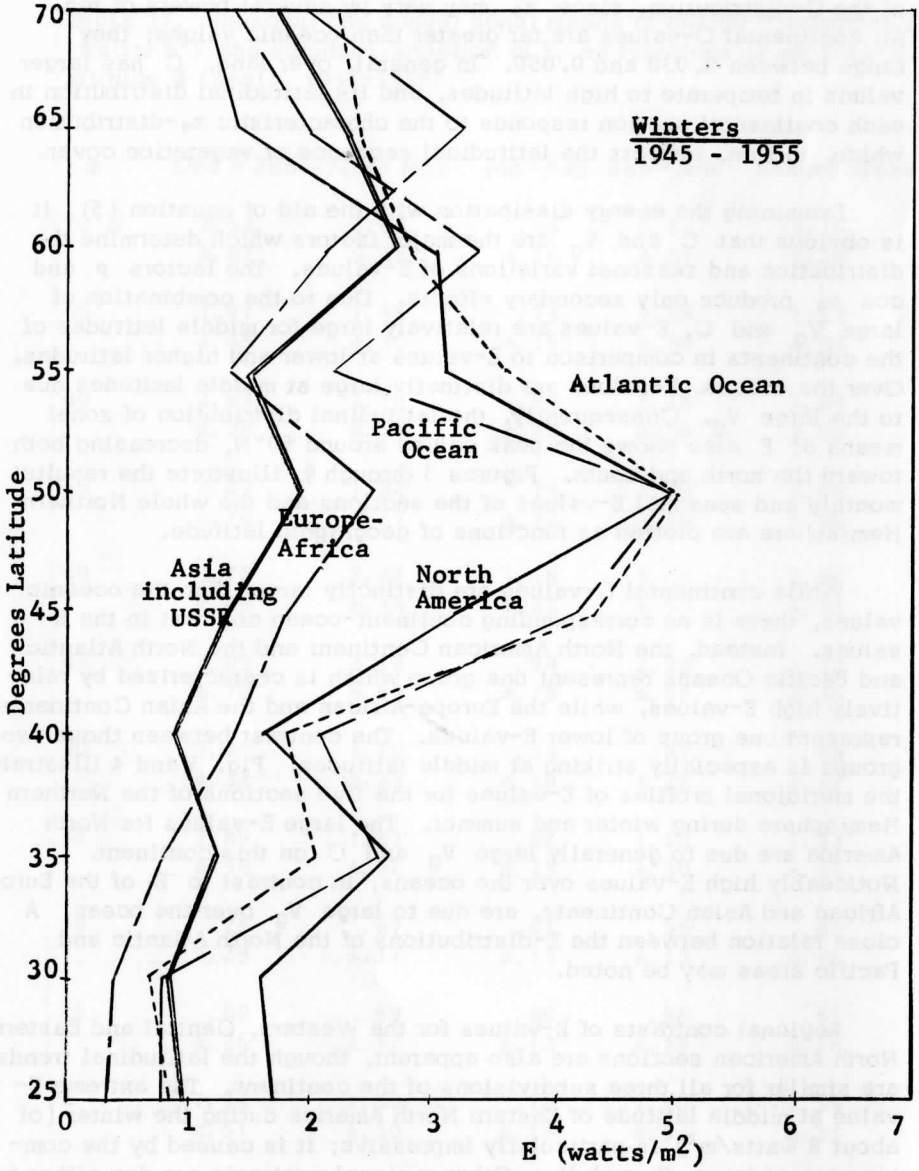

FIGURE 3. Area contrast of mean seasonal energy dissipation E over the Northern Hemisphere. (December through February).

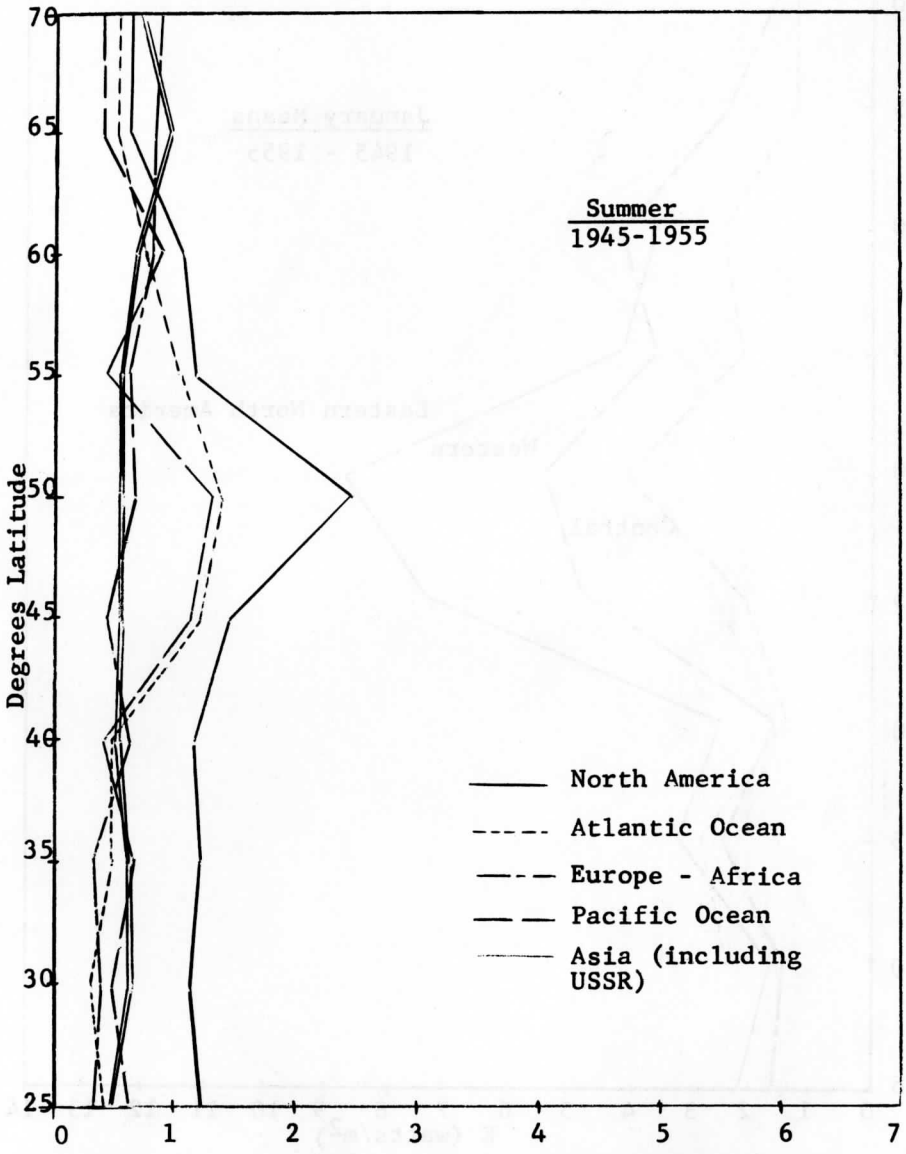

FIGURE 4. Area contrast of mean seasonal energy dissipation E over the Northern Hemisphere (June through August).

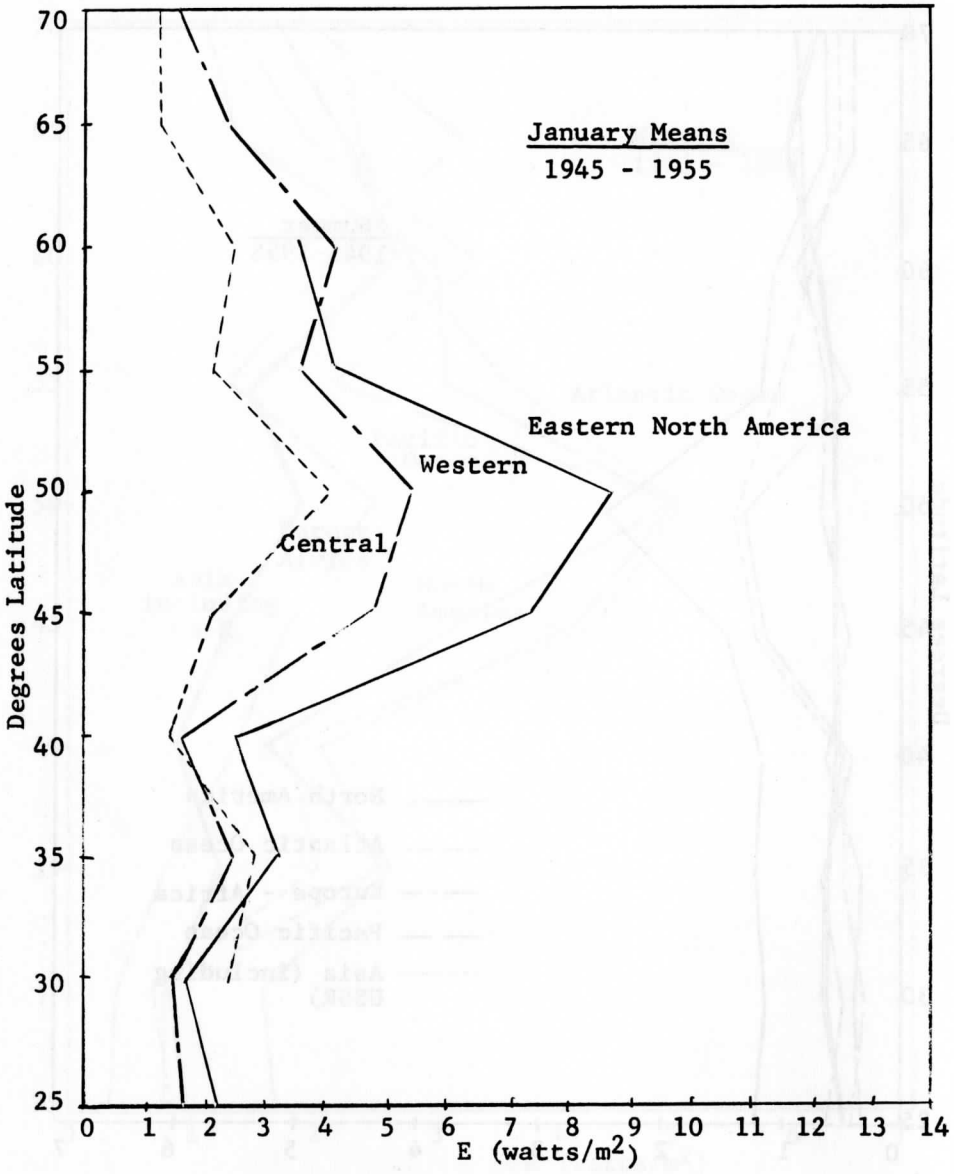

FIGURE 5. Regional contrast of January energy dissipation E over the North American continent.

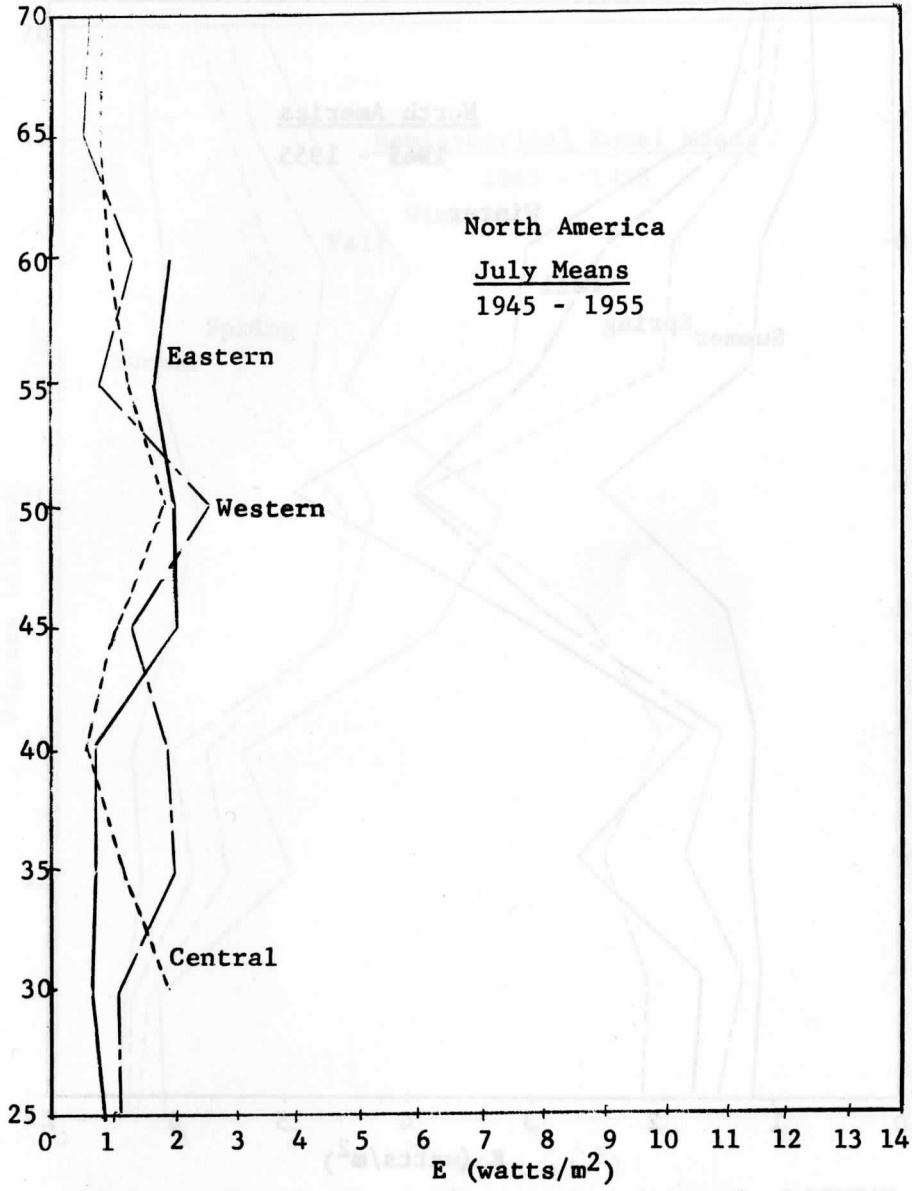

FIGURE 6. Regional contrast of July energy dissipation over the North American Continent.

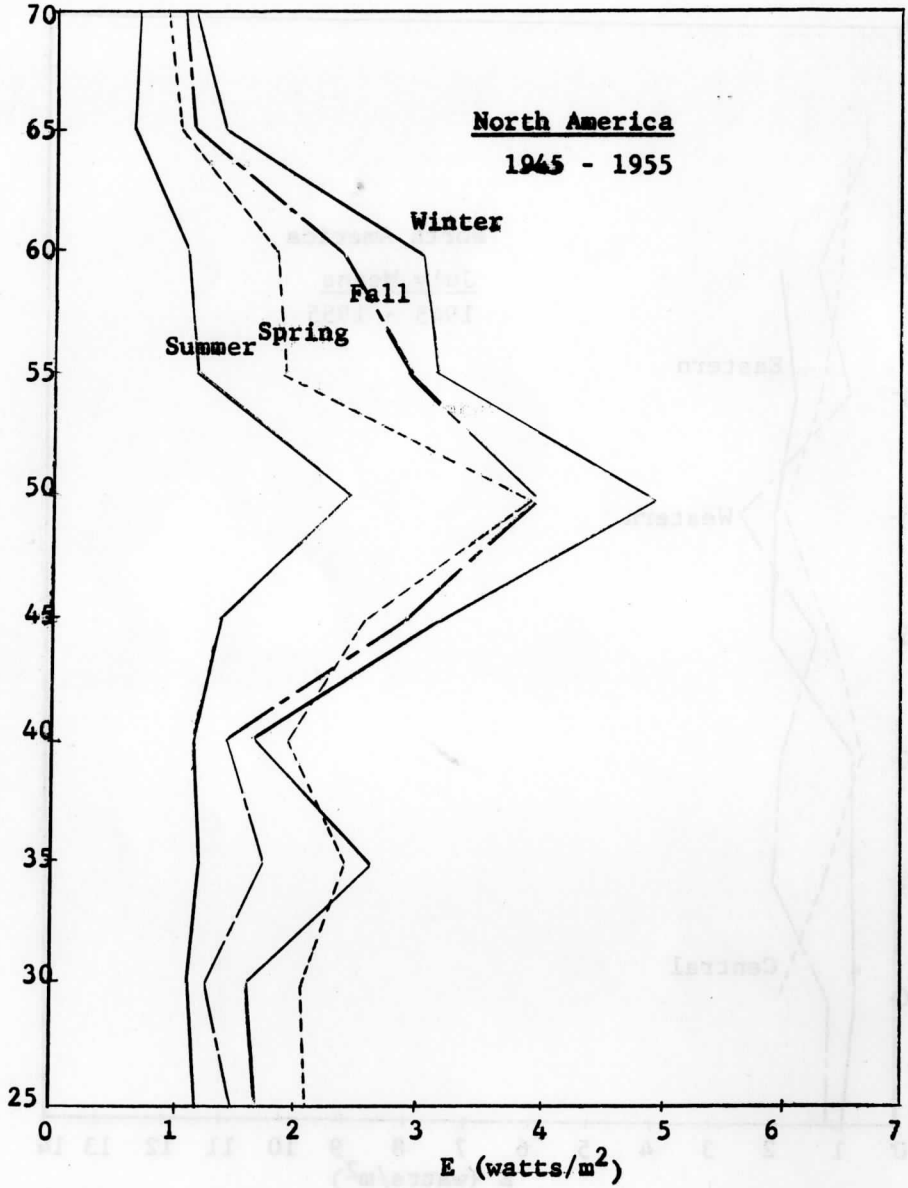

FIGURE 7. Seasonal mean energy dissipation E over the North American Continent.

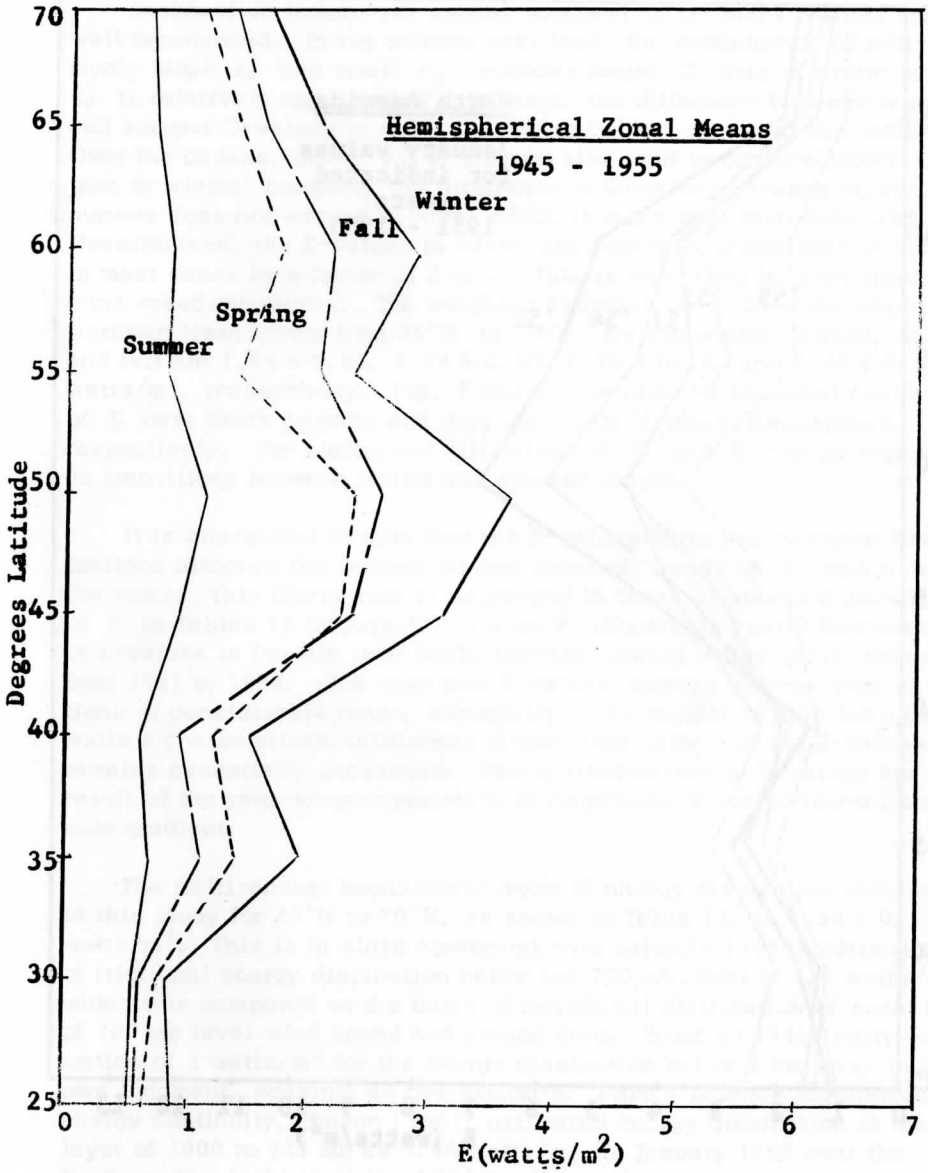

FIGURE 8. Seasonal mean energy dissipation E over the Northern Hemisphere.

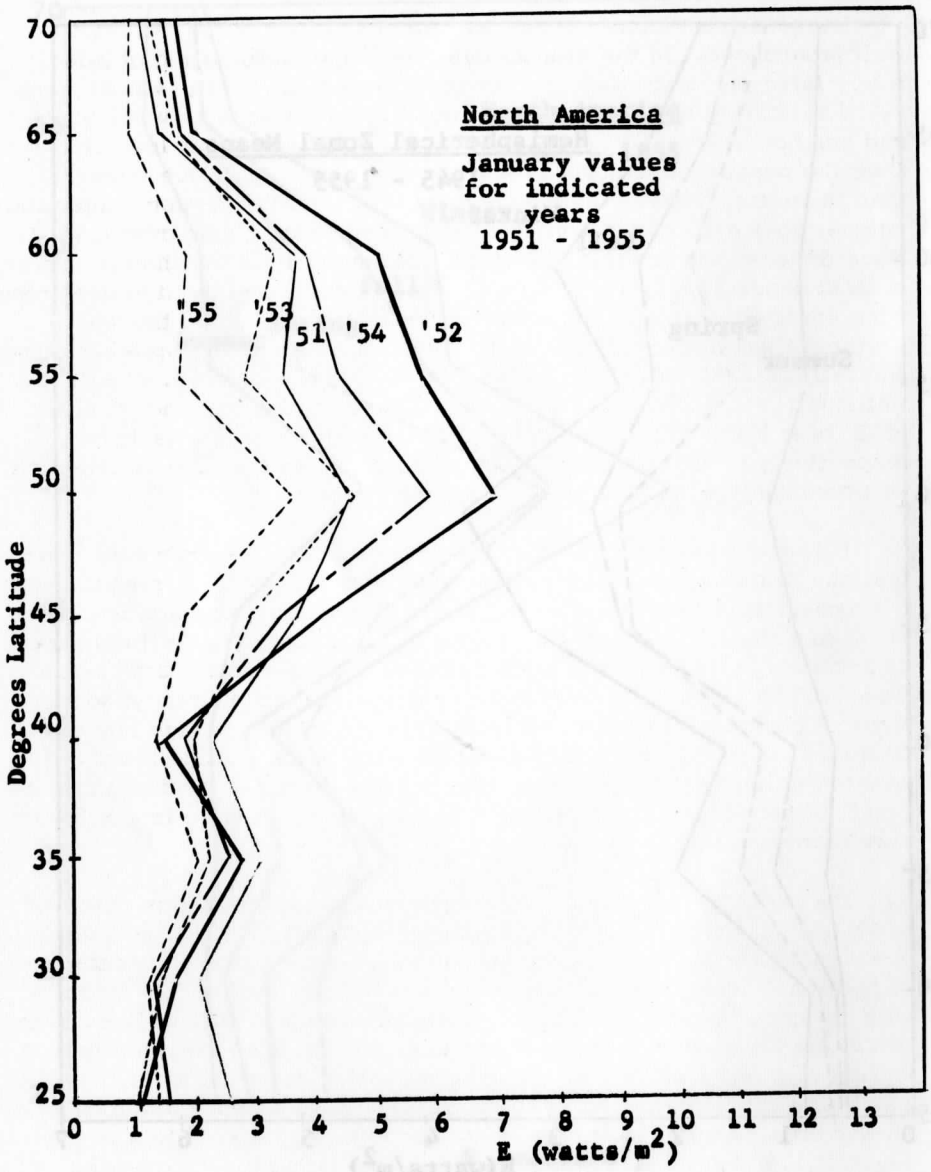

FIGURE 9. Year to year contrast in January energy dissipation E over the North American Continent from 1951 to 1955.

Seasonal variations (or annual marches) of C- and E-values are well pronounced. In the summer over land, the combination of relatively large z_0 and small V_g produces larger C than in winter when z_0 is relatively small and V_g is large; the difference between winter and summer C-values is about 0.0050 to 0.1000 except at low latitudes. Over the oceans, small V_g in summer also tend to produce larger C than in winter; however, the difference of C-values between winter and summer does not exceed 0.0008, which is much less than over land. Nevertheless, the E-values in winter are generally larger than in summer; in most cases by a factor of 2 or 3. This is explained by high geostrophic wind speeds in winter. The weighted averages of E over the whole Northern Hemisphere from 25°N to 70°N for the winter, spring, summer, and fall are 1.94 ± 0.51, 1.33 ± 0.30, 0.70 ± 0.16, and 1.40 ± 0.33 watts/m^2, respectively. Fig. 7 and 8 illustrate the seasonal contrast of E over North America and over the whole Northern Hemisphere, respectively. The spring and fall values of C and E can be regarded as transitions between winter and summer values.

It is interesting to note that the E-values show year-to-year fluctuations although the latitudinal and seasonal trends of E remain about the same. This fluctuation is expressed in terms of standard deviation of E in Tables 13 through 17. Figure 9 illustrates yearly fluctuations of E-values in January over North America, during a five years' period from 1951 to 1955. One sees that E-values undergo year-to-year variations of considerable range, especially in the middle to high latitudes, while a characteristic latitudinal distribution pattern of the E-values remains essentially unchanged. Yearly fluctuations of E-values are the result of the year-to-year variation in magnitude of the horizontal pressure gradient.

The multi-annual hemispheric mean of energy dissipation obtained in this study for 25°N to 70°N, as shown in Table 17, is 1.34 ± 0.33 watts/m^2. This is in close agreement with Lettau's (1954) estimation of frictional energy dissipation below the 700 mb level of 1.4 watts/m^2, which was computed on the basis of meridional distribution of zonal means of 700 mb level wind speed and ground drag. Brunt's (1941) early estimation of 3 watts/m^2 for the energy dissipation below 1 km was, in his own judgment, possibly an overestimate. From a balance requirement of energy continuity, Jensen (1961) estimated energy dissipation in the layer of 1000 to 925 mb as 3.36 watts/m^2 for January 1958 over the Northern Hemisphere north of 20°N. This value can be compared with the winter zonal mean of 1.94 ± 0.51 watts/m^2 for 25°N to 70°N in this study. White and Saltzman (1956) obtained 5 watts/m^2 over North America (35°N to 60°N and 70° to 120°W) in January 1953, which was estimated from the conversion between potential and kinetic energy;

this value is larger than the corresponding figures in this study (see Table 8 and Figure 9), but it includes dissipation in the entire troposphere. Johnson (1962) computed E for four aerological stations in the United States and found a range of boundary-layer dissipation between 0.5 and 4.0 watts/m^2, which is in agreement with the corresponding values in this study (see Tables 8 and 22 through 25).

2.2.3 Regional Distribution and Seasonal Variation of Energy Dissipation over the North American Continent

2.2.3.1 Estimates based on geostrophic drag coefficients

Geostrophic drag coefficients and energy dissipation were computed at 58 mesh points over the North American Continent. The CDC 1604 computer output includes, for all available individual months during the period 1945 to 1955, monthly means of V_g, C, E, and the standard deviation of E.

Seasonal means of V_g, C, E, and standard deviation of E were calculated from the monthly mean values of these quantities. The seasonal means of the 1000 mb geostrophic wind speed and geostrophic drag coefficient are listed in Tables 18 through 21 for areas centered at indicated geographic latitudes and longitudes. Corresponding seasonal means of energy dissipation and standard deviation of energy dissipation are shown in Tables 22 through 25. Together with the corresponding z_0-tabulations in Table 4, this is an effort to establish the geographical distribution pattern of significant boundary layer characteristics over the North American Continent.

The continent-wide distribution of C shows pronounced north-to-south as well as east-to-west variation, in response to characteristic distributions of z_0- and V_g-values. In general, the distribution of C-value is more influenced by z_0 than by V_g. The C-values are relatively large at 30°N to 35°N, and around 55°N latitude. Lower C-values appear where field crops or low vegetation dominate. An annual cycle of C is significant over the whole continent. The drag coefficient is high in summer, as a consequence of large z_0 and small V_g, with transition values in spring and fall.

Energy dissipation patterns over the North American Continent show a prominent regional contrast. In general, the distribution of E follows the same trend as that of V_g as long as V_g is significantly different regionally. However, C also imposes a secondary effect.

TABLE 18. December-through-February: Regional distribution of means of geographic wind speed at 1000 mb surface V_g (cm/sec) and geostrophic drag coefficient C (unit of 10^{-4}) over the North American Continent. 1945-1955.

Latitude		70°N	65	60	55	50	45	40	35	30	25
Longitude											
65°W	V_g			1305	1246						
	C			413	413						
75	V_g	816	936	1176	1161	1482	1393	1050			
	C	334	329	417	415	404	388	378			
85	V_g	880	940		1059	1446	1216	1159	1155	935	
	C	332	329		415	397	339	329	424	453	
95	V_g	944	945	943	1012	1328	1180	931	1164	1073	
	C	330	329	367	415	345	303	371	393	423	
105	V_g	832	916	868	896	1276	1277	972	1206	1098	1218
	C	333	330	379	432	358	315	383	366	371	363
115	V_g	915	890	917	1005	1518	1465	1031	1196	853	
	C	331	331	377	437	365	325	381	373	378	
125	V_g	866	910	1447	1353	1567					
	C	332	331	364	424	364					
135	V_g		1038	1579							
	C		328	361							
145	V_g	951	1174								
	C	339	329								
155	V_g	1072	1182	1421							
	C	336	334	328							

TABLE 19. March-through-May: Regional distribution of means of geostrophic wind speed at 1000 mb surface V_g (cm/sec) and geostrophic drag coefficient C (unit of 10^{-4}) over the North American Continent. 1945-1955.

Latitude		70°N	65	60	55	50	45	40	35	30	25
Longitude											
65°W	V_g			1120	1006						
	C			422	424						
75	V_g	742	892	1086	962	1262	1207	880			
	C	336	331	423	425	414	412	420			
85	V_g	816	942		1018	1369	1141	990	1088	900	
	C	334	329		417	404	385	366	436	462	
95	V_g	889	946	894	1001	1365	1129	1031	1143	1070	
	C	332	329	371	422	376	356	377	404	434	
105	V_g	858	915	865	900	1178	1123	1079	1070	1320	998
	C	333	330	382	441	391	367	385	380	371	375
115	V_g	824	872	819	856	1279	1112	1397	1181	1074	
	C	333	331	384	453	402	381	377	382	378	
125	V_g	810	863	951	921	1281					
	C	334	331	381	451	402					
135	V_g		863	1153							
			332	374							
145	V_g	894	884								
	C	364	348								
155	V_g	1018	947	1148							
	C	360	362	355							

TABLE 20. June-through-August: Regional distribution of means of geostrophic wind speed at 1000 mb surface V_g (cm/sec) and geostrophic drag coefficient C (unit of 10^{-4}) over the North American Continent. 1945-1955.

Latitude		70°N	65	60	55	50	45	40	35	30	25
Longitude											
65°W	V_g			914	875						
	C			492	491						
75	V_g	749	767	918	843	885	947	608			
	C	377	375	491	493	487	465	465			
85	V_g	778	831		844	992	865	622	731	625	
	C	376	373		488	477	435	425	469	482	
95	V_g	807	818	751	792	1036	843	744	784	944	
	C	374	373	427	493	447	419	419	439	450	
105	V_g	743	784	721	693	952	870	755	703	815	661
	C	377	373	434	507	454	424	418	409	389	391
115	V_g	762	748	649	686	1192	925	1489	1071	1060	
	C	376	375	438	513	447	425	394	397	381	
125	V_g	652	691	697	719	1235					
	C	381	378	435	511	446					
135	V_g		626	850							
	C		382	427							
145	V_g	657	608								
	C	422	402								
155	V_g	744	642	881							
	C	417	420	408							

TABLE 21. September-through-November: Regional distribution of means of geostrophic wind speed at 1000 mb surface V_g (cm/sec) and geostrophic drag coefficient C (unit of 10^{-4}) over the North American Continent. 1945-1955.

Latitude		70°N	65	60	55	50	45	40	35	30	25
Longitude											
65°W	V_g			1163	1178						
	C			456	453						
75	V_g	876	935	1150	1147	1328	1238	802			
	C	332	330	456	454	445	438	445			
85	V_g	887	980		1115	1373	1179	909	976	855	
	C	332	329		450	438	411	391	442	463	
95	V_g	898	968	941	1053	1261	1110	813	985	1014	
	C	332	329	383	455	402	385	391	412	435	
105	V_g	1063	932	882	919	998	1075	901	994	928	1064
	C	333	330	392	470	419	385	397	386	381	372
115	V_g	887	900	791	897	1210	1174	1144	1041	835	
	C	332	330	395	479	420	387	389	389	384	
125	V_g	775	855	1124	1051	1353					
	C	335	332	385	472	416					
135	V_g		839	1271							
	C		333	381							
145	V_g	922	916								
	C	369	350								
155	V_g	1064	992	1259							
	C	365	366	358							

TABLE 22. December-through-February: Regional distribution of means of energy dissipation E (watts/m^2) and standard deviation of E over the North American Continent. 1945-1955.

Latitude	70°N	65	60	55	50	45	40	35	30	25
Longitude										
65°W			4.79 ±2.17	4.16 ±1.77						
75	.81 ± .24	1.19 ± .44	3.54 ±1.57	3.36 ±1.51	6.30 ±1.74	5.11 ±1.65	1.90 ± .42			
85	.04 ± .39	1.20 ± .47		2.47 ± .90	5.76 ±1.86	2.59 ± .87	2.01 ± .58	3.09 ± .98	1.84 ± .75	
95	1.26 ± .53	1.24 ± .51	1.48 ± .55	2.20 ± .82	3.07 ±1.26	1.89 ± .70	1.31 ± .41	2.80 ± .98	2.41 ± .67	
105	.90 ± .41	1.19 ± .61	1.20 ± .48	1.64 ± .64	2.91 ±1.28	2.76 ±1.14	1.58 ± .54	2.84 ± .82	2.07 ± .70	2.76 ±1.26
115	1.17 ± .40	1.07 ± .55	1.49 ± .86	2.55 ±1.77	5.06 ±1.67	4.25 ± .65	1.86 ± .65	2.83 ± .69	1.00 ± .31	
125	.98 ± .41	1.10 ± .43	5.39 ±2.67	5.86 ±2.75	5.54 ±1.66					
135		1.68 ± .74	6.90 ±3.59							
145	1.36 ± .54	2.41 ±1.10								
155	1.92 ± .84	2.48 ±1.00	3.98 ±1.09							

TABLE 23. March-through-May: Regional distribution of means of energy dissipation E (watts/m^2) and standard deviation of E over the North American Continent. 1945-1955.

Latitude	70°N	65	60	55	50	45	40	35	30	25
Longitude										
65°W			3.07 ±1.23	2.21 ± .81						
75	.60 ± .20	.99 ± .35	2.77 ± .92	1.93 ± .79	4.28 ± .30	3.52 ± .99	1.45 ± .53			
85	.81 ± .27	1.14 ± .37		2.13 ± .64	4.95 ± .29	2.57 ± .88	1.53 ± .35	2.80 ± .81	1.67 ± .49	
95	1.02 ± .34	1.15 ± .34	1.21 ± .46	2.05 ± .58	3.88 ±1.55	2.15 ± .76	1.77 ± .52	2.77 ± .89	2.49 ± .80	
105	.94 ± .39	1.06 ± .32	1.14 ± .34	1.62 ± .45	2.68 ±1.18	2.27 ± .83	2.17 ± .85	2.00 ± .63	3.52 ±1.15	1.73 ± .76
115	.81 ± .22	.94 ± .35	.98 ± .28	1.60 ± .58	3.60 ± .97	2.39 ± .90	4.39 ±1.02	2.83 ± .94	1.93 ± .33	
125	.76 ± .19	.92 ± .32	1.72 ± .74	1.54 ± .96	3.61 ± .98					
135		.95 ± .31	2.82 ±1.46							
145	1.21 ± .34	1.15 ± .38								
155	2.62 ± .50	1.47 ± .43	2.45 ±1.09							

TABLE 24. June-through-August: Regional distribution of means of energy dissipation E (watts/m^2) and standard deviation of E over the North American Continent. 1945-1955.

Latitude	70°N	65	60	55	50	45	40	35	30	25
Longitude										
65°W			1.92 ± .47	1.70 ± .53						
75	.70 ± .21	.73 ± .26	1.95 ± .53	1.52 ± .44	1.73 ± .66	1.96 ± .55	.52 ± .21			
85	.79 ± .25	.93 ± .38		1.51 ± .55	2.32 ± .69	1.31 ± .37	.48 ± .15	.95 ± .30	.60 ± .27	
95	.87 ± .29	.89 ± .32	.85 ± .23	1.29 ± .51	2.29 ± .50	1.13 ± .25	.83 ± .23	1.04 ± .31	1.76 ± .46	
105	.72 ± .38	.78 ± .25	.77 ± .23	.90 ± .30	1.83 ± .82	1.29 ± .39	.82 ± .24	.66 ± .19	.94 ± .30	.48 ± .18
115	.79 ± .41	.69 ± .22	.58 ± .19	.89 ± .30	3.49 ± .94	1.49 ± .57	5.59 ±1.17	2.91 ± .38	1.87 ± .35	
125	.55 ± .26	.56 ± .19	.74 ± .40	1.02 ± .41	3.87 ±1.97					
135		.43 ± .17	1.26 ± .54							
145	.59 ± .18	.44 ± .18								
155	.82 ± .25	.57 ± .22	1.33 ± .49							

TABLE 25. September-through-November: Regional distribution of means of energy dissipation E (watts/m^2) and standard deviation of E over the North American Continent. 1945-1955.

Longitude \ Latitude										
65°W			3.69	3.80						
			± .88	±1.15						
75	.98	1.12	3.76	3.51	5.47	4.12	1.20			
	± .32	± .38	±1.20	±1.14	±2.14	±1.32	± .48			
85	1.01	1.30		3.24	5.79	3.21	1.42	2.01	1.43	
	± .29	± .46		±1.26	±1.92	±1.00	± .61	± .73	± .57	
95	1.03	1.28	1.46	2.77	3.45	2.38	.94	1.82	2.12	
	± .27	± .51	± .49	±1.03	± .90	± .59	± .25	± .58	± .67	
105	.86	1.15	1.23	1.93	1.84	2.10	1.29	1.68	1.35	2.06
	± .24	± .53	± .33	± .66	± .64	± .59	± .46	± .47	± .51	± .98
115	1.01	1.02	.91	1.89	3.29	3.00	2.59	1.96	.94	
	± .38	± .45	± .26	± .61	±1.31	±1.04	± .92	± .60	± .28	
125	.70	.89	3.00	3.29	4.52					
	± .22	± .32	±1.15	±1.09	±2.03					
135		.86	3.82							
		± .44	±1.08							
145	1.42	1.30								
	± .49	± .59								
155	2.11	1.73	3.14							
	± .82	± .64	±1.18							

In winter, peaks of energy dissipation are obtained along the Pacific northwestern and Atlantic northeastern coasts. In the Northwest, peak values of E (5.86 to 6.90 watts/m^2) are found at 55 to 60°N, while in the Northeast, a corresponding range of high E-values (5.11 to 6.30 watts/m^2) occurs at 45 to 50°N; both core regions of high dissipation extend toward the interior at about 50°N. Regions of low E-values (around 1 watt/m^2) are common in the northern part of Canada; and occur also south of 35°N latitude at the west coast.

In summer, peaks of energy dissipation at the northwestern and northeastern coasts still exist but are weaker than in winter; for example, 3.87 watts/m^2 at 50°N, 125°W, and 1.96 watts/m^2 at 45°N, 75°W. The interesting fact is that another core of high dissipation values appears at the west coast at latitudes 35°N to 40°N with E-values ranging from 2.91 to 5.59 watts/m^2. Most other areas on the continent have low E-values in summer, usually smaller than 1 watt/m^2. Spring and fall can be regarded as transition seasons between winter and summer.

Year-to-year fluctuations of E-values over the continent exist and are evidenced by the standard deviation of E. The coefficient of variability (i.e., the ratio of standard deviation to the seasonal mean of E) is around 30% to 50%; coefficients above 50% are found in the core regions of high dissipation. However, as noted previously, the yearly fluctuations of E-values do not alter appreciably the geographical distribution pattern nor the seasonal cycle of energy dissipation.

2.2.3.2 Comparison with results using Cressman's Skin-Drag Coefficient

Cressman (1960) attempted to estimate an atmospheric skin-drag coefficient C_d, which was defined by

$$C_d = \tau_0 / \rho V_H^2 \qquad (6)$$

where V_H is the wind speed at the top of the frictional layer. Cressman postulated that C_d is a function of the number and height of mountain ridges per unit length of air trajectory, and estimated C_d-values from topographical charts. From his hemispheric map of skin-drag coefficient, C_d-values were interpolated for mesh points over North America, though interpolation was somewhat subjective due to crudeness of the map. If it is assumed that V_H corresponds to geostrophic wind speed at the 1000 mb surface, C_d must correspond to C^2, or $\sqrt{C_d}$ should correspond to the geostrophic drag coefficient, C. The C_d-values

interpolated from Cressman's map and our corresponding C-values for winter and summer are compared in Table 26 at three selected longitudes across North America (40, 50, and 60°N latitude). Due to its definition, $\sqrt{C_d}$ has no seasonal variation since it is a measure of topographical variation. While there is satisfactory agreement in the eastern half of the continent, it is apparent that Cressman's $\sqrt{C_d}$-values are significantly larger than our C-values in the Rocky Mountain region. In contrast to Cressman's concept, we consider topographical variation as change of surface height rather than roughness structure.

Assuming the same α_0 which was determined as a function of the surface-Rossby number, dissipation can be computed using C_d instead of C^2. Table 27 shows examples of January E-values over North America, computed with both the geostrophic drag coefficient C and Cressman's skin drag coefficient. It is found that mean E-values computed with Cressman's C_d-values are larger than any other estimates discussed in Section 2.2.2, and produce extremely high dissipation value, over the Rocky Mountain terrain. It appears that Cressman has overestimated the friction effect of mountains. Cressman's (1960) tentative assumption that $C_d = 0$ for oceanic surfaces would require that there is no energy dissipation over the oceans, which appears unrealistic.

When reference is made to Section 2.1.3, it can be concluded that the validity-test of drag coefficients with the aid of the ratio between climatological means of wind speed (at station anemometer height) and geostrophic speed will hardly support $\sqrt{C_d}$ values which are more than twice as large as our C-values.

2.3 Discussion of Results

The method presented here of evaluating continental and regional roughness parameters has certain obvious restrictions. In the survey of land use and vegetation cover, a great variety of heterogeneous sources were employed. Since the statistical data were frequently incomplete, certain adjustments had to be made. Extrapolations, supported by economic maps were necessary, especially for the USSR. Since vegetation height was considered the major factor in causing aerodynamic roughness over the land areas, forests play an important role. It must be expected that details of density distribution and morphology, especially for high vegetation, are additional factors. However, due to lack of pertinent information these factors could not be considered here. The problem may be solved by detailed experimental investigations in relatively small areas. Other restrictions are imposed by the adoption of Deacon's

TABLE 26. Examples of geostrophic drag coefficient C by Kung and skin-drag coefficient C_d by Cressman (1960) for the North American Continent. 1945-1955. C and $\sqrt{C_d}$ in unit of 10^{-4}.

Longitude		135	125	115	105	95	85	75	65°W
Latitude									
60°N	$\sqrt{C_d}$	775	632	387	387	387	---	447	447
	C winter	361	364	377	379	367	---	417	413
	C summer	427	435	438	434	427	---	491	492
50	$\sqrt{C_d}$	---	616	748	387	387	387	500	---
	C winter	---	364	365	358	345	397	404	---
	C summer	---	446	447	454	447	477	487	---
40	$\sqrt{C_d}$	---	---	837	775	387	424	469	---
	C winter	---	---	381	383	371	329	378	---
	C summer	---	---	394	418	419	425	465	---

TABLE 27. Comparison of January means (1945-1955) of energy dissipation E (watts/m^2) over the North American Continent, computed in line (I) with geostrophic drag coefficient by Kung and in line(II) with skin drag coefficient by Cressman (1960).

		Longitude (°W)								
Latitude		135	125	115	105	95	85	75	65	Mean
60°N	I	8.17	6.94	1.74	.94	1.39	----	3.58	4.94	3.96
	II	38.54	21.58	1.88	.98	1.55	----	4.19	5.86	10.65
50	I	-----	6.07	5.37	3.58	3.22	5.90	6.93	----	5.18
	II	-----	19.14	25.11	4.73	4.61	5.64	10.73	----	11.66
40	I	-----	-----	1.92	1.67	1.18	2.13	2.22	----	1.82
	II	-----	-----	9.35	6.90	1.29	3.57	3.46	----	4.91

z_0-values for desert and snow. However, it is believed that the roughness parameters for large areas presented in this study are fairly representative, and that only relatively minor revisions will be necessary.

Because of the lack of reliable information, a constant of 0.1 cm was assumed for the oceanic roughness parameter. This eliminates one dynamic degree of freedom in evaluating geostrophic drag coefficient. However, for the treatment of large-scale climatological data this restriction can be tolerated as long as the oceanic roughness parameter varies only relatively little with the wind speed.

In computing energy dissipation, an equation was used which is strictly valid for a barotropic atmosphere. For the computation of energy dissipation in a baroclinic atmosphere, Lettau (see Johnson, 1962) developed an approximate formula for constant "thermal wind,"

$$E = \tau_0 (V_0 + V_H)/2 \qquad (7)$$

where V_0 and V_H are geostrophic wind components (parallel to τ_0) at the surface and the top of the friction layer, respectively. Lettau (1959) examined also the dependency of the geostrophic drag coefficient on the variation of Richardson number variation at a 100 cm reference

height, $\underline{Ri}_{100}$. The ratio of geostrophic drag coefficients for diabatic and adiabatic conditions may be assumed to depend on $\underline{Ri}_{100}$; the ratio varies from 1.0 at neutral conditions to a maximum of about 1.2 at slight instability, and decreases toward both higher (i.e., increasing stability) and lower (i.e., increasing instability) $\underline{Ri}_{100}$-values. It may be assumed that the geostrophic drag coefficient is smaller than the adiabatic value for surface cooling and larger under conditions of moderate surface heating. On the average, computations based on neutral conditions can produce the correct order of magnitude. Thus, when diabatic effects are taken into account, some modification of energy dissipation values may be necessary. However, the revisions will be again of relatively secondary nature, and will not change radically the climatological pattern given in this study.

An eleven years' period of 1000 mb pressure data over the Northern Hemisphere was examined; after elimination of all suspicious data, seven to nine years were available for each month. This should be sufficient to obtain the general climatological patterns, concerning both spatial distribution and seasonal variations.

The dependency of energy dissipation on the cube of the geostrophic wind speed is a source of error in the averaging process. Even if it is possible to derive C and α_0 from $\bar{V}_g$ (where the bar indicates the monthly mean of daily data) it must be expected that

$$\overline{(V_g^3)}\,(\bar{V}_g)^3 \equiv r \geq 1 \qquad (8)$$

Also, the effect caused by taking the zonal average of V_g is not negligible, when differences of individual V_g-values within a zone are significant. In severe cases the ratio r in the defining equation (8) may reach a value of 1.3. This is due to the fact that deviation of V_g-values is not evenly distributed within a zone. In this study, continental E-values were computed by zonal averages of monthly V_g-values in accordance with latitudinal values of continental roughness parameters. Thus, zonal means of E-values and consequent multi-annual global mean of E-values, which was approximated from zonal mean E-values, are possibly underestimated by approximately 30%, and occasionally slightly more.

2.4 References

BALCHIN, W. G. V.; Geography and Man. New Era Publication Co., London, 1955.

BAUMGARTNER, A.; Untersuchungen über den Wärme—und Wasserhaushalt eines jungen Waldes. Berichte des Deutschen Wetterdienstes No. 28 (Band 5), 1956.

BAUMGARTNER, A.; Beobachtungswerte und weitere Studien zum Wärme und Wasserhaushalt eines jungen Waldes. Universität München — Meteorologisches Institut, Wissenschaftliche Mitteilungen No. 4, 1957.

BROCKS, K.; Measurement of wind profiles over the sea and drag at the sea surface. International Oceanographic Congress (Preprint), New York, 1959.

BRUNT, D.; Physical and dynamical meteorology. Cambridge Univ. Press, 1941.

BRYSON, R. A.; Oral communication with the author, 1962.

CURTIS, J. T.; The vegetation of Wisconsin, Univ. of Wisconsin Press, 1959.

DALRYMPLE, P., H. H. LETTAU, and S. WOLLASTON; South Pole micrometeorological program, Part II, Data Analysis. Quartermaster Res. and Eng. Comm. Techn. Report ES-7, 1963.

DEACON, E. L.; Vertical profiles of mean wind in the surface layer of the atmosphere. Geophys. Memoirs No. 91, 1953.

DEACON, E. L.; Aerodynamic roughness of the sea. J. Geophys. Research 67: 3167 - 3172, 1962.

DOMINION BUREAU OF STATISTICS: Canada Yearbook 1957-1958, Ottawa, 1958.

FONS, W. L.; Influence of forest cover on wind velocity. J. Forestry 38: 481-486, 1940.

FOOD AND AGRICULTURE ORGANIZATION OF THE UNITED NATIONS; Yearbook of Food and Agricultural Statistics, 1956, Rome, 1958.

FROST, R.; Atmospheric turbulence. Quart. J. Roy, Meteor. Soc. 74: 316-338, 1948.

GENTILLI, J.; A geography of climate. Univ. of Western Australia Press, 1958.

HAINES, D.A., and R. A. BRYSON; An empirical study of wind factor in Lake Mendota. Limn. Oceanogr. 6: 356-364, 1961.

HAMMOND, C.S. and Co.; Hammond's Comparative World Atlas.

HUTCHINS, C.W.; Geostrophic wind computation program. (A FORTRAN program). 1960.

JENSEN, C.E.; Energy transformation and vertical flux processes over the Northern Hemisphere. J. Geophys. Research 66: 1145-1156, 1961.

JOHNS HOPKINS UNIV. Lab. of Climatology; Publication in climatology vol. V, No. 7, 1952.

JOHNSON, W.B. Jr.; Seasonal and regional variations of atmospheric boundary-layer parameters and energy dissipation, derived from Gregg's aerological survey of the U.S., MS Thesis, Univ. of Wisconsin, 1962.

KLAGES, U.H.W.; Ecological crop geography. Macmillan Co., New York, 1942.

KUNG, E.C.; Ecological data of crops and natural vegetations. (Data collected at the Univ. of Wisconsin by personal communication), 1959.

KUNG, E.C.; Average aerodynamic roughness length of vegetation near Drexel, Nebraska. (Unpublished data) 1959.

KUNG, E.C.; Derivation of roughness parameter from wind profile data above tall vegetation. Sec. 3 of "Studies of three-dimensional structure of the planetary boundary layer," Dept. of Meteor., Univ. of Wisconsin, Annual Report, Contract DA-36-039-SC-80282, 1961.

KUNG, E.C. and H. H. LETTAU; Regional and meridional distribution of continental vegetation cover and aerodynamic roughness parameters. Sec. 5 of "Studies of three-dimensional structure of the planetary boundary layer," Dept. of Meteor., Univ. of Wisconsin, Annual Report, Contract DA-36-039-SC-80282, 1961.

KUTZBACH, J. E.; Investigations of the modification of wind profiles by artificially controlled surface roughness. Sec. 7 of "Studies of three-dimensional structure of the planetary boundary layer," Dept. of Meteor., Univ. of Wisconsin, Annual Report, Contract DA-36-039-SC-80282, 1961.

LAUSCHER, F.; Über der Verteilung der Windgeschwindigkeit auf der Erde. Arch. Meteor., Wien, Ser. B, Band II: 427-447, 1951.

LENSCHOW, D. H.; Technique and results of surface-temperature determination with aid of an airborne bolometer. MS Thesis, University of Wisconsin, 1962.

LETTAU, H. H.; A study of the mass, momentum and energy budget of the atmosphere. Arch. Meteor., Wien, Ser. A 7: 135-157, 1954.

LETTAU, H.H.; Computation of Richardson numbers, classification of wind profiles, and determination of roughness parameters. Sec. 7. 4 in Vol. I of "Exploring the atmosphere's first mile." (H. H. Lettau and B. Davidson, ed.), Pergamon Press, London and New York, 1957.

LETTAU, H. H.; Wind profile, surface stress and geostrophic drag coefficients in the atmospheric surface layer. In "Atmospheric diffusion and air pollution." (F. N. Frenkiel and P. S. Sheppard, ed.) Vol. 6 of "Advances in Geophysics," Academ. Press, New York and London, 1959.

LETTAU, H. H.; A generalized mathematical model of the mean-velocity distribution in fully turbulent duct flow. Sec. 8 of "Studies of the three-dimensional structure of the planetary boundary layer," Dept. of Meteor., Univ. of Wisconsin, Annual Report, Contract DA-36-039-SC-80282, 1961a.

LETTAU, H. H.; Theoretical wind spirals in the boundary layer of a barotropic atmosphere. Sec. 9 of "Studies of the three-dimensional structure of the planetary boundary layer," Dept. of Meteor., Univ. of Wisconsin, Annual Report, Contract DA-36-039-SC-80282, 1961b.

MUNK, W. H.; A critical wind speed for air-sea boundary processes. J. Mar. Research 5: 203-218, 1943.

NIKURADSE, J.; Stroemungsgesetze in Rauhen Rohren. V. D. I. Forschungsheft, No. 361, 1933.

OXFORD REGIONAL ECONOMIC ATLAS; the USSR and eastern Europe. Oxford Univ. Press, 1956.

PACKARD, R. L.; Ecological geography of certain Wisconsin feed crops. Ph. D. Thesis, Univ. of Wisconsin, 1957.

PAESCHKE, W.; Experimentalle Untersuchungen zum Rauhigkeitsund Stabilitatsproblem. Beitr. Phys. fr. Atm, 24: 163-189, 1937.

POPPENDIEK, H. F.; Investigation of velocity and temperature profiles in air layers within and above tree and brush. Contract N6-ONT-275, Taks Order VI, NR-082-036, Dept. of Eng., Univ. of California, Los Angeles, 1959.

PANOFSKY, H. H.; The budget of turbulent energy in the lowest 100 meters. J. Geophys. Research 67: 3161-3165, 1962.

PROUDMAN, J.; Dynamical oceanography, Wiley and Sons, New York, 1953.

ROSSBY, G. G.; and Montgomery, R. B.; On the momentum transfer at the sea surface. Pap. Phys. Oceanogr. Meteor. 4, No. 3, M. I. T., 1936.

SCHOOLEY, A. H.; Mean roughness factor as a function of wind velocity. J. Geophys. Research 66: 2863-2866, 1961.

SHEN, T. H.; Agricultural resources of China. Cornell Univ. Press, 1951.

SUTTON, O. G.; Micrometeorology, McGraw-Hill, New York, 1953.

TAYLOR, R. J.; The dissipation of kinetic energy in the lowest layer of the atmosphere. Quart. J. Roy. Meteor. Soc. 78: 179-185, 1952.

THE TIMES OF INDIA; Directory and Yearbook, 1956-1960. Coleman Ltd., Bennett.

UNITED STATES DEPARTMENT OF AGRICULTURE; Agricultural Statistics, 1957. Washington, D.C. 1958a.

UNITED STATES DEPARTMENT OF AGRICULTURE; Forest timber resources for America's future. Washington, D.C., 1958b.

VAN ROYEN, W.; The agricultural resources of the world. Prentice-Hall, Inc., New York, 1954.

WHITE, R. N., and B. SALTZMAN; On conversions between potential and kinetic energy in the atmosphere. Tellus 6: 357-363, 1956.

WILSON, F. G.; Forest trees of Wisconsin, Wisconsin Conservation Department Publication 507-55, 1955.

3

The Modification of Temperature Variance Spectra in Airflow over Artificially Controlled Surface Roughness

John P. Kearns
and
Raymond J. Deland

Department of Meteorology
University of Wisconsin

Abstract: Temperature spectra were measured over a field of bushel baskets set on the frozen surface of Lake Mendota, and also over the unmodified ice surface. Comparison of the spectra shows the effects of turbulence generated by the bushel basket field as a whole and by the spacing of the bushel baskets.

List of Contents

3.1 Introduction

3.2 Experimental Procedure
- 3.2.1 Measurement and Recording of Temperature Fluctuations
- 3.2.2 Calibration of Temperature Sensors
- 3.2.3 Computation of Spectra
- 3.2.4 Richardson Numbers
- 3.2.5 Modification of Boundary Roughness
- 3.2.6 Conditions of the Experiment

3.3 Results

3.4 Conclusions

3. 5 Acknowledgments

3. 6 References

3. 1 Introduction

The aim of the experiment described in this section is to determine the effect of controlled variations of the surface roughness on variance spectra of temperature in the atmospheric surface layer. The experiment uses the technique of active control, as described by Lettau (1959). Passive control means the careful selection of external conditions, such as terrain and boundary structure, weather type, stability, etc. Active control means the altering of one or more of these conditions in a specified manner. In this experiment the roughness of the boundary was changed over a limited area, by placing bushel baskets on the frozen surface of Lake Mendota. Temperature variance spectra obtained over the natural ice surface and over the field of bushel baskets are compared.

For the spectra obtained in this experiment the emphasis is on their characteristics in the inertial sub-range of atmospheric turbulence. At one or two meters above the surface, where the measurements reported here were made, the inertial sub-range includes the wave-numbers in the approximate range 0. 01/m to 100/m. For this spectral range it is well established by theory and experiment — see Panofsky and McCormick (1960), Monin (1962), Zwang (1960) — that, for steady-state turbulent flow, the variance spectra of vertical velocity, turbulent heat flux, and temperature all tend to obey the "-5/3 law," i. e.

$$d(\log S)/d(\log f) = d(\log S)/d(\log n) = -5/3$$

where S is the variance spectral density, f the frequency, and n the wave-number.

The spectra determined in this experiment lie in the wave-number range of 0. 003/m to 0. 6/m, so that only the higher-frequency portions of the spectra can be considered to fall within the inertial sub-range.

When the roughness is changed artificially the resulting non-steady conditions, due to the finite area over which the roughness is varied, result in deviations of the high-frequency portions of the spectra from the -5/3 law.

3.2 Experimental Procedure

3.2.1 Measurement and Recording of Temperature Fluctuations

A detailed description of the fine-wire thermocouple sensors is given by Hamilton (1962), who constructed them. Since they were designed for the same requirements of fast response time, very small radiation error, and good ventilation, they proved satisfactory.

The sensors were found to have a time constant of 0.2 sec for an air speed of 1 m/sec. Direct calibration of the sensors by Hamilton showed a conversion factor of 20 mv/°C from 4° to 14°C for the five junctions in series, sensibly constant over the range of temperatures encountered during the experiment. Two of the sensors were mounted on a mast, one above the other, at heights of 113 and 226 cm above the ice surface, about 1 m ahead of the mast facing the wind.

Two Kintel Microvoltmeter-Amplifiers, Model 202, manufactured by Cohu Electronics, were used to raise the level of the signals from a few to a few hundred millivolts. The signals were then transmitted by about 500 m of cable to the shore, where they were fed into two Hewlett-Packard Digital Voltmeters, Model 405-AR. In order to insure that the digital voltmeter would neither change scales automatically (which would require time-consuming correction processes), nor go off scale if the scale were fixed (which would result in either an interruption in the sampling or an inaccurate re-reading), the inputs were biased by a precision potentiometer. This bias was checked frequently. The digital voltmeters measured the signal to three places with an accuracy of 0.2% of full scale. They have a maximum sampling rate of five per second, as does the recorder.

The two temperatures were printed simultaneously, at the rate of four samples per second by a single Hewlett-Packard Digital Recorder, Model 561 B, in two columns of three digits each. A triggering pulse, four times a second, from a clock mechanism was connected to the external trigger input of the digital voltmeters. Tests proved this technique to be satisfactory, but special care had to be taken to insure that there would be no interaction between the two voltmeters. This was accomplished by careful grounding.

A vexing problem was presented by a persistent malfunction of the recorder. This affected the lefthand column only, corresponding to the upper sensor. Occasionally the second digit would be misprinted, either as an illegible number, or as a zero, which was obviously out of sequence

with the series of numbers, such as in an actual example: ...856, 865, 864, 806, 853... Rather than guess the proper value, either the number before or the number after the misprint was substituted for it.

To test this procedure, the data from a run taken on a different day, which has relatively far more misprints than those of the runs considered here (about 1 per 40 compared to about 1 per 150), was analyzed. The run was divided in two halves and a variance spectrum was computed for each half by two procedures. In the first case, the number before the misprint was substituted; in the second case, the number after. No significant differences were noted among the four spectra thus obtained.

3.2.2 Calibration of Temperature Sensors

The output of the amplifiers was calibrated against temperature. The following procedure was applied for both sensor-and-amplifier combinations used in the experiment.

The reference junctions were placed in an insulated icewater bath and the temperature sensor was placed in an insulated bath which was constantly agitated by a small propeller driven by an electric motor. A precision mercury-in-glass thermometer was placed as near to the thermocouple junctions as possible. Water of different temperature was added to this bath.

The thermocouples were connected to the amplifiers, which were connected to the digital voltmeter. When the water bath had reached thermal equilibrium, a reading was taken. Some thirty readings were taken for each sensor from 0°C to 14°C. This resulted in a nearly linear calibration curve with a mean slope of 36.6 mv/°C.

As a further check, three different reference voltages were connected to the Kintel amplifiers and the reading of the digital voltmeters noted for each. These reference voltages were directly measured by a Brown Electronix Potentiometer, manufactured by Minneapolis-Honeywell. The amplification factor of both Kintel amplifiers on the 3 mv scale was established to be 185.

The theoretical output from the sensors, as found in standard tables, when multiplied by the amplification factor of the Kintel amplifiers as found above, resulted in a calibration curve virtually identical to that obtained by calibration of the sensor-amplifier combination.

Before a given run, a reference voltage and a short circuit were connected across the input of the amplifiers. The corresponding outputs did not change detectably between runs.

3.2.3 Computation of Variance Spectra

The output from the digital recorder was card punched, for spectral analysis on the Control Data 1604 Electronic Computer of the Numerical Analysis Laboratory of the University of Wisconsin. A standard program for the evaluation of variance spectra (normalized by dividing by the variance), prepared by C. W. Hutchins of the Department of Meteorology, after the method of Blackman and Tukey (1958), was used.

To enable comparisons to be made between the spectra and those obtained by others, the computed variances for the various runs are given in Table 1. The spectra as computed are in terms of frequency (cycles per unit time). They are presented in terms of wave-number, defined for this purpose as the frequency divided by the average wind speed, at the level of the sensor, during the run.

3.2.4 Richardson Numbers

As a basis for comparison with other observations, the Richardson number was computed from measurements of average wind and temperature profiles. The wind and temperature profile instrumentation has been described in detail by Stearns (1962). During the bushel basket runs, wind profile measurements were available at two locations, one within the bushel basket field (the "main mast") and one over the bare ice (the "remote mast"). Temperature profiles were obtained only within the bushel basket field (on the "temperature mast," which also carried the sensors for the measurement of temperature fluctuations).

Due to insufficient number of anemometers, there was no anemometer at the highest level (320 cm) on the main mast during the bushel basket runs. Since the results of Kutzbach (1961) show that there is little difference between the average wind speeds over ice and over the bushel baskets (for the relatively small bushel-basket fields used) the wind speed over the bushel baskets at this level was taken to be the same as that measured at the remote mast.

During the second bushel basket run the wind profile was not measured close to the location of the temperature mast. In order to estimate the winds at the location of the temperature mast, it was assumed (for each level) that the ratio of velocity at the temperature mast during Run No. 2 to that measured during Run No. 1 was equal to the ratio of

TABLE 1. Characteristics of temperature as measured by the fast response temperature sensors for four variance spectra runs of ten minute duration, over Lake Mendota, 23 March, 1963. V_m = mean of digital voltmeter reading minus the bias voltage; σ_V^2 = the variance of these readings; T_m = mean of temperature; σ_T^2 = the variance of temperature; σ_T = the standard deviation of temperature. The conversion factor is 36.6 mv/°C.

	V_m (mv)	σ_V^2 $(mv)^2$	T_m (°C)	σ_T^2 $(°C)^2$	σ_T (°C)
Ice Run No. 1					
16:32 - 16:42 CST					
226. cm	433.	2267.	11.7	1.70	1.31
113. cm	324.	3217.	8.8	2.40	1.55
Ice Run No. 2					
16:51 - 17:01 CST					
226. cm	401.	934.5	12.9	.71	.84
113. cm	381.	2423.	10.5	1.83	1.35
Bushel Basket Run No. 1					
14:06 - 14:16 CST					
226. cm	217.	2343.	5.86	1.76	1.33
113. cm	117.	2930.	3.12	2.21	1.49
Bushel Basket Run No. 2					
14:21 - 14:31 CST					
226. cm	237.	1331.	6.40	1.00	1.00
113. cm	130.	1518.	3.46	1.14	1.07

the measured velocity at the remote mast during Run No. 1 to that during Run No. 2.

For the computation of the Richardson number, the approximation as presented by Lettau (1957) is used:

$$Ri = g(z_1 \cdot z_2)^{\frac{1}{2}}(T_2-T_1)\,\ell n(z_2/z_1)/T_2(V_2-V_1)^2,$$

where the subscript 2 refers to the upper level and the subscript 1 to the lower level. For runs taken with the lower sensor: $z_1 = 80$ cm, $z_2 = 160$ cm and $(z_1 \cdot z_2)^{\frac{1}{2}} = 113$ cm = sensor level.

For runs taken with the upper sensor: $z_1 = 160$ cm, $z_2 = 320$ cm, and $(z_1 \cdot z_2)^{\frac{1}{2}} = 226$ cm = sensor level.

The evaluation of Richardson number by this method gives a representative value at the sensor height as obtained from smoothed profiles. Values for temperature, wind velocity and Richardson number as obtained from smooth profiles are presented in Table 2. Note that the Richardson number increases with height and that it is relatively great for the ice runs. This is to be expected as the wind shear is greater near the surface and in the bushel baskets. The estimated Richardson numbers over the ice during the bushel-basket runs are not greatly different from those directly measured over the ice during the ice runs.

3.2.5 Modification of Boundary Roughness

Two-hundred and thirty white bushel baskets were placed in a random fashion in a rectangular field 20 m wide at the leading and back edges, and 21 m long in the direction of the wind. Other specifications of the field follow Kutzbach (1961). The obstacle density of the field was 0.55 bushel basket per square meter, and its reciprocal, the "specific area" of the field was 1.82 m^2. The ratio of specific area to lateral silhouette area (A) is 16.3. The mean distance between bushel baskets, D_{BB}, is 1.35 m; $1/D_{BB} = 0.74$/m.

Kutzbach's empirical relationship

$$\text{Log } z_0 = 3.32 - 1.13 \text{ Log } A,$$

produces $z_0 = 1.85$ cm. From Kutzbach's Figure 12, a zero point displacement, d, of about 15 cm was estimated.

TABLE 2. Temperature, wind speed and representative Richardson number over Lake Mendota, 23 March, 1963, obtained as smoothed profiles from the measurements of the wind and temperature profile systems during four ten-minute variance spectra runs. T = average temperature; V = average wind speed; Ri = Richardson number; Ri (est) = estimated Ri over ice in front of bushel basket field.

	T (°C)	V (m/sec)	Ri	Ri (est)
Ice Run No. 1				
16:32 - 16:42 CST				
226. cm	7.84	3.55	.23	
113. cm	6.79	3.05	.14	
Ice Run No. 2				
16:51 - 17:01 CST				
226. cm	7.08	2.88	.22	
113. cm	6.40	2.54	.25	
Bushel Basket Run No. 1				
14:06 - 14:16 CST				
226. cm	3.24	5.19	.095	.19
113. cm	1.86	4.10	.026	.078
Bushel Basket Run No. 2				
14:21 - 14:31 CST				
226. cm	4.37	5.80*	.068	.21
113. cm	2.94	4.59*	.020	.064

* = estimated

3.2.6 Conditions of the Experiment

In the afternoon of March 23, 1963, relatively warm air flowed over the melting ice surface of Lake Mendota and the micrometeorological site of the Department of Meteorology of the University of Wisconsin. The observations were made far enough from shore that fully developed flow could be expected. The temperature of the surface was equal to that of melting ice.

The bushel basket runs were obtained during the periods 14: 06 to 14: 16 CST and 14: 21 to 14: 31 CST. The wind direction was from the west-southwest with a fetch of at least 2000 m during both runs.

The temperature mast was placed 18 m behind the leading edge of the roughness field. This distance is D_{LE}; $1/D_{LE} = 0.056/m$. The remote anemometer mast was placed 20 m ahead of the leading edge.

Due to the demands of the wind profile studies conducted before, during, and after the bushel basket runs on 23 March, 1963, the ice runs could not be made until two hours after the bushel basket runs. The first was taken from 16: 32 to 16: 42 CST; the second from 16: 51 to 17: 01 CST.

The wind direction was generally from the southwest resulting in a maximum fetch of some 2000 m over ice. However, fluctuations in wind speed combined with a general turning into a southerly flow probably reduced this fetch to somewhat less than 800 m during parts of these runs.

To the eye the ice surface appeared very smooth and flat with irregularities of less than an inch on the surface. Kutzbach (1961) obtained values of the roughness parameter, z_0, over ice between 0.009 and 0.024 cm; his values for the zero displacement, d, ranged from 1.05 to 2.95 cm.

3.3 Results

The spectra are shown in Figures 1 to 4, two in each figure to facilitate comparison. The spectra as shown are normalized with respect to the total variance in each case, so that they represent the form only of the distribution according to frequency, not the absolute values of variance in each frequency range. Reference lines have been drawn for

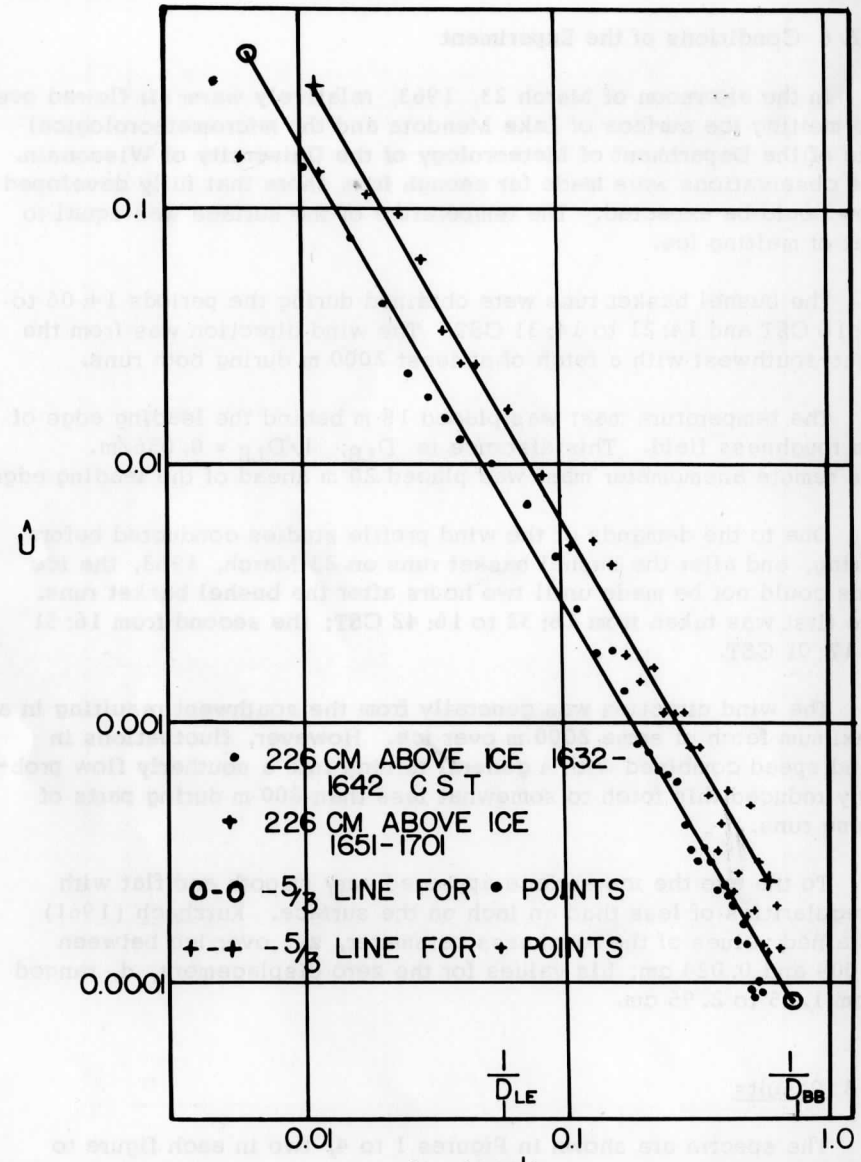

FIGURE 1. Comparison of spectra for two runs over ice surface at 226 cm.

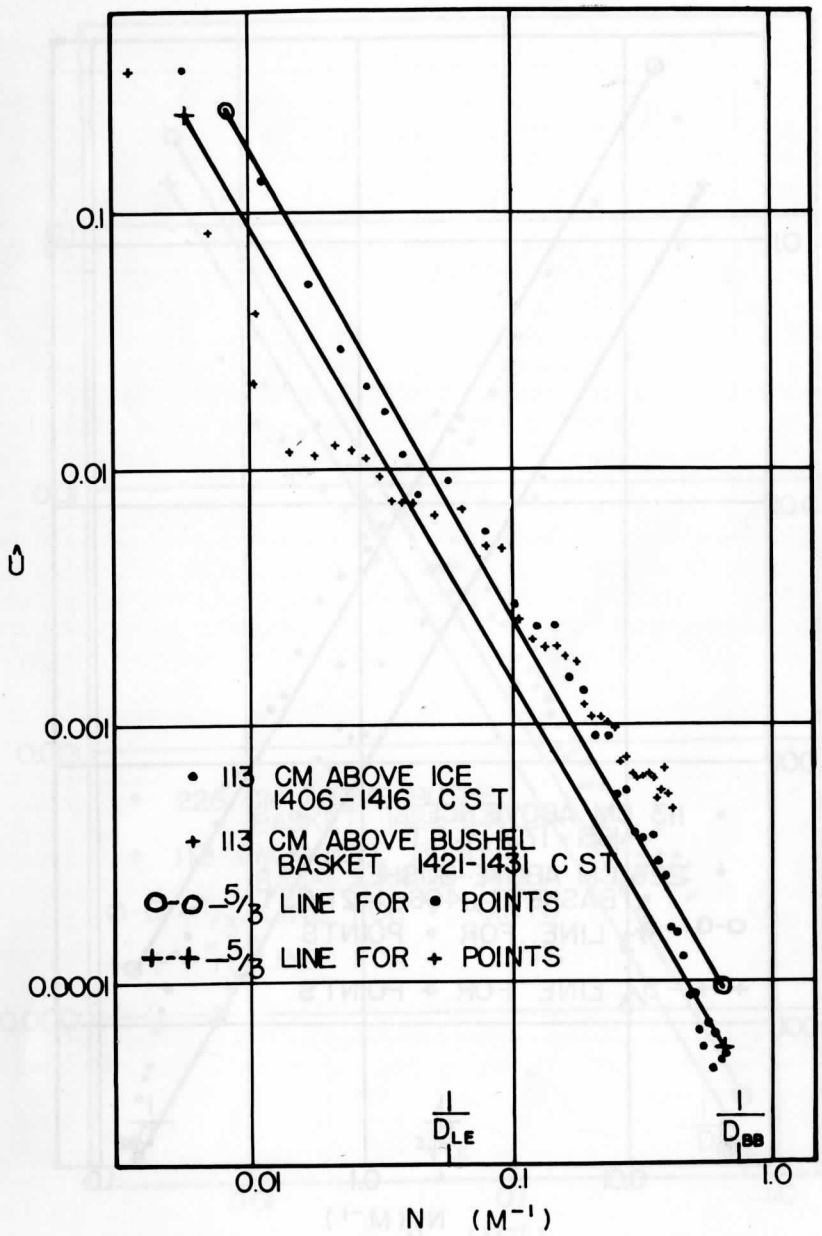

FIGURE 2. Comparison of spectra: 113 cm above bushel baskets vs 113 cm over ice surface.

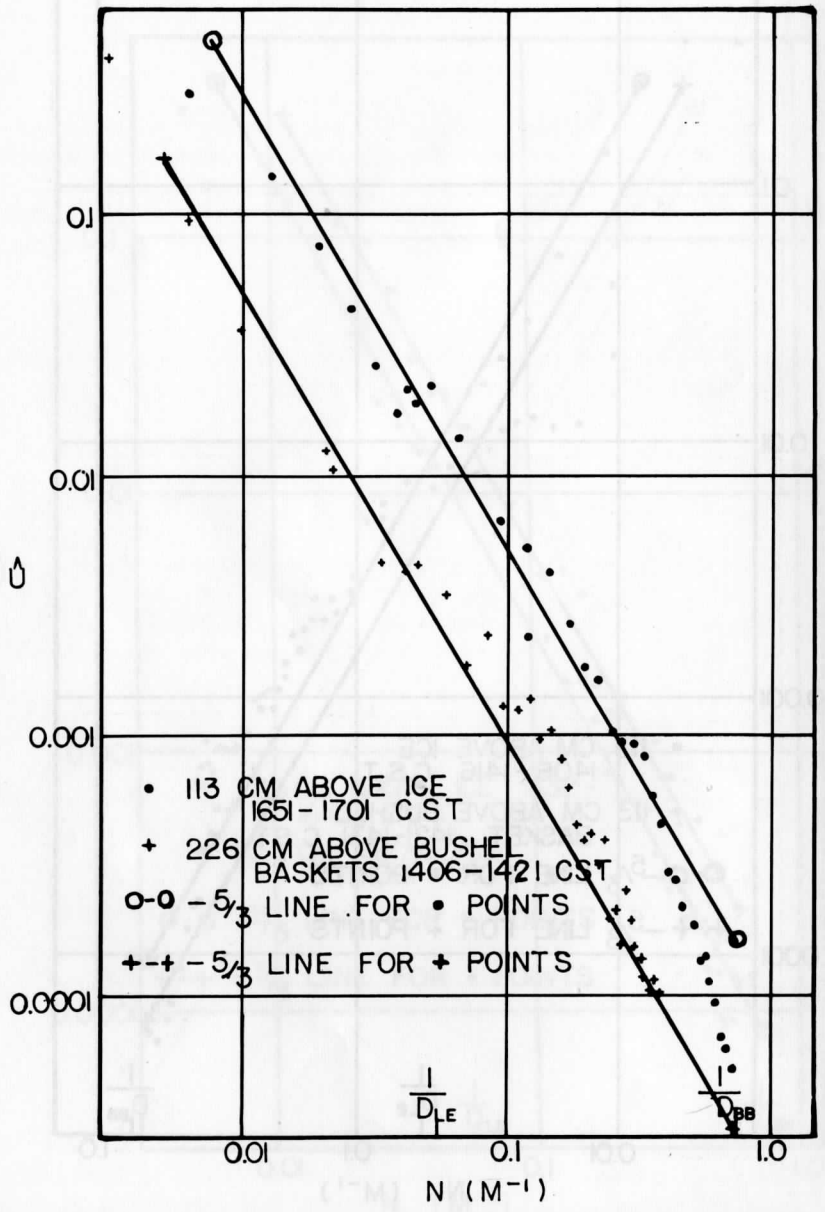

FIGURE 3. Comparison of spectra: 226 cm above bushel baskets vs 113 cm over ice surface.

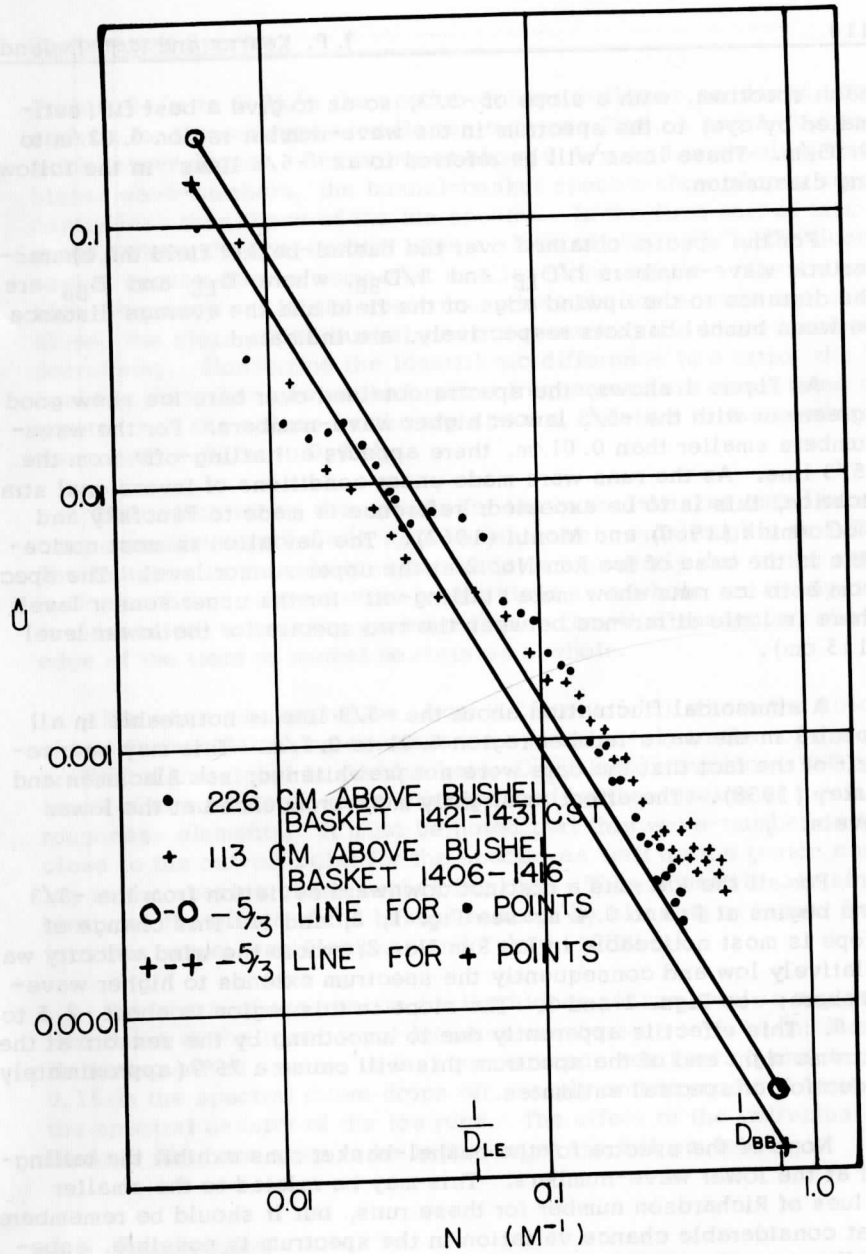

FIGURE 4. Comparison of two bushel basket runs; 226 cm vs 113 cm

each spectrum, with a slope of -5/3, so as to give a best fit (estimated by eye) to the spectrum in the wave-number region 0.02/m to 0.05/m. These lines will be referred to as "-5/3 lines" in the following discussion.

For the spectra obtained over the bushel-basket field the characteristic wave-numbers $1/D_{LE}$ and $1/D_{BB}$, where D_{LE} and D_{BB} are the distance to the upwind edge of the field and the average distance between bushel baskets respectively, are indicated.

As Figure 1 shows, the spectra obtained over bare ice show good agreement with the -5/3 law at higher wave-numbers. For the wave-numbers smaller than 0.01/m, there appears a "tailing-off" from the -5/3 line. As the runs were made under conditions of inversional stratification, this is to be expected: reference is made to Panofsky and McCormick (1960) and Monin (1962). The deviation is most noticeable in the case of Ice Run No. 2 at the upper sensor level. The spectra from both ice runs show more "tailing-off" for the upper sensor level. There is little difference between the two spectra for the lower level (113 cm).

A sinusoidal fluctuation about the -5/3 line is noticeable in all spectra in the wave-number region 0.01 to 0.1/m. This may be a result of the fact that the data were not prewhitened; see Blackman and Tukey (1958). The effect is slightly more pronounced at the lower levels.

For all the ice runs a distinct downward deviation from the -5/3 line begins at 0.3 to 0.4/m; see Fig. 1, 2, and 3. This change of slope is most noticeable in Ice Run No. 2, where the wind velocity was relatively low and consequently the spectrum extends to higher wave-numbers; see Figs. 1 and 3. The slope in this region is about -2.5 to -2.8. This effect is apparently due to smoothing by the sensor: at the extreme right end of the spectrum this will cause a 75% (approximately) reduction of spectral estimates.

None of the spectra for the bushel-basket runs exhibit the tailing-off at the lower wave-numbers. This may be related to the smaller values of Richardson number for these runs, but it should be remembered that considerable chance variation in the spectrum is possible, especially since the spectrum in this region is not averaged over several frequencies as it is at higher wave-numbers.

The spectra for both bushel-basket runs at the lower level fit the -5/3 law in the region from 0.015/m to 0.04/m: see Figs. 2 and 4.

From 0.04/m to 0.06/m the spectra appear to flatten suddenly. The spectra for the ice runs also flatten out—see Figs. 1 and 2—but to a much lesser degree. Beginning at about 0.1/m and proceeding toward higher wave-numbers, the bushel-basket spectra show slopes significantly less than those of the ice spectra. In the first part of this range, where the ice-spectra have a slope of about -5/3, the bushel-basket spectra have a somewhat smaller slope, while at the extreme high-frequency end of the spectrum, where the ice spectra increase in slope, the slope of the bushel-basket spectra at the lower level is still decreasing. Converting the logarithmic difference to a ratio, the bushel-basket spectral values at the highest frequencies are about three times greater than the values for the ice spectra, relative to their values in the range 0.02/m to 0.05/m.

The region where the spectra for the bushel-basket runs flatten out (approximately 0.04/m to 0.06/m) corresponds roughly to $1/D_{LE}$. The increase in the relative magnitude is apparently due to the contribution to the variance caused by the field as a whole, or in physical terms to mechanical turbulence generated when the wind encounters the leading edge of the field of bushel baskets as a whole.

The wave-number region (from 0.25 to 0.5/m) where the spectra shows further flattening corresponds approximately to that of the separation of individual bushel baskets, D_{BB}, indicating increased turbulence of about this wave-length produced by the spacing of the individual roughness elements. It must be noted that this wave-number region is close to the cut-off point for the spectra as well as the region corresponding to the spacing of the bushel-baskets. This is unfortunate since it obscures the effect of the bushel baskets by aliasing of higher frequencies into this range; see Blackman and Tukey (1958).

The shape of the spectra for the higher sensor level is a great deal like those of the lower level for wave-numbers up to 0.10/m, but the flattening of the spectra is less pronounced; see Figs. 3 and 4. Beyond 0.15/m the spectral curve drops off sharply and beyond 0.3/m it approaches the spectral density of the ice runs. The effect of the individual bushel-baskets does not seem to be important at the 226 cm level.

3.4 Conclusions

The changes in the temperature spectra caused by the bushel baskets have been related to the geometry of the bushel-basket field, enabling some deductions to be made about the response of the turbulent boundary layer to a change in roughness. The results are, however, of a preliminary

nature. More detailed observations of the same kind would enable more quantitative conclusions, especially about the upward propagation of the bushel-basket-induced turbulence.

3.5 Acknowledgments

The authors wish to express their gratitude to their colleagues, especially Messrs. Charles R. Stearns, Harry L. Hamilton, Jr., Arlin B. Super, and John C. Turner, for their aid in gathering the data upon which this report is based.

3.6 References

BLACKMAN, R. B., and J. W. Tukey, 1958. The Measurement of Power Spectra. New York, Dover Publications, Inc., 190 pp.

GURVICH, A. S., 1960. Frequency spectra and functions of distribution of probabilities of vertical wind velocity components. Bull. (Izv) Akad. Sci. U. S. S. R. Geophys. Series (Eng. edition) 695-703.

HAMILTON, H. L., Jr., 1962. Spacially continuous measurement of temperature profiles through an air-water interface. Final Report, Studies of the Three-Dimensional Structure of the Planetary Boundary Layer, Contract DA-36-039-SC-80282 (USEPG, Fort Huachuca, Arizona) University of Wisconsin.

KUTZBACH, J. E., 1961. Investigations of the modification of wind profiles by artificially controlled surface roughness. Annual Report, Studies of the Three-Dimensional Structure of the Planetary Boundary Layer, Contract DA-36-039-SC-80282 (USEPG, Fort Huachuca, Arizona) University of Wisconsin.

LETTAU, H. H., 1957. Computation of Richardson numbers, classification of wind profiles, and determination of wind profiles. Exploring the Atmosphere's First Mile, Vol. 1 (H. H. Lettau and B. Davidson, eds.); New York, Pergamon Press, Inc., Sec. 7.4, 328-366.

LETTAU, H. H., 1959. Final Report, Research Problems in Micrometeorology. Contract DA-36-039-SC-80063 (USEPG, Fort Huachuca, Arizona) University of Wisconsin.

MONIN, A.S., 1962: On the turbulence spectrum in a thermally stratified atmosphere. Bull. (Izv) Akad. Sci. U.S.S.R. Geophys. Series, (Eng. edition) 266-271.

PANOFSKY, H.A., and R. A. McCORMICK, 1960. The spectrum of vertical velocity near the surface. Quart. J. R. Meteor. Soc. 86: 495-503.

STEARNS, C.R., 1962. Micrometeorological installation on Lake Mendota. Final Report, Studies of the Three-Dimensional Structure of the Planetary Boundary Layer, Contract DA-36-039-SC-80282.

STEARNS, C.R., 1963. Oral communication.

ZWANG, L.R., 1960. Measurements of temperature pulse frequency spectra in the surface layer of the atmosphere. Bull. (Izv) Akad. Sci. U.S.S.R. Geophys. Series, (Eng. edition) 833-838.

Scanner's note:

This page is blank.

4

Report on Two Wind Profile Modification Experiments in Air Flow over the Ice of Lake Mendota

Charles R. Stearns
and
Heinz H. Lettau

Department of Meteorology
University of Wisconsin

Abstract: Two different wind profile modification experiments in air flow over the ice of Lake Mendota were made in March of 1963. In the first experiment an array of conifer saplings (Christmas trees) and in the second, adjacent fields of black and white bushel baskets were employed. Wind profile modification was measured with the aid of a moving and a stationary anemometer mast. An analysis of the results is primarily presented in terms of horizontal momentum budgets, as a function of wind fetch across and downwind of the obstacle fields. The efficiency of obstacles, when expressed in specific terms of momentum extraction per unit silhouette-area, is about twice as large for trees in comparison to bushel baskets, and slightly but significantly larger for black in comparison with white bushel baskets, with solar heating being present.

List of Contents

4.1 Introduction

4.2 Layout of Obstacle Fields
- 4.2.1 Christmas Tree Array
- 4.2.2 Bushel Basket Array

4.3 Results of Data Collection
4.3.1 Data Collection System
4.3.2 Christmas Tree Experiment of 21 March 1963
4.3.3 Bushel Basket Experiment of 23 March 1963

4.4 Results of Momentum Budget Analysis
4.4.1 Theoretical Background
4.4.2 Discussion of Results

4.5 Conclusions

4.6 References

4.1 Introduction

Typical of atmospheric boundary layer conditions are extremely large values of the Reynolds number and relatively high Richardson numbers. The large magnitude of these two important similarity parameters is the reason why it is difficult to simulate atmospheric boundary and surface layer conditions in the wind tunnel, and, thus, to solve micrometeorological problems conclusively by laboratory experiments. Lettau (1959) has outlined the concept of controlled micrometeorological experimentation in the open air. Of special interest are wind-stress experiments with the objective to obtain

(i) a theoretical understanding of the effect of surface roughness on turbulent flow in the lower atmosphere, and

(ii) the ability to calculate the effect of surface roughness from measurements of the roughness elements alone.

As examples of obstacles to be employed in such outdoors experimentation Lettau (1959, page 47 to 48) listed pine and fur saplings or branches, bushel baskets, etc. A first series of bushel basket experiments in air flow over the ice of Lake Mendota was reported by Kutzbach (1961) who demonstrated the magnitude of reproducible changes in wind shear artificially produced by controlled surface roughness modification.

Of a total of 460 bushel baskets available for micrometeorological experimentation at the Meteorology Department of the University of Wisconsin, 230 were painted white and 230 black in the summer following Kutzbach's experimentation. The average albedo of the baskets was 65 and 15%, respectively. In the late winter of 1961/62 the first feasibility studies were made concerning the possibility of artificial control of the Richardson number, by systematic interchange of white and black

obstacles in a given layout. Tentative results were reported by Lettau (1962).

From the first initiation of wind-stress experimentation on the ice of Lake Mendota on, there was discussion of the possibilities of using other types of obstacles. Among various things, a collection of Christmas trees discarded annually after the holidays had been taken under consideration. In the early winter of 1962/63, Professor Bryson of the Department of Meteorology at the University of Wisconsin stimulated the group to take the action described in the following sections.

However, generally unfavorable weather and ice-surface conditions (extreme cold in January, and relatively deep and unsettled snow cover in February and during most of March) permitted only a limited number of actual wind-stress experiments in late March. In spite of the cold winter, the lake opened relatively early, on the 3rd of April, 1963. In addition to the Christmas tree experiment, a study was made on wind profile modification using adjacent fields of black and white bushel baskets. Concurrently, a first investigation of the effect of controlled surface roughness modification on temperature variance spectra was completed; the results of this experiment are discussed by Kearns and Deland in Section 3 of this report.

4.2 Layout of Obstacle Fields

4.2.1 Christmas Tree Array

The trees for the wind-stress experiment were obtained in January of 1963, partly from left-overs at a commercial Christmas tree lot, the city dump, and private donations. The collection represented a wide variety in kind, sizes and shapes with the dominant species being white and jack pine, and blue spruce. A total number of 228 trees was obtained and brought to the micrometeorological site at Second Point of Lake Mendota. Because of the heterogeneity in size and shape, each tree was trimmed or cut so that the overall height was about 175 cm. Shorter trees remained untrimmed. The bottom branches were removed at the trunk so that a 60 cm length of the stem was available for supporting the tree in the ice. The estimated average crown diameter of the individual trees at the lowest branch level was about 80 cm.

The area for "planting" the artificial forest on the ice of Lake Mendota extended from approximately 30 to 65 m south of the base-tower location. In the pre-planning phase of the experiment it was decided to lay out a circular pattern because the trees would be frozen

to the ice and not movable after "planting"; thus, the field would offer the same fetch for any wind direction. The main anemometer mast was planned to be located at the center point of the circular array. Based on results obtained with bushel basket fields, a specific area of 4 m^2 per tree was selected, and it was assumed that an obstacle fetch represented by approximately 9 rows of trees would be sufficient to produce a significant modification of wind profile structure. Thus, the average spacing between trees was to be 2m.

From the chosen center point of the array, concentric circles were drawn on the ice at intervals of 2m, starting with a radius of 2m so that the largest circle had a radius of 18m. Beginning at the radial line pointing south, distances of 2m were measured and marked along each circle to indicate the position of individual trees. The southeast quadrant had only the four inner rows of trees since it was to be expected that wind directions in this quadrant were highly unlikely. Fig. 1 illustrates the layout for the Christmas tree experiment.

A hole of approximately 12 cm diameter and about 40 cm deep was drilled in the ice at each marked position. A tree was placed in each hole, snow was packed in, and water was poured into the hole to permit freezing of the tree into the ice. For the outermost row rather scraggly species were selected; the purpose was to establish a relatively gentle transition for the air flow at the leading edge. If more abrupt changes would have been desired, this row should have had the fullest trees. Lanes were present in certain directions; with a given limited number of individual obstacles this is nearly unavoidable. By visual sighting over the tree tops towards the main anemometer mast it was found that the average tree height was fairly close to the 140 cm-level.

Snow is rather common in Wisconsin winters, and the last season was no exception. Drift-snow in the artificial forest made experiments impossible until the snow pack receded which did not happen until the last third of March, as the consequence of meltings and re-freezings. At the time of the experiment reported here, small banks of drift-snow up to 25 cm were still present, generally at the northside of each individual tree. There were spots of clear ice in the area, and all lower branches of the trees were out of the drifts. Fig. 2 provides an illustration of the field on the day following the wind profile experiments. In the terms of forestry it can be said that the stand was poorly stocked.

4.2.2 Bushel Basket Array

Previous attempts to control the Richardson number and demonstrate the effect of boundary heating on wind profile modification experiments, with the aid of black and white bushel baskets in the presence of solar heating — see Lettau (1962) — were inconclusive; in some part this was due to the scheme adopted in 1962 of systematic interchanging of black and white baskets with time, in a given layout. One reason for the lack of clear-cut results in 1962 was that wind and temperature profile structure in the ambient air would undergo certain changes which obscured the differences due to albedo, and differential heating of the obstacle field. Thus, for the experiments in the winter of 1963 it was decided to change the method so that the direct comparison of profile structure over white and black baskets was possible at the same time. This was feasible because a sufficient number of masts, anemometers, and temperature sensors had been made available.

Based on previous experience a specific area of $2m^2$ per basket was selected. This obstacle-density is sufficient to produce significant changes in wind profile structure when the fetch is of the order of 20m. With 210 black and 210 white baskets available, each field was 21m wide in the crosswind direction, and 20m long in the downwind direction. The two fields were placed adjacent to each other, with the electrical terminal box at the downwind end of the dividing line. Fig. 3 illustrates the array.

At the time the baskets were being laid out on 23 March of 1963, the wind direction was due West. Before actual measurements were begun the wind had shifted to WSW. It was decided not to change the layout, in view of the time-loss involved, and the inherent uncertainty whether or not the wind would hold to the new direction. However, it did, and therefore, the downwind movements of the wind masts followed a line which formed an angle of about 70 degrees with the leading and back edges of the field.

4.3 Results of Data Collection

4.3.1 Data Collection System

Anemometers of the three-cup type manufactured by C. W. Thornthwaite Associates, Elmer, New Jersey, were used. The individual anemometers are matched so that they agree within 1% with the average of a set when they are simultaneously exposed on a horizontal beam. Only two individual anemometers showed slightly larger departures but

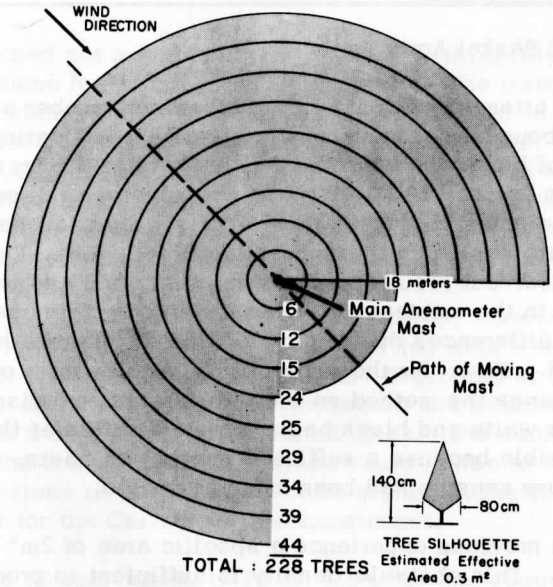

FIGURE 1. Layout for the "Christmas Tree Experiment" on the ice of Lake Mendota, 21 March, 1963.

FIGURE 2. View of the artificial forest on the ice of Lake Mendota.

still less than 2% from the mean. Each full rotation of the cup-shaft alternately exposes and shields a photocell from a light source. The output of the photocell is amplified at the field site, transmitted to shore by underwater cables, further amplified and registered on electro-mechanical counters. All counters were started and stopped simultaneously, and counts were noted manually for the period of each measurement. The system is described in detail by Stearns (1962). Two masts were used for the Christmas tree experiment (see Section 4. 3. 2) and three masts were used for the bushel basket experiment (see Section 4. 3. 3).

Temperature profiles were obtained by aspirated shielded thermocouples measuring the temperature differences between adjacent levels. Two masts were used for the bushel basket experiment, with sensors at 0, 20, 40, 80, 120, 160, 240, and 320 cm for Mast I, and 0, 20, 40, 80, 160, and 320 cm for Mast II. The thermocouple output was amplified, digitalized, and recorded on punch cards, with two complete profiles being sampled once each minute. The absolute temperature is determined by a thermistor at the surface level.

Short-wave radiation was measured by an Eppley pyrheliometer, and net radiation by a Suomi net-radiometer. These radiation values were recorded on the same punch cards used for the temperature profiles. The system is described in detail by Stearns (1962).

The preselected recording period for wind profile measurement at each station was 10 min. According to previous experience with similar experimentation this is a reasonable compromise, in view of the divergent requirements of a stable and representative mean, and limitation of the total duration of the experiment. The masts were moved on skids along a path parallel to the wind through the center of each obstacle field. The moving was done between observation periods, and no data was taken when personnel was in the obstacle field or upwind of the masts.

4. 3. 2 Christmas Tree Experiment of 21 March 1963

Anemometer levels up to 320 cm above the ice surface were used. The main mast with eleven anemometers at levels of 20, 40, 60, 80, 100, 120, 140, 160, 200, 240, and 320 cm remained stationary at the center point of the layout; see Fig. 1. The moving mast carried five anemometers at levels of 20, 40, 80, 160, and 320 cm. A series of 10-min mean wind profiles were observed at a total of 15 positions (x) forming a line from 16m upwind to 78m downwind of the leading edge. Information on timing and positioning of the individual profile

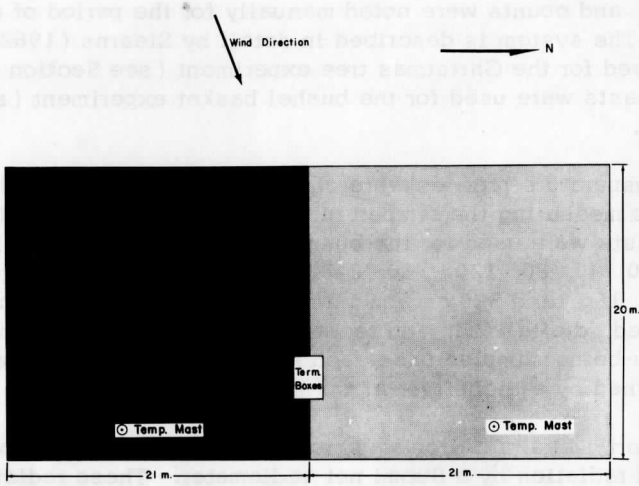

FIGURE 3. Dimensions of "black" and "white" field in the layout for the Bushel Basket Experiment on the ice of Lake Mendota, 23 March, 1963.

observations is given in Table 1, and reference speeds are listed in Table 2. Supporting weather data are summarized in Table 3.

In general, the atmospheric conditions were favorable for the experimentation. Table 2 shows that the wind speeds were relatively strong and steady, with unsystematic fluctuations of reference speed during the total period which remained within reasonable limits. For an analysis of the data see Section 4. 4. 2. Figs. 4 through 7 illustrate a few selected profiles of the series.

TABLE 1. Christmas tree experiment, 21 March 1963. CST = medium time of 10-min periods; x = downwind position (in m) with zero at leading edge; z = anemometer level (in cm). Tabulated is ratio of wind speed at indicated levels of the moving mast, to simultaneous wind speed at 320-cm level of main mast.

CST:	13: 44	14: 02	14: 18	14: 35	14: 51	15: 10	15: 27
x:	-16	-8	-4	0	4	8	16
z							
320	.983	.977	.972	.988	.980	.990	.993
160	.929	.928	.908	.923	.912	.834	.738
80	.864	.858	.842	.838	.508	.453	.453
40	.794	.788	.769	.750	.362	.438	.329
20	.740	.727	.704	.662	.472	.383	.307

CST:	15: 43	16: 00	16: 17	16: 35	16: 48	17: 08
x:	26*	30	34	42	58	78
z						
320	1.023	.995	.980	.959	.967	1.003
160	.669	.680	.682	.706	.821	.833
80	.392	406	.477	.552	.748	.334
40	.297	294	.374	.477	.694	.784
20	.278	260	.337	.446	.654	.747

*Back edge of artificial forest

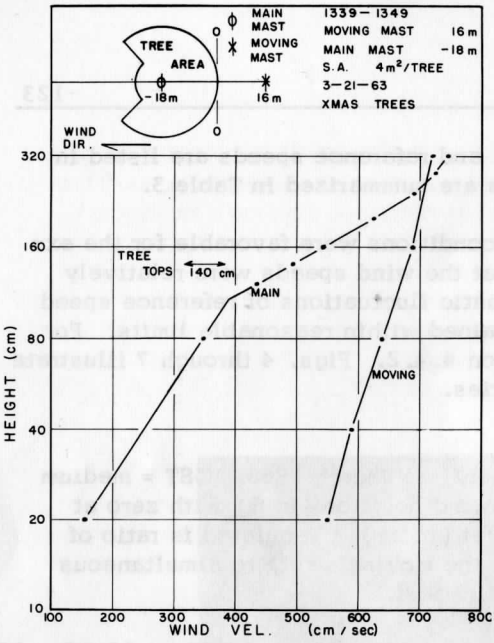

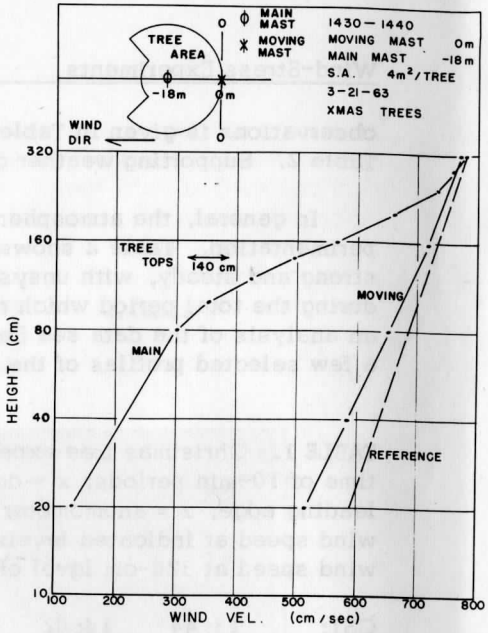

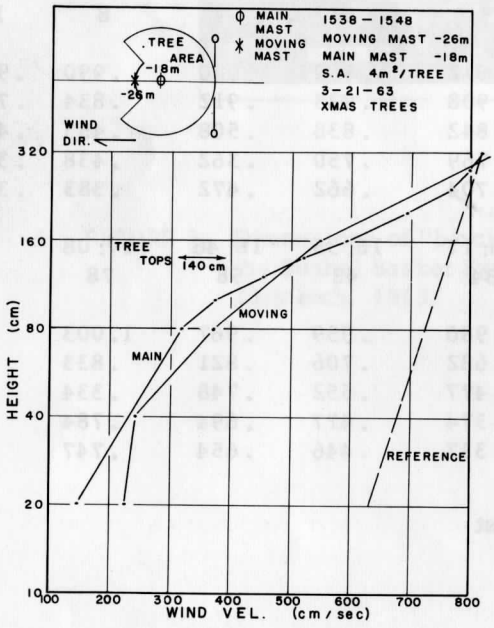

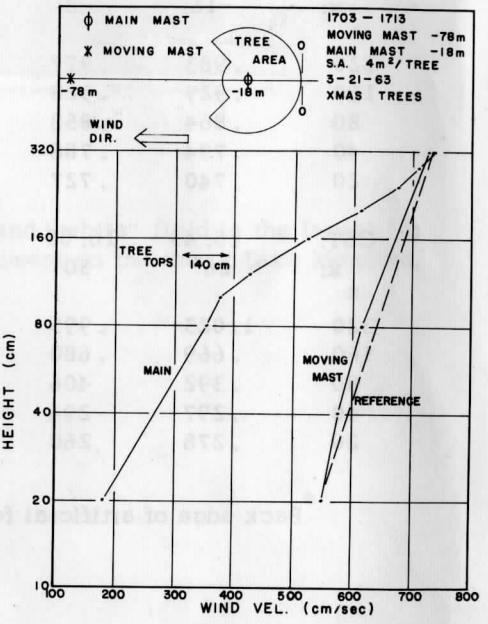

Fig. 4 (upper left) through Fig. 7 (lower right) — Christmas tree experiment, 21 March, 1963; examples of wind profiles at center-point of array (main mast) and at four positions of moving mast (16m upwind, at leading edge, at back edge, and 78m downwind of leading edge) as indicated on upper left corner of individual figures. The log-profile labeled "reference" is approximately representative of upwind conditions over clear ice.

TABLE 2. Christmas tree experiment, 21 March 1963. CST = medium time of 10-min periods; V = 10-min mean wind speed (in cm/sec) at 320 cm level of main mast, R_0 = net radiation (ly/min) over ice. Average Reference Speed = 733 cm/sec (at 320-cm level)

CST (hr: min)	V	R_0	CST (hr: min)	V	R_0	CST (hr: min)	V	R_0
13: 44	746	.526	15: 10	772	.259	16: 17	701	.014
14: 02	699	.485	15: 27	802	.172	16: 35	648	-.033
14: 18	674	.433	15: 43	819	.082	16: 48	610	-.072
14: 35	779	.402	16: 00	788	.060	17: 08	736	-.116
14: 51	729	.287						

TABLE 3. Christmas tree experiment, 21 March, 1963. Summary of supporting weather data recorded hourly at USWB Station Madison, Truax Field. p_0 = station pressure (mb); T = dry-bulb temperature (°F); RH = relative humidity (%); DD = wind direction; V = wind speed (knots)

CST (hour)	Sky cover	p_0	T	RH	DD	V
13	0.0	996	32	56	NNW	16
14	0.0	996	33	56	NW	16
15	0.6[1]	996	34	49	NNW	16
16	0.7[1]	996	34	49	NW	14
17	0.0	997	33	45	NW	14

[1] Thin broken

The ratio of fir to pine in the artificial forest was approximately 50 to 50. The silhouette area of individual trees varied and was not easy to obtain in view of varying degrees of compactness; see Fig. 2. As a compromise figure between estimates by various observers at the site the mean silhouette area can be given as $0.3 m^2$. Thus, the nondimensional similarity parameter A, which is defined as the ratio of specific area over silhouette area, and which characterizes the aerodynamic effects of an ensemble of obstacles—reference can be made to the discussion by Kutzbach (1961)—equals 4/0.3 = 13.3 for this experiment, with a possible error tolerance of 33%.

4.3.3 Bushel Basket Experiment of 23 March 1963

In view of the relatively low height of the obstacles, anemometer levels not in excess of 160 cm above the ice surface were used, and, with regard to the relatively short wind trajectory over the basket field, special care was applied to produce wind-profile data with extraordinary detail. Three anemometer masts were in operation. Mast I, with only three anemometers at 40, 80, and 160 cm remained stationary at a position approximately 15m upwind of the leading edge of the obstacle field, to monitor the ambient flow, and to provide reference wind speeds over the undisturbed ice of Lake Mendota. Mast II, carrying four anemometers at levels of 20, 40, 80 and 160 cm, was one of the moving system, Mast III with eight anemometers at levels of 20, 40, 60, 80, 100, 120, 140, and 160 cm the other. From upwind positions crosswind of Mast I, Masts II and III were gradually transgressed downwind along two parallel lines. Mast II was moved towards and through the white field, and Mast III towards and through the black field. After a sequence of five mast positions and simultaneous 10-min mean profile measurements, the two masts were interchanged, and Mast III now was moved upwind towards and through the white field, Mast II towards and through the black field, each occupying a station previously held by the other moving mast, until finally they were lined up again crosswind of Mast I.

An inspection of the results showed that data from Masts II and III confirmed each other for a given trajectory position. Because of its greater detail only the wind data obtained from Mast III is listed in Table 4. This table also supplies information on time, and position of individual profile measurements. Ambient speeds are given in Table 5, and supporting weather information is summarized in Table 6. It should be noted that wind speeds listed in Table 4 are reduced to uniform ambier speed by the application of the factor $\bar{V}_m/V_m$ (see Table 5) to directly observed speeds at a given time.

The two masts carrying the temperature sensors were located approximately 18m downwind from the leading edge, one in the white and the other in the black field, both towards the outer side so as to minimize any interference with the path of the moving anemometer masts; see Fig. 3. Temperature profile information is summarized in Table 7, also Richardson number estimates for the black and white fields. Data on solar heating, i.e., short-wave radiation flux-density from sun and sky, received by the Eppley pyrheliometer on the site is included in Table 5. The ice on Lake Mendota was melting on this day, and a substantial inversion prevailed over the undisturbed regions as well as the white obstacle field. Table 7 shows that the relatively intense solar heating produced lapse conditions over the black obstacle field.

TABLE 4. Bushel Basket Experiment "White versus Black Field," 23 March 1963. CST = medium time of 10-min period; x = downwind position (in m) with zero at leading edge; z = anemometer level (in cm). Tabulated is wind speed (in cm/sec) at indicated levels of Mast III after the observed values were reduced to average wind speed at the remote control mast.

Path across Black Field

CST:	11:22	11:47	12:05	12:28	12:40
x:	-15	6	16.5	30	50
z					
160	532	527	500	497	495
140	523	516	485	478	486
120	512	499	465	457	473
100	492	470	432	426	452
80	465	431	378	394	426
60	448	398	357	371	411
40	412	332	303	341	384
20	372	263	263	317	352

Path across White Field

CST:	14:40	14:26	14:11	13:51	13:37
x:	-15	6	18	30	50
z					
160	490	494	504	492	456
140	482	489	484	459	448
120	472	477	458	450	435
100	450	454	417	416	417
80	423	419	378	383	393
60	417	389	333	361	382
40	384	303	255	355	354
20	346	215	239	302	330

TABLE 5. Bushel Basket Experiment, 23 March 1963. CST = medium of time of 10-min periods; V_m = average wind speed (in cm/sec) at 40, 80, and 160 cm levels of control mast (No. I); $\overline{V_m}$ = average of column-listings. Epp = 10-min of Eppley recordings (ly/min).

CST (hr: min)	V_m	$V_m/\overline{V_m}$	Epp	CST	V_m	$V_m/\overline{V_m}$	Epp
11: 22	442	0. 954	1. 208	13: 37	402	0. 917	1. 112
11. 47	403	0. 870	1. 224	13: 51	373	0. 851	1. 068
12: 05	508	1. 096	1. 232	14: 11	414	0. 945	1. 006
12: 28	549	1. 185	1. 214	14: 26	471	1. 075	0. 957
12: 40	415	0. 896	1. 206	14: 40	531	1. 212	0. 907
$\overline{V_m}$:	463. 4				438. 2		

TABLE 6. Bushel Basket Experiment, 23 March 1963. Summary of supporting weather data recorded hourly at USWB Station Madison, Truax Field. p_0 = station pressure (mb); T = dry-bulb temperature (°F); RH = relative humidity (%); DD = wind direction; V = wind speed (knots)

CST (hour)	Sky cover	p_0	T	RH	DD	V
11	0. 1[1]	986	52	54	SSW	10
12	0. 0	985	56	51	SSW	12
13	0. 0	985	59	49	SSW	13
14	0. 0	984	62	44	SSW	13

[1] Thin scattered

TABLE 7. Bushel Basket Experiment, 23 March 1963. Average vertical differences of air temperature (T, °C) and wind speed (V, cm/sec) at indicated height differences (z, cm), and computed Richardson numbers (Ri) for indicated layers.

	Black Field				White Field			
z_2-z_1	T_2-T_1	V_2-V_1		Ri	T_2-T_1	V_2-V_1		Ri
		Mast II	Mast III			Mast III	Mast II	
160-80	0.22	99	122	0.005	0.68	126	111	0.014
80-40	-0.23	89	75	-0.005	0.40	123	97	0.005
40-20	-0.21	60	40	-0.006	0.09	16	64	0.004

The lateral silhouette area of the individual bushel basket was determined by Kutzbach (1961) to be $0.118 m^2$. With the specific area of $2m^2$ per bushel basket selected for this experiment, the similarity parameter, as given by the ratio of specific area over silhouette area, was A = 17. When the basket is viewed from above, Kutzbach determined its horizontal silhouette area as $0.138 m^2$, which is nearly the same as the lateral one. Thus, in order to obtain the heating of the field by short-wave radiation from the sun and the sky, we multiply the Eppley value, I_0, by the factor 1 - a where a = albedo of the obstacle, and divide by a compromise value of the similarity parameter, A = 15. For example, with I_0 = 1.20 ly/min (see Table 5), and a = 0.15, or 0.65, respectively, the heating of the black field will amount to 0.068 ly/min, and of the white field to 0.028 ly/min, i.e. a differential heating rate of 0.040 ly/min.

4.4 Results of Momentum Budget Analysis

4.4.1 Theoretical Background

The vertical extent of the profile modification is relatively small and the changes of wind speed in the downwind direction are relatively large, in the two experiments. This makes it permissible to neglect the effects of the pressure gradient force and of compressibility of the air, also the Coriolis force, and viscous forces. Two-dimensionality of flow, and steady states are assumed. Then the continuity equation permits us to estimate the mean vertical motion w, with the aid of a height-integration of horizontal convergence,

$$\partial u/\partial x + \partial w/\partial z = 0; \quad \text{or,} \quad w_z = -\int_0^z (\partial u/\partial x)\, dz, \tag{1}$$

assuming that $w_0 = 0$ at the horizontal ice surface ($z = 0$). Disregarding also possible changes (with x) of the squared turbulent x-component of air motion, momentum continuity is expressed by

$$\rho_0[\partial u^2/\partial x + \partial(uw)/\partial z] = \partial\tau/\partial z, \tag{2}$$

where τ = Reynolds stress. When equation (1) is combined with a height-integrated form of equation (2) we obtain after rearrangement of terms

$$\tau_0 = \tau_h - \rho_0[u_h \cdot w_h + \int_0^h (\partial u^2/\partial x)\, dz] \tag{3}$$

where h is the highest level up to which the wind profile is measured and integrations can be performed. Profiles of mean vertical motion are obtained with the aid of equation (1), and also, the bracketed term of the righthand side of equation (3) can be evaluated when detailed wind profile information at a sufficient number of x-positions is available. To obtain the Reynolds stress at $z = h$, and finally the surface drag τ_0, the following method was employed.

For the undisturbed profile over ice, in the farthest upwind position of the masts, the "surface-layer assumption" is made, i.e., that the shearing stress at height h is practically equal to the ground drag. The value of τ_0 is obtained with the aid of diabatic wind profile theory. A model described by Dalrymple, Lettau and Wollaston (1963) was employed in which the Deacon number of the wind profile is assumed to deviate systematically from unity by an expression which is directly proportional to height. This permits the evaluation of the diabatic influence function, (φ), and the integral-diabatic influence function, (Φ), in closed form. The method produces not only ground drag, but also zero-level displacement D and surface roughness length, z_0, in diabatic states. A complete scheme of the method is given in Fig. 8.

After determination of $\tau_0 = \tau_h$ at the undisturbed upwind position, let say, at $x = x_1$, we estimate the Reynolds stress at $z = h$ for the next-following position x_2 with the aid of the shear values (u') at $z = h$, which are taken from the measured profiles, using the proportionality

$$(\tau_h)_2 = (\tau_h)_1 \cdot (u'_h)_2/(u'_h)_1, \tag{4}$$

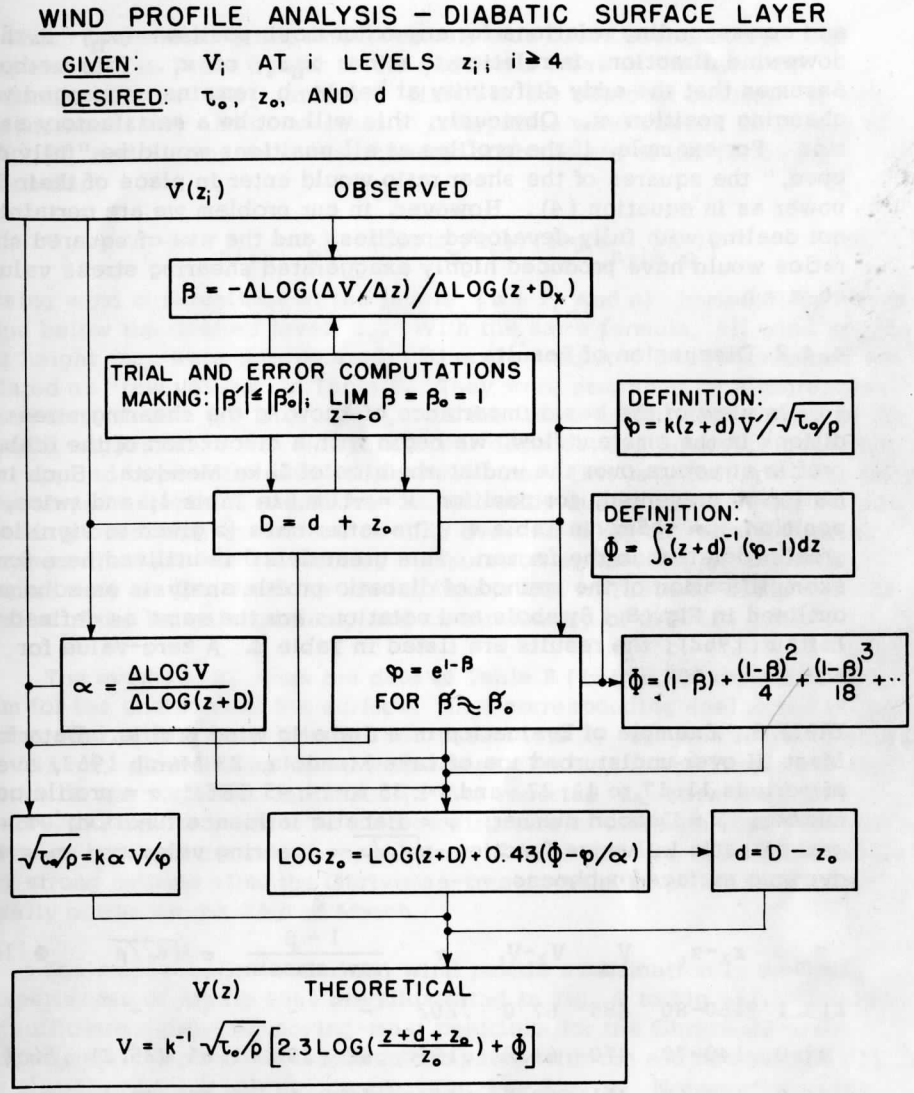

FIGURE 8. Schematic illustration of wind profile evaluation using the 1963-model. α = profile contour number, φ = diabatic influence function, and Φ = integral-diabatic influence function.

and corresponding relations for any other mast-position (x_n) in the downwind direction, in relation to either x_{n-1}, or x_1. This method assumes that the eddy diffusivity at height h remains unchanged with changing position x. Obviously, this will not be a satisfactory assumption. For example, if the profiles at all positions would be "fully developed," the squares of the shear ratio would enter in place of their first power as in equation (4). However, in our problem we are certainly not dealing with fully developed profiles, and the use of squared shear-ratios would have produced highly exaggerated shearing stress values at z = h.

4.4.2 Discussion of Results

In view of the basic importance of knowing the shearing stress conditions in the ambient flow, we begin with a discussion of the diabatic profile structure over the undisturbed ice of Lake Mendota. Such information is presented, for position x = -16m, in Table 1, and twice, for position x = -15m, in Table 4. The latter case is given in significantly greater detail than the former. This great detail is utilized here for an examplification of the method of diabatic profile analysis as schematically outlined in Fig. 8. Symbols and notations are the same as defined by Lettau (1962); the results are listed in Table 8. A zero-value for D

TABLE 8. Example of Evaluation of a diabatic wind profile. Data from Mast III over undisturbed ice of Lake Mendota, 23 March 1963, average of periods 11:17 to 11:27, and 14:35 to 14:45 CST. α = profile contour number; β = Deacon number; φ = diabatic influence function; Φ = integral diabatic influence function; $\sqrt{\tau_0/\rho}$ = shearing velocity; z_0 = aerodynamic surface roughness

z_m	z_2-z_1	V_m	V_2-V_1	α	$\frac{1-\beta}{\text{raw}}$	$\frac{1-\beta}{\text{smooth}}$	$\varphi\sqrt{\tau_0/\rho}$		Φ	$\log_{10} z_0$
113.1	160-80	485	67.0	.202	-	-	-	-	-	-
99.0	140-70	470	63.8	.195	.42	.50	1.65	(25.2)	.56	(-1.43)
84.8	120-60	451	59.5	.186	.50	.56	1.75	20.5	.64	-1.89
70.7	100-50	439	54.0	.175	.63	.52	1.68	19.6	.59	-2.07
56.6	80-40	406	46.0	.158	.54	.46	1.58	17.4	.51	-2.38
42.4	60-30	399	40.8	.180	.24	.34	1.40	21.8	.37	-1.60
28.3	40-20	379	39.0	.149	-	.23	1.26	19.2	.24	-2.13

$$K \equiv \sqrt{\frac{(n+1)^2 + n^2}{2}}$$

$$V_x = V_{n+1} \cdot (n - K) + V_n \cdot ([n+1] - K)$$

(which is the zero-point displacement) was found satisfactory. The levels z_m in Table 8 refer to the geometric mean of the pairs of "double heights" (z_2 and z_1) listed in the adjacent column. It was found necessary and convenient to interpolate wind speeds for levels of 70, 50, and 30 cm; this was achieved with the aid of the following formula:

OR,

$$V_x = V_n + (V_{n+1} - V_n) \cdot (\log z_x/z_n)/(\log z_{n+1}/z_n), \qquad (5)$$

using wind observations at the levels (n + 1, and n) immediately above and below the desired level z_x. With the same formula, all wind speeds at height z_m were interpolated. Directly computed Deacon numbers are listed as "raw values" in Table 8. They were smoothed by a regression line to produce $\beta = 1$ at $z = 0$, and the linear height dependency of the model suggested in Fig. 8. This linear dependency, however, could not be applied beyond the level of about 100 cm. This may indicate "not fully developed" states at and above 1m, probably due to change from surface heating over land, to surface cooling over the lake, in spite of fetches of more than 2000m. Therefore, computation of shearing stress was based only on data from the lowest five levels in Table 8, using a 0.428 value of the Karman constant, and an air density of 0.00126 g/cm^3.

The average z_0 from the data in Table 8 (below 100 cm) is 0.010 cm for the undisturbed ice surface. In a corresponding evaluation of the first wind profile on 21 March 1963 (see Table 1) z_0 was found to equal 0.033 cm. Both values agree with what is known, in the literature, for snow on ice surfaces. Kutzbach (1961) reported z_0 between 0.009 and 0.073 cm, dependent on surface structure of Mendota-ice. The difference between the two days in March of 1963 appears to be explainable by strong melting after the Christmas-tree experiment which was especially active on the 23rd of March.

The main results concerning wind profile modification in the two experiments of March 1963 are illustrated in Fig. 9 to Fig. 11. Due to a sufficient number of moving-mast positions for the Christmas-tree experiment, mean vertical motion computed with the aid of equation (1) is illustrated by isopleth-construction; see Fig. 9. Noteworthy is the contrast between strong and concentrated updrafts at the leading edge, and gentler downdrafts in the lee of the obstacle field. The five positions of the moving masts in the bushel basket experiment did not produce sufficient detail to permit the construction of isopleth lines. However, the computed w-profiles, together with the velocity-defect profiles, demonstrate clearly the effect of the obstacle field, and illustrate that the effects are more pronounced for the black than for the white field. This is well supported by the corresponding differences in Richardson

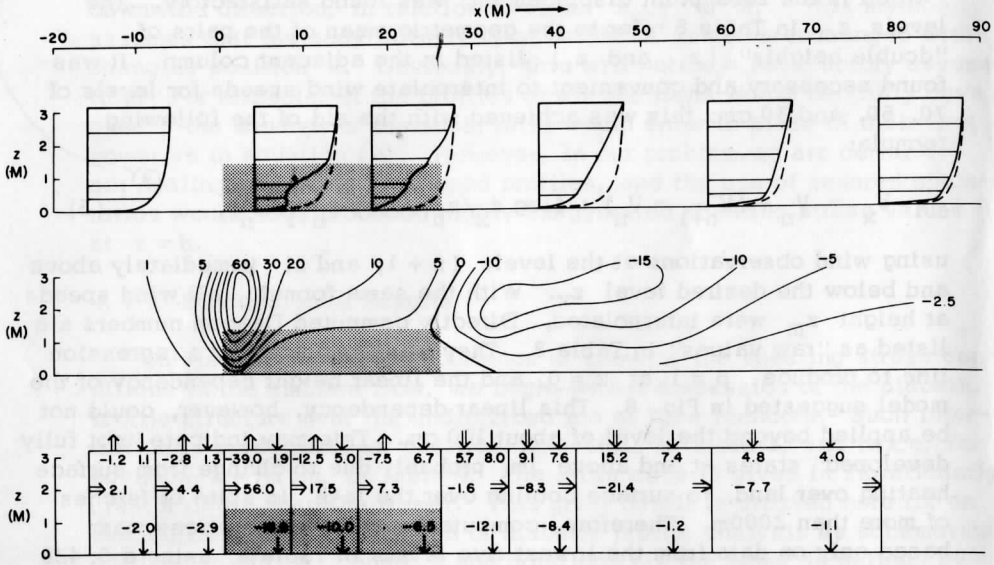

FIGURE 9. Christmas tree experiment on the ice of Lake Mendota, 21 March, 1963, 13:15 to 17:13 CST.

A: Velocity profiles at six selected positions (x);

B: Isopleths of computed mean vertical motion in cm/sec;

C: Local momentum budget constituents for nine adjacent air volumes.

The shaded area outlines vertical and horizontal extent of the artificial forest.

The four numbers in each column represent dynes/cm^2 and indicate horizontal divergence of x-momentum transport (horizontal double arrows), vertical transport (by mean vertical motion) of x-momentum (vertical double arrows), and eddy transport (single arrows) of x-momentum at the top and bottom of each volume.

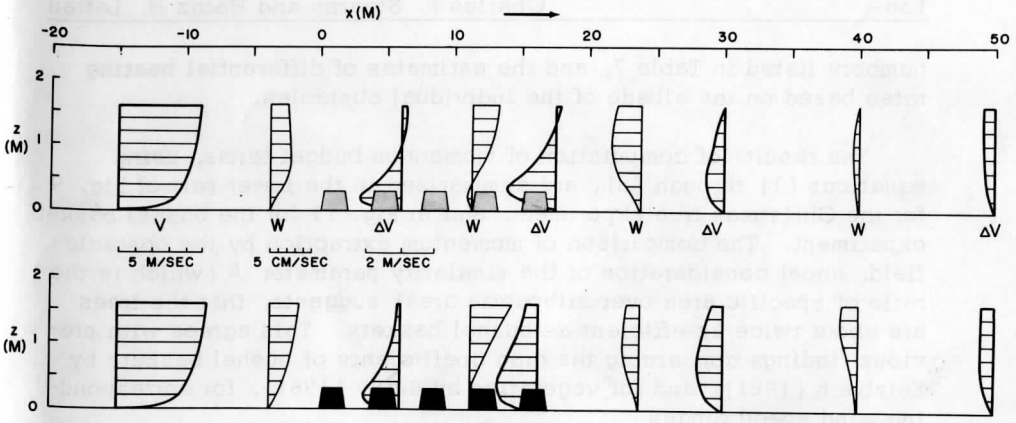

FIGURE 10. Bushel Basket Experiment on the ice of Lake Mendota, 23 March, 1963, 11:17 to 12:45 (white basket field, upper part), 13:32 to 14:45 (black basket field, lower part). V = profile of undisturbed velocity; W = profile of computed vertical motion; ΔV = profiles of velocity-defect (disturbance).

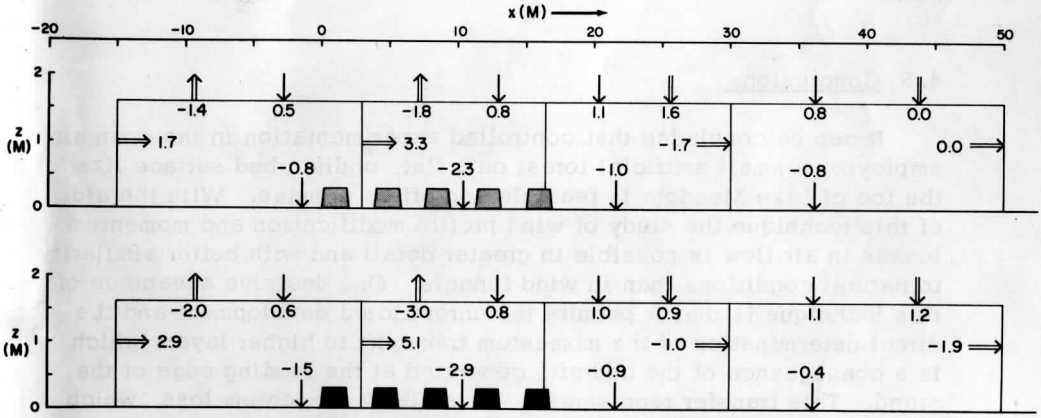

FIGURE 11. Bushel Basket Experiment on the ice of Lake Mendota, 23 March, 1963. Local momentum budget constituents for four air volumes along trajectories across the white and black fields. Symbols are explained in caption for Fig. 9.

numbers listed in Table 7, and the estimates of differential heating rates based on the albedo of the individual obstacles.

The results of computation of momentum budget terms, using equations (1) through (3), are summarized in the lower part of Fig. 9 for the Christmas tree experiment, and in Fig. 11 for the bushel basket experiment. The comparison of momentum extraction by the obstacle field, under consideration of the similarity parameter A (which is the ratio of specific area over silhouette area) suggests, that the trees are about twice as efficient as bushel baskets. This agrees with previous findings concerning the drag coefficients of bushel baskets by Kutzbach (1961), and for vegetation by Burgy (1961), for corresponding wind speed ranges.

During recent years the question of drag and momentum extraction in natural vegetation has been discussed and investigated at a variety of places, and in connection with different practical applications. Examples are the work by Jensen (1954) related to shelter effects, by Fraser (1962) on wind-throw and stem-breakage, by Reifsnyder (1955) related to forest fire research, and by Lemon (1962) on the energy budget in plant communities, to name only a few of the widely varying problems. For more detailed references see the literature survey given by Burgy (1961), or the work reported by Kung in Section 2 of this report.

4.5 Conclusions

It can be concluded that controlled experimentation in the open air employing a small artificial forest on a flat, undisturbed surface like the ice of Lake Mendota is feasible and offers promise. With the aid of this technique the study of wind profile modification and momentum losses in air flow is possible in greater detail and with better similarity to natural conditions than in wind tunnels. One decisive advantage of this technique is that it permits the unrestricted development and the direct determination of the momentum transport to higher layers which is a consequence of the updrafts generated at the leading edge of the stand. This transfer represents a "reversible" momentum loss, which will be recovered downwind of the back-edge. Only the Reynolds stress, at the lower boundary and at the ensemble of the obstacles, is an "irreversible" loss which is of prime interest in micrometeorology. The interaction between momentum transfer processes for individual cross sections of the flow along the obstacle fetch, as illustrated in the lower part of Fig. 9, can be well documented only for a relatively small

artificial forest. The author knows of only one other open-air experimentation with an artificial forest, namely that reported by Reifsnyder (1955); about the same amount of trees, roughly 200, were used, but Ponderosa pines of much larger size which made it difficult to study details of wind profiles above the canopy.

However, the results of the first experiment of this kind on the ice of Lake Mendota are restricted due to several uncertainties. One important question concerns the validity of the assumption of two-dimensional flow. It must be concluded that in future experiments the array should more closely resemble a truly two-dimensional obstacle field. Observational checks on the parallelity of flow over the center region of the field will be desirable, possibly using smoke puffs or smoke trails as tracers. The uncertainties of the budget of momentum, due to the assumption of two-dimensional flow, in spite of the circular shape of the array, prohibit the discussion of downwind conditions in detail for the 1963 experiment. High surface stress values behind the back-edge of the Christmas tree array appear conspicuous; also the suggestion that eddy momentum flux, coming in at $z = h$ farther down the trajectory, can possibly serve, at least partly, to restore mean horizontal momentum, rather than supporting fully the ground drag.

Likewise, the wind profile experimentation by differentially heated but otherwise identical obstacle fields are in need of more detailed information. However, it can now be concluded definitely, from the results of the 1963 bushel baskets experiments, that not only artificial control of the Richardson number has been achieved on the scale of micrometeorological processes, but also the quantitative demonstration of its effect on momentum exchange in the lower atmosphere. In the future improvements will be necessary concerning details of temperature profile modification, and the heat budget of the air over the obstacle field.

4.6 References

BURGY, R. H. "Aerodynamic Drag in Tall Vegetation," pages 37 to 43 of Annual Report, Contract DA-36-039-SC-80282 (USEPG, Fort Huachuca, Arizona) Univ. of Wisconsin, 1961.

DALRYMPLE, P., H. LETTAU, and S. WOLLASTON. "South Pole Micrometeorology Program, Part II: Data Analysis," Technical Report ES-7, Quartermaster R and E Center, Natick, Mass., 1963.

FRASER, A. I. "Wind Tunnel Studies of the Forces Acting on the Crown of Small Trees," pages 178 to 184 of Report on Forest Research in England for 1962, The North Western Printers Ltd., 1963.

JENSEN, M. Shelter Effect; Investigations into the Aerodynamics of Shelter and its Effects on Climate and Crops, The Danish Technical Press, Copenhagen, 1954.

KUTZBACH, J. E. "Investigations of the Modification of Wind Profiles by Artificially Controlled Surface Roughness," pages 71 to 114 of Annual Report, Contract DA-36-039-SC-80282 (USEPG, Fort Huachuca, Arizona) Univ. of Wisconsin, 1961.

LEMON, E. R. "The Energy Budget at the Earth's Surface; Energy and Water Balance in Plant Communities," Research Report No. 359, Northeast Branch, Soil and Water Conservation Research Division, Agricultural Research Service, U. S. Dept. of Agriculture, Ithaca, N.Y., 1962.

LETTAU, H. "Research Problems in Micrometeorology," Final Report, Contract DA-36-039-SC-80063 (USEPG, Fort Huachuca, Arizona) Univ. of Wisconsin, 1959.

LETTAU, H. "General Introduction," pages 1 to 5 of Final Report, Contract DA-36-039-SC-80282 (USEPG, Fort Huachuca, Arizona), Univ. of Wisconsin, 1962.

LETTAU, H. "Notes on Theoretical Models of Profile Structure in the Diabatic Surface Layer," Final Report, pages 195-226 of Contract DA-36-039-SC-80282 (USEPG, Fort Huachuca, Arizona) Univ. of Wisconsin, 1962.

REIFSNYDER, W. "Wind Profiles in a Small isolated Forest," Forest Science, Vol. 1, No. 4, page 288, 1955.

STEARNS, C. R. "Micrometeorological Installation on Lake Mendota," pages 7 to 46, Final Report, Contract DA-36-039-SC-80282 (USEPG, Fort Huachuca, Arizona), Univ. of Wisconsin, 1962.

5

Preliminary Note on the Theory of Steady Katabatic Flow for Height-Dependent Eddy Diffusivity

Heinz H. Lettau

Department of Meteorology
University of Wisconsin

Abstract: The classical theory of katabatic flow, as first presented by Prandtl, is reviewed; it is essentially a laminar-flow solution for constant viscosity and heat conductivity. The characteristic equations of katabatic flow for height-dependent eddy diffusivity are derived; it is demonstrated that the mathematical problem is similar to that of spiral-flow in the planetary boundary layer of a barotropic atmosphere. Possibilities of model solutions are discussed.

List of Contents

5.1 The Classical Theory of Katabatic Flow
- 5.1.1 Prandtl's Theoretical Model
- 5.1.2 Prandtl's Solution

5.2 Theory of Katabatic Flow for Height-Dependent Eddy Diffusivity
- 5.2.1 Derivation of the Characteristic Equations
- 5.2.2 Discussion of Possible Model Solutions

5.3 Conclusions and Outlook for Future Work

5.4 References

5.1 The Classical Theory of Katabatic Flow

5.1.1 Prandtl's Theoretical Model

A relatively complete theoretical model of steady katabatic (or, anabatic) air flow was presented by L. Prandtl in 1942 in his renowned textbook entitled "Fuehrer durch die Stroemungslehre"; reference can also be made to the "Compendium of Meteorology" article by F. Defant (1951) who has reviewed Prandtl's theory, and extended it to include non-steady cases. The general assumption which underlies the model is that gravity (g) is the only external acceleration. As in other types of gravity-induced currents, the Boussinesq-Rayleigh assumption is introduced, i.e., the air density (ρ) is considered a variable only in the product $g\rho$, and assumed to be a constant (ρ_0) in all other terms of the fluid dynamics equation. In comparison with the intensity of boundary heating or cooling rates ($\pm Q_0$) and the resulting heat advection and heat diffusion, the effect of any internal heat source or sink (especially, effects of infrared radiation-flux divergence, or heat generated by dissipation of mechanical energy) is considered negligible. Then, the equations of continuity, momentum, and energy are:

$$\nabla \cdot \vec{V} = 0, \tag{1}$$

$$\rho_0 \, d\vec{V}/dt + \nabla p + \vec{k} g\rho = \mu \nabla^2 \vec{V} = \rho_0 \nu \nabla^2 \vec{V}, \text{ and} \tag{2}$$

$$d\theta/dt = \partial\theta/\partial t + \vec{V} \cdot \nabla\theta = \kappa \nabla^2 \theta, \tag{3}$$

where $\vec{V}$ = vector of motion, p = atmospheric pressure, $\vec{k}$ = vertical unit vector, μ = dynamic viscosity = $\rho_0 \nu$, when ν = kinematic viscosity, θ = potential temperature, and κ = thermal diffusity. The discussion is restricted to two-dimensional motion in the vertical plane parallel to the fall-line of an uniform flat slope. Let $\vec{V}$ be independent of the horizontal cross-wind coordinate. In order to eliminate pressure gradient effects, we take the curl of equation (2) and consider the lateral component (η) of vorticity. Disregarding the temperature dependency of viscosity, equation (2) yields the following equation for the vorticity in the x, z-plane

$$\rho_0 d\eta/dt - g\partial\rho/\partial x = \rho_0 \nu \nabla^2 \eta \tag{2'}$$

We want to apply the system of equations to steady-state conditions in potential temperature and lateral vorticity, i.e., for $\partial\theta/\partial t = 0$ and $\partial\eta/\partial t = 0$. Moreover, it will be assumed that the vector of motion is completely described by the component parallel (or, anti-parallel) to the fall-line of the slope. We introduce a new system of rectangular coordinates, n (normal to the slope and positive into the air), and s (parallel

to the slope and positive towards higher ground). Let the slope inclination be given by the constant angle ε. This angle is assumed to be sufficiently small so that $\tan\varepsilon = dz/dx \approx \varepsilon$ and, also, $\sin\varepsilon = dz/ds \approx \varepsilon$, when ε is expressed in radians. It follows from simple geometry that, together with $dz = \varepsilon ds$, we have also that $dn = -\varepsilon dx$. This means that in equation (2') we may write $-\varepsilon\partial\rho/\partial n$ in place of $\partial\rho/\partial x$. Considering that the air moves parallel to the fall line of the slope, the wind speed is $ds/dt = u$. It is assumed that u is only a function of the independent variable n so that $\eta = \partial u/\partial n$.

With all the above assumptions the system of equations (1) to (3) can be reformulated as

$$\partial u/\partial s = 0, \tag{4}$$

$$\varepsilon g\partial\rho/\partial n = \rho_0 \nu \partial^3 u/\partial n^3, \tag{5}$$

$$u\partial\theta/\partial s = u\varepsilon\partial\theta/\partial z = \kappa\nabla^2\theta \tag{6}$$

Concerning the temperature field Prandtl assumed that potential temperature is initially a linear function of height (z) and that a disturbance (ϑ) is superimposed which is only a function of the normal coordinate (n), so that

$$\theta = \theta_0 + \gamma z + \vartheta(n); \quad \text{with} \quad \gamma = \text{const}; \quad \nabla^2\theta = \partial^2\vartheta/\partial n^2. \tag{7}$$

Furthermore, consistent with the above restrictions it is assumed that the density disturbance is related to the temperature disturbance by the simplified version of the equation of state $d\rho/\rho_0 = -d\theta/\Theta_0$, where θ is in Kelvin degrees. Thus, equations (5) and (6) become

$$-\varepsilon g\partial\vartheta/\partial n = \theta_0 \nu \partial^3 u/\partial n^3, \text{ and} \tag{8}$$

$$u\varepsilon\gamma = \kappa\partial^2\vartheta/\partial n^2 \tag{9}$$

The physical meaning of equation (9) is that heat advection balances heat diffusion. Note that the expression of heat advection on the left-hand side of equation (9) is exact as long as air motion is actually restricted to being downslope or upslope. Inasmuch as $\partial\vartheta/\partial s = 0$, and $u = ds/dt$, only the initial vertical temperature gradient (γ) contributes to the advection term $\vec{V}\cdot\nabla\theta$. The physical meaning of equation (8) is that vorticity diffusion is balanced by vorticity generation through gravity and the temperature disturbance, as represented by the left-hand side of this equation.

5.1.2 Prandtl's Solution

To facilitate the solution of the system of the two simultaneous equations (8) and (9) a dimensionless independent variable $\zeta = n/Z$ is introduced, where the scale-length Z is defined in the relation

$$Z^4 = 4\kappa\nu\theta_0/g\gamma\varepsilon^2 \qquad (10)$$

Then, separation of the two dependent variables produces the two characteristic equations:

$$\partial^4 u/\partial\zeta^4 + 4u = 0; \quad \text{and,} \quad \partial^5\vartheta/\partial\zeta^5 + 4\partial\vartheta/\partial\zeta = 0. \qquad (11)$$

The boundary conditions are:

at the interface ($\zeta = 0$): $u = u_0 = 0$, $\vartheta = \vartheta_0 \neq 0$;

at large normal distance ($\zeta \gg 1$): $u = u_\infty = \vartheta = \vartheta_\infty = 0$.

A solution satisfying these conditions is:

$$u = U^* e^{-\zeta}.\sin\zeta\,; \quad \vartheta = \vartheta_0\, e^{-\zeta}.\cos\zeta, \qquad (12)$$

where the two integration constants U^* (cm/sec) and ϑ_0 (deg) are interrelated by

$$U^* = \vartheta_0\sqrt{g\kappa/\gamma\nu\theta_0} = \vartheta_0\sqrt{g/\gamma\,\theta_0\,\underline{Pr}} \qquad (13)$$

where $\underline{Pr} = \nu/\kappa$ = Prandtl number of air.

Even though Prandtl's theoretical model is strictly valid only for the laminar case it has been assumed—see Defant (1951)—that it applies also for steady turbulent flow, provided that the coefficients of eddy transfer of momentum and heat are height-independent over a sufficiently large cross section of the flow. It is well known that eddy coefficients are not constants for ordinary atmospheric boundary layer conditions, that is, when a large-scale pressure gradient exists (with subsequent quasi-geostrophic motion at the top of the boundary layer), considering the suppression of eddy size close to the interface. However, the shear conditions of katabatic flow are significantly different in comparison with ordinary boundary layer, or, surface layer profile structure. It may appear tolerable to use here a height-independent coefficient of eddy conductivity (K_0) in place of both ν and κ, thus assuming equality of eddy diffusivity for momentum and heat. Then, the effective Prandtl number is unity, and the relationships (13) of Prandtl's model of katabatic flow can be reformulated as

$$U^* = \vartheta_0\sqrt{g/\gamma\theta_0}\ ; \quad \text{and} \quad Z^2 = (2K_0/\gamma\varepsilon)\sqrt{\theta_0\gamma/g}. \tag{14}$$

The second equation, when solved for eddy diffusivity, yields $K_0 = 0.5\varepsilon Z^2\sqrt{g\gamma/\theta_0}$.

Immediately obtainable from the solution are the surface stress (τ_0) and the boundary value of heat flux (Q_0). These quantities follow from the defining equations, with the aid of equations (12) and (13), as

$$\tau_0 = \rho_0 K_0(\partial u/\partial n)_0 = \rho_0 K_0 U^*/Z, \text{ and} \tag{15}$$

$$Q_0 = -c_p\rho_0 K_0(\partial\theta/\partial n)_0 = -c_p\rho_0 K_0(\gamma + \vartheta_0/Z) \tag{16}$$

where c_p = specific heat of the air.

A characteristic of katabatic flow is that the wind profile must show a maximum speed (u^*) at a relatively small normal distance (n^*) from the interface. For a sufficiently small value of slope inclination the normal distance (n) is practically indistinguishable from the vertical distance (z). Thus at a given micrometeorological mast installation on the sloping surface, we can also say that a maximum wind speed (u^*) will occur at a certain height (z^*). The differentiation of the wind profile equation (12) once with respect to ζ produces the shear profile equation,

$$\partial u/\partial\zeta = U^* e^{-\zeta}(\cos\zeta - \sin\zeta) = Z\partial u/\partial n \approx Z\partial u/\partial z. \tag{17}$$

It follows that the first level of maximum wind speed (i.e., where $\partial u/\partial\zeta = 0$) occurs at $\zeta^* = \pi/4 \approx z^*/Z$. The original wind profile equation (12) then gives the maximum speed,

$$u^* = U^* e^{-\pi/4} \sin\pi/4 = 0.323\ U^*. \tag{18}$$

It is usually concluded that inspection of an observed wind profile (which is supposed to be katabatic) will yield directly a pair of u^*, z^* values, and consequently, $U^* = u^*/0.323$, and $Z = 4z^*/\pi$. Together with other independent information concerning the values of the external parameters ε, θ_0, γ, and g, the knowledge of U^* and Z appears to be sufficient for the verification of equations (14) through (16).

However, in a decisive test of the katabatic nature of an observed flow-case one must also consider the thermal structure of the lower atmosphere. The observed vertical temperature profile must agree with equation (12) and the model relationship equation (7), namely,

$$\theta = \theta_0 + \gamma z + \vartheta_0 e^{-\zeta} \cos \zeta \; ; \quad \text{with} \quad \vartheta_0 = U^* \sqrt{\gamma \theta_0 / g}, \tag{19}$$

when U^* and $Z = z/\zeta$ are the same as derived from wind profile data with the aid of Prandtl's model.

Furthermore, the Q_0-value estimated with the aid of equation (16) must satisfy energy budget requirements. These are established by independent determination of the boundary values of net radiation (R_0), sub-surface heat flux (S_0), and heat of evaporation-condensation (E_0), in the balance equation

$$Q_0 = R_0 - S_0 - E_0 .$$

In view of the above requirements we can hardly expect the classical solution to be realistic. It appears in order to re-examine Prandtl's model and to search for a solution which is more in line with turbulence concepts in shear flow past a solid flat boundary. The foremost problem will be to remove the restriction imposed by the assumption of height-independency of eddy diffusivities for heat and momentum.

5.2 Theory of Katabatic Flow for Height-Dependent Eddy Diffusivity

5.2.1 Derivation of the Characteristic Equations

The general assumptions listed at the beginning of Section 5.1.1 will not be changed. While equation (1) remains the same, we rewrite the momentum, and energy equation for turbulent flow as follows,

$$\rho_0 \, d\vec{V}/dt + \nabla p + \vec{k} g \rho = \partial \vec{\tau} / \partial z, \tag{20}$$

$$c_p \rho_0 (\partial \theta / \partial t + \vec{V} \cdot \nabla \theta) = - \partial Q / \partial z . \tag{21}$$

For the laminar case, shearing stress ($\vec{\tau}$) and heat flux (Q) are given by the products of respective gradients times the molecular viscosity or heat conductivity, so that the previous equations (2) and (3) are special cases of the more general forms (20) and (21).

The procedures, described in Section 5.1.1 which resulted in equations (4) and (5), are applied to equations (20) and (21) and yield the following system

$$\partial u / \partial s = 0 \tag{4}$$

$$\varepsilon g \partial\rho/\partial n = \partial^2\tau/\partial n^2, \tag{22}$$

$$-c_p \rho_0 u \partial\theta/\partial s = -\partial Q/\partial z, \tag{23}$$

when the vector of shearing stress is written $\vec{\tau} = \vec{s}\tau + \vec{j}\tau_y$, so that $\vec{j}(\nabla \times \vec{\tau}) = \partial\tau/\partial n$, while, as before, $\partial\tau/\partial n \approx \partial\tau/\partial z$. Utilizing the assumptions quoted in Section 5.1.1 concerning the structure of the temperature field, that is to say, accepting the validity of equation (7), equations (22) and (23) yield

$$-\varepsilon g \rho_0 \partial\theta/\partial n = \theta_0 \partial^2\tau/\partial n^2, \tag{24}$$

$$c_p \rho_0 \varepsilon \gamma u = -\partial Q/\partial n. \tag{25}$$

Assuming gradient-type eddy diffusion we have as the defining equations of the effective, or eddy, diffusivities K_H for heat, and K for momentum,

$$Q = -c_p \rho_0 K_H \partial\theta/\partial n = -c_p \rho_0 K_H (\gamma + \partial\vartheta/\partial n), \tag{26}$$

$$\tau = \rho_0 K \partial u/\partial n. \tag{27}$$

Now, we multiply both sides of equation (24) by K_H and consider equation (26); then, we differentiate equation (25) once with respect to the independent variable n, multiply both sides of the resulting equation by K, and consider equation (27). After slight rearrangement of terms the following is obtained

$$\varepsilon g Q/c_p \theta_0 = K_H \partial^2\tau/\partial n^2, \tag{28}$$

$$\varepsilon c_p \gamma\tau = -K \partial^2 Q/\partial n^2. \tag{29}$$

Here, shearing stress and heat flux are the dependent variables, the normal distance from the slope is the independent variable, and the eddy diffusivities can be either height-dependent coefficients or constants.

It is useful to transform the variables and the equations into dimensionless forms. Let X denote a parameter having the physical dimension of length; X corresponds to the scale-length of Prandtl's model as defined in Section 5.1.2. The dimensionless form of the independent variable will be denoted by $x = n/X$, and differentiations with respect to x by primes. We define dimensionless forms of the dependent variables, including heat flux (s), shearing stress (t), wind speed (U), and temperature disturbance (V), and also a dimensionless eddy

diffusivity (γ) by the following five identities:

$$s = Q/Q_0 \tag{30}$$

$$t = \tau/\tau_0 \tag{31}$$

$$U = u\rho_0 K_1/\tau_0 X \tag{32}$$

$$V = \vartheta c_p \rho_0 r K_1/Q_0 X \tag{33}$$

$$y = K/K_1 \tag{34}$$

where $r = K_H/K$ is the reciprocal of the eddy Prandtl number; r will be assumed to be independent of height. This may, or may not, be a realistic assumption. In addition to scale-height X, three other reference or scale values are introduced in the system (30) through (34); τ_0 and Q_0 are the boundary values of shearing stress (ground drag), and heat flux (rate of surface heating or cooling), respectively, and K_1 is the eddy diffusivity for momentum at $x = 1$ (or, $n = X$). Upon inserting the expression for Q, τ, and K as given by (30), (31), and (34), into equations (28) and (29), the following interrelationships between the scale values Q_0, τ_0, K_1, and X are suggested

$$X^4 = \theta_0 K_1^2 r/g\varepsilon^2\gamma \tag{35a}$$

$$Q_0/\tau_0 = c_p\sqrt{\theta_0\gamma r/g} \tag{35b}$$

This produces dimensionless forms of equations (28) and (29):

$$s = y\,t' \tag{36}$$

$$t = -y\,s' \tag{37}$$

which can be referred to as the characteristic equations of the katabatic flow problem. The corresponding dimensionless forms of equations (26) and (27), $t = yU'$ and $s = -yV'$, transform, with the aid of equations (36) and (37), into

$$U' = t/y = -s'; \quad \text{or} \quad U - U_0 = -s', \tag{38}$$

$$V' = -s/y = -t'; \quad \text{or,} \quad V - V_0 = -t' \tag{39}$$

where U_0 and V_0 are integration constants or boundary values to be determined later. Thus the problem is to solve the scalar system of two differential equations of second order, equations (36) and (37),

which is equivalent to one scalar fourth-order differential equation,

$$s = -y(ys'')'' \qquad (40)$$

or the identical form in t. It can be readily verified that Prandtl's model is the special case for height-independent diffusivity, i.e., for $y = y_1 = 1$ in equation (40), which produces, for $Z^4 = 4X^4$, the form presented in Section 5.1.1; reference is made to equations (10) and (11). Note that the integral forms of equations (38) and (39) describe clearly how the dimensionless wind speed (U) is directly related to divergence of heat flux (s'), and dimensionless temperature disturbance (V) to the frictional force per unit volume (t'). Such interrelationships are typical for natural, or gravity-buoyancy-induced flow of which katabatic wind is an interesting example.

5.2.2 Discussion of Possible Model Solutions

The problem is to solve the basic equation (40), or the equivalent system of equations (36) and (37), in order to obtain the vertical profiles of wind speed, shearing stress, temperature disturbance and heat flux, in katabatic flow for given boundary conditions of cooling rates and slope inclinations. Obviously, the solution depends exclusively on the analytical formulation of the height-dependency of K, or the x-dependency of the function $y(x)$. The simplest possible case, that of $y = y_0 = y_1 = \text{const}$ (or, $y' = 0$), results in the classical Prandtl solution, as was demonstrated at the end of Section 5.2.1.

It is highly interesting that the characteristic equations (36) and (37) of katabatic flow represent formally the same mathematical problem as the characteristic equations of the planetary boundary layer in a barotropic atmosphere; reference is made to equations (3b) in Lettau (1961, page 145). In other words, the computation of vertical profiles of the two rectangular components of horizontal shearing stress in the barotropic (thermally neutral) planetary boundary layer corresponds exactly to the computation of the vertical profiles of uni-dimensional shearing stress and heat flux of katabatic motion in diabatic states. The classical solution (i.e., for $y = y_0 = y_1 = \text{const}$) leads in the former case to the Ekman spiral. The mathematical structure of Prandtl's classical solution for katabatic flow—see equations (12)—is obviously closely related to the well-known Ekman-spiral solution.

In view of this similarity it is immediately possible to apply to the katabatic flow problem any of the variety of known wind-spiral solutions reported in the literature, for a certain choice in the mathematical formulation of the function $y(x)$. For y being a linear or exponential

function, or a power law of x, closed solutions exist and are given by Bessel functions (Hankel functions). For y being a quadratic function of x, the closed solution is expressed by elementary functions and results in "equiangular" spirals; reference is made to Lettau (1962). However, as was pointed out earlier—see Lettau (1961, page 146)—none of these, or related solutions, using preconceived explicit formulations of $y(x)$, has produced satisfactory agreement with observational results concerning boundary layer structure, and similar shortcomings must be expected for katabatic flow structure.

The universal solution of atmospheric boundary layer flow presented by Lettau (1961) rests essentially on the concept that the absolute value of the shearing velocity, $\sqrt{\tau/\rho}$, decreases monotonically with height, and enters as a factor in the formulation of the height-dependent eddy diffusivity for momentum. The other factor of K is a height-dependent length-scale of turbulent eddies. This model with its inherent non-linearity cannot be applied directly to katabatic winds, because the typical feature here is that wind shear goes through zero at the level $z^* = n^*$, while the structure of the temperature profile at such relatively close proximity to the ground indicates that heat conduction is finite, and certainly different from zero at this level. Thus, the thermal diffusivity of the air at a given height cannot be taken as being proportional to the local shearing velocity which, in turn, must still be proportional to the local wind shear.

5.3 Conclusions and Outlook for Future Work

It can be concluded that new concepts must be explored to solve the problem of katabatic flow in a realistic manner. The purpose of this preliminary note is, first of all, to outline the background of the problem and to demonstrate the need for continuation of theoretical effort. W. Knapp of the University of Wisconsin Meteorology Department has begun to investigate theoretical models of this problem, employing numerical integration methods similar to that discussed by Lettau (1961) for the boundary layer problem. The results will be presented in a later annual report. Another purpose of this preliminary note is an appeal to observers. For the conclusive testing of any theoretical model of steady katabatic flow it is desirable that details of wind and temperature profiles, including turbulence structure, together with surface heat budget determinations, are procured in higher resolution and with greater representativeness than before. The most promising locations for improved observations of this flow type should be found on the sloping plateaus of Greenland and Antarctica, in sufficient distance from the coast lines.

An improved understanding of the steady-state problem of katabatic flow is also the prerequisite for the discussion of development, i.e., onset and decay of unsteady katabatic flow, including the question of inherent instability, possibly related to the existence of a critical value of slope inclination, as discussed by Defant (1951), and the vehement nature of this flow type when influenced by topography as recently investigated by Ball (1960) at the rim of the antarctic plateau.

5.4 References

BALL, F.K. "Winds on the Ice Slope of Antarctica," pages 9 to 16 of "Antarctic Meteorology" (Proceedings of the Symposium in Melbourne, Feb. 1959) Pergamon Press, Oxford, London, New York, Paris, 1960.

DEFANT, F. "Local Winds," page 655 of "Compendium of Meteorology," Boston, Massachusetts, 1951.

LETTAU, H. "Theoretical Wind Spirals in the Boundary Layer of a Barotropic Atmosphere," pages 143 to 170 of "Annual Report," Contract DA-36-039-SC-80282 (USEPG, Fort Huachuca, Arizona) University of Wisconsin, 1961.

LETTAU, H. "Equiangular Wind and Current Spirals," pages 159 to 172 of "Final Report," Contract DA-36-039-SC-80282 (USEPG, Fort Huachuca, Arizona) University of Wisconsin, 1962.

Scanner's note:

This page is blank.

INDEX OF DISTRIBUTION

Hqs, U. S. Army Materiel Command
Research Division
ATTN: AMCRD-RS-ES-A
Washington, D.C., 20315 1

Hqs, U. S. Army Materiel Command
Development Division
ATTN: AMCRD-DE-MI
Washington, D.C., 20315 1

Office of Chief of Research and Development
Department of the Army
ATTN: CRD/M
Washington, D.C., 20315 2

Hqs, U.S. Army Combat Development Command
ATTN: CDCMR-E
Fort Belvoir, Virginia, 22060 1

Hqs, U.S. Continental Army Command
ATTN: ATINT-P and O
Fort Monroe, Virginia, 23351 1

Office of the Chief Signal Officer
Department of the Army
Washington, D.C., 20315 1

Hqs, U.S. Army Electronics Command
Research Division
ATTN: AMSEL-RE-C
Fort Monmouth, New Jersey, 07703 2

Hqs, U.S. Army Missile Command
ATTN: AMSMI-RPA
Redstone Arsenal, Alabama 35809 2

Hqs, U.S. Army Munitions Command
ATTN: AMSMU-RC
Dover, New Jersey, 07801 2

Hqs, U.S. Army Mobility Command
ATTN: Research Division
Centerline, Mich., 48015 2

Hqs, U.S. Army Test and Evaluation Command
Directorate of NBC Testing
Aberdeen Proving Ground, Maryland, 21005 2

CO, U.S. Army Cold Regions Research and Engineering Laboratory
ATTN: Environmental Research Branch
Hanover, N.H., 03755 2

CG, U.S. Army GSR and E Laboratory
ATTN: Earth Sciences Division
Natick, Massachusetts, 01760 2

CO, U.S. Army Ballistic Research Laboratories
ATTN: AMXBR-B
Aberdeen Proving Ground, Maryland, 21005 2

Director, U.S. Army Engineer Waterways Experiment Station
ATTN: WESSR
Vicksburg, Miss., 39181 1

CO, U.S. Army Electronics R and D Agency
ATTN: Meteorology Division Surveillance Department
Fort Monmouth, N. J., 07703 2

CO, U.S. Army Electronics
R and D Activity
ATTN: Meteorology Dept
Fort Huachuca, Ariz., 85613 50

CO, U.S. Army Electronics
R and D Activity
ATTN: Missile Meteorology
Division
White Sands Missile Range,
New Mexico, 88002 2

CO, U.S. Army Biological
Laboratories
ATTN: CB Cloud Research Office
Fort Detrick, Frederick
Maryland 1

CO, U.S. Army Frankford
Arsenal
ATTN: MEIE Division
Philadelphia, Penn., 19103 1

CO, Picatinny Arsenal
ATTN: Special Weapons Group
Dover, N.J., 07801 1

CO, U.S. Army Engineering
R and D Laboratory
Fort Belvoir, Virginia, 22060 1

CO, U.S. Army Transportation
Research Command
Fort Eustis, Virginia, 23604 1

CO, U.S. Army Dugway
Proving Ground
ATTN: Meteorological
Division
Dugway, Utah, 84002 1

President
U.S. Army Artillery Board
Fort Sill, Oklahoma, 73504 1

CO, U.S. Army Artillery
Combat Developments Agency
Fort Sill, Oklahoma, 73504 1

CO, U.S. Army Communica-
tions-Electronics
Combat Developments Agency
Fort Huachuca, Arizona, 85613
1

Commandant
U.S. Army Artillery and
Missile School
ATTN: Target Acquisition Dept
Fort Sill, Okla., 73504 1

Commander
Air Weather Service (MATS)
U. S. Air Force
ATTN: AWSSS/TIPD
Scott Air Force Base,
Illinois, 62226 1

Commander
USAF Cambridge Research Center
ATTN: CRXL, Hanscom Field
Bedford, Mass., 01730 2

Chief of Naval Research
ATTN: CODE 427
Department of the Navy
Washington, D.C., 20315 1

Office of U.S. Naval
Weather Service
U.S. Naval Air Station
Washington, D.C., 20315 1

Officer-in-Charge
U.S. Naval Weather Research
Facility
U.S. Naval Air Station,
Bldg R-28
Norfolk, Virginia, 23501 1

Director, Atmospheric
Sciences Programs
National Science Foundation
Washington, D.C., 20315 1

Director, Bureau of
Research and Development
Federal Aviation Agency
Washington, D.C., 20315 1

Director, Bureau of Research
and Development
Federal Aviation Agency
National Aviation Facilities
Experimental Center
ATTN: Technical Library
Bldg 3
Atlantic City, N.J., 08401 1

Chief, Fallout Studies Branch
Division of Biology and
Medicine
Atomic Energy Commission
Washington, D.C., 20315 1

Office of the Assistant
Secretary of Defense
(Research and Engineering)
The Pentagon
ATTN: Technical Library,
Room 3E1065
Washington, D.C., 20315 1

Director of Meteorological
Systems
Office of Applications
(FM)
National Aeronautics and
Space Administration
Washington, D.C., 20315 1

Chief, U.S. Weather Bureau
ATTN: Librarian
Washington, D.C., 20315 2

CO, Defense Documentation
Center for Scientific and
Technical Information
Cameron Station
Alexandria, Virginia 20

Mr. R. A. McCormick
Chief, Met Section
4676 Columbia Parkway
Cincinnati, Ohio, 45226 1

Commander
Air Force Cambridge Research
Laboratories
ATTN: CRZW
1065 Main Street
Waltham, Mass., 02154 1

Commanding General
Deseret Test Center
Fort Douglas, Utah, 84113 1

President
U.S. Army Artic Test Board
Fort Greely, Alaska 1

Hqs, U.S. Army Test and Evaluation Command
ATTN: AMSTE-EL
Aberdeen Proving Ground,
Maryland, 21005 1

Hqs, U.S. Army Test and
Evaluation Command
ATTN: AMSTE-BAF
Aberdeen Proving Ground,
Maryland, 21005 1

Hqs, U.S. Army Missile
Command
ATTN: AMSMI-RB
Redstone Arsenal, Alabama 1
35809

Hqs, U.S. Army Missile
Command
ATTN: AMSMI-RR
Redstone Arsenal,
Alabama, 35809 1

Commanding Officer
U. S. Army Biological
Laboratories
ATTN: Technical Library
SMUFD-12 TI
Ft. Detrick, Frederick, Md., 1

Commanding Officer
U.S. Army CBR Operations Research Group
Army Chemical Center
Maryland 1

Commanding Officer
U. S. Army Chemical Research and Development Labs
ATTN: Director of Development Support
Army Chemical Center, Maryland 1

Office of the Chief Signal Officer
ATTN: The Technical Director Command and Control Systems Directorate
Department of the Army
Washington, D.C., 20315, 1

Scientific and Technical Information Facility
ATTN: NASA Representative (S-AK/DL)
P. O. Box 5700
Bethesda, Md., 20014 1

U. S. Army Polar R and D Center
Fort Belvoir, Va., 22060 1

Commanding General
U.S. Army Combat Developments Command
Experimentation Center
Fort Ord, Calif., 93941 1

Director, Meteorology Dept
University of Arizona
Tucson, Ariz., 85717 1

Director, U. S. Water Conservation Lab
Agricultural Rsch Service
U.S. Dept of Agriculture
Route 2, Box 816-A
Tempe, Arizona, 85281 1

Director, Pacific Southwest Forest and Range Experiment Station
U.S. Dept of Agriculture
Forest Service
P. O. Box 245
Berkeley , Calif., 94704 1

Director, Meteorology Dept
University of California at Los Angeles
Los Angeles, Calif., 90052 1

Director, U. S. Salinity Lab
P. O. Box 672
ATTN: Dr. L. A. Richards
Riverside, Calif., 92502 1

Department of Irrigation
University of California
Davis, Calif., 95616 1

Department of Agricultural Engineering
University of California
ATTN: Dr. F. A. Brooks
Davis, Calif., 95616 1

Meteorology Dept
San Jose State College
San Jose, Calif., 95113 1

Chief, Radio Propagation Laboratory
U.S. National Bureau of Standards
Boulder, Colo., 80301

Dept of Civil Engineering
Colorado State University
Fort Collins, Colo., 80521 1

Director
ATTN: M. Martinelli, Jr.
Rocky Mountain Forest and
Range Experiment Station
U.S. Dept of Agriculture
Forest Service
Room 221, Forestry Building
Colorado State University
Fort Collins, Colo., 80521 1

Director, Meteorology Dept
Florida State University
Tallahassee, Florida, 32301 1

Director, Southern Piedmont
Soil Conservation Field
Station
U. S. Dept of Agriculture
P. O. Box 33
Watkinsville, Ga., 30677 1

Meteorology Department
University of Hawaii
Honolulu, Hawaii, 96822 1

Director, Meteorology Dept
The University of Chicago
Chicago, Ill., 60607 1

Deaprtment of Agronomy
Iowa State University
ATTN: Dr. R. H. Shaw
Ames, Iowa, 50010 1

Director, Soil and Water
Conservation Division
Agricultural Research Service
U. S. Dept. of Agriculture
Beltsville, Md., 20705 1

Director, Dept of Civil
Engineering
Johns Hopkins Univ
Baltimore, Md., 21233 1

Executive Secretary
American Meteorological
Society
45 Beacon Street
Boston, Mass., 02109 1

Director, Meteorology Dept
Massachusetts Institute of
Technology
Cambridge, Mass., 02138 1

Dept. of Meteorology
Mass. Institute of Technology
Round Hill Field Station
South Dartmouth,
Massachusetts, 02748 1

Director, Meteorology Dept
University of Michigan
Ann Arbor, Michigan, 48105 1

University of Minnesota
ATTN: Dean Spilhouse
Minneapolis,
Minnesota, 55041 1

Director, NSSP
ATTN: Library
Federal Office Building
Room 710
911 Walnut Street
Kansas City, Mo., 64108 1

Director, Meteorology Dept
St. Louis University
St. Louis, Mo., 63120 1

Dept of Geophysics
Washington University
St. Louis, Mo., 63120 1

Department of Soils
University of Missouri
Columbia, Mo., 62501 1

Director, Meteorology Dept
New York University
University Heights
New York, N.Y., 10001 1

Soil and Water Conservation
Research Division
Agricultural Rsch Service
U. S. Dept of Agriculture
Cornell University,
Bailey Hall
Ithaca, N.Y., 14851 1

Atmospheric Science Branch
Scientific Research Institute
Oregon State College
Corvallis, Ore., 97330 1

Director, Meteorology Dept
Pennsylvania State Univ
University Station,
Pennsylvania, 16802 1

Dept of Oceanography and
Meteorology
The Agricultural and
Mechanical College of Texas
College Station, Texas
77840 1

Electrical Engineering Rsch
Laboratory
The University of Texas
Austin, Texas, 78761 1

Department of Agronomy
Utah State University
ATTN: Dr. S. A. Taylor
Logan, Utah, 84321 1

Dept. of Meteorology
University of Utah
Salt Lake City, Utah, 84116 1

Director, National Research
Council
National Academy of Sciences
2101 Constitution Avenue
Washington, D.C., 20315 1

Director, Meteorology Dept
University of Washington
Seattle, Wash., 99703 1

Director, Meteorology Dept
University of Wisconsin
Madison, Wis., 53705 1

Department of Soils
University of Wisconsin
ATTN: Dr. C. B. Tanner
Madison, Wisconsin, 53705 1

Commander
U.S. Navy Electronics Lab
ATTN: Dr. M. Halstead
San Diego, Calif., 92101 1

Officer-in-Charge
Meteorological Curriculum
U.S. Naval Post Graduate
School
Monterey, Calif., 92801 1

Director, Geophysical Rsch
Directorate
ATTN: CRZHB
USAF Cambridge Rsch Center
Hanscom Field
Bedford, Mass., 01730 2

Commandant
ATTN: Weather Br DST
U. S. Army Signal School
Fort Monmouth, N.J., 07703 1

Commanding Officer
U.S. Army Electronics R and D
Laboratory
Fort Monmouth, N.J., 07703 1

Deputy for Defense
Research and Engineering
ATTN: Geophysical Sciences
Office of the Secretary of
Defense
Washington, D.C., 20315 1

Climatic Center, USAF
ATTN: COCAD
Air Weather Service (MATS)
Annex 2, 225 D. Street, S.E.
Washington, D.C., 20315 1

Director
Department of Transport
315 Bloor Street West
Toronto 5, Ontario
Canada 1

Forestry Library
260 Walter Mulford Hall
University of California
Berkeley, Calif., 94704 1

Micrometeorology Branch
Technical Division
U. S. Army Chemical School
Fort McClellan, Ala., 36201 1

Commanding General
U. S. Army Edgewood Arsenal
ATTN: Operations Rsch Group
Edgewood Arsenal, Maryland
21040 1

Department of Soil Science
Ontario Agricultural College
Guelph - Ontario, Canada 1

CO, U.S. Army R and D Office,
Panama
P.O. Drawer 942
Fort Clayton, C.Z. 1

AD _____ Accession Nr _____

University of Wisconsin, Madison
STUDIES OF THE EFFECTS OF VARIATIONS IN BOUNDARY CONDITIONS ON THE ATMOSPHERIC BOUNDARY LAYER
by H. H. Lettau and others. Annual Report (1 Oct 62 to 30 Sep 63). Pub. Nov 63, ERDAA Technical Program, DA Task 1-A-0-11001-B-021-08. 157 p. incl. illus. tables. Unclassified report.

Data from two classical flat plate boundary layer experiments were used to determine values of Karman's constant through the approach of a limiting wall condition for an explicit function described by flow structure. The constant was found to vary with Reynolds numbers.

A theoretical model of the atmospheric boundary layer was used to make a survey of the aerodynamic roughness of natural surfaces of the northern hemisphere and to compute the distribution and seasonal variations of geostrophic drag coefficients and energy dissipation.

Temperature spectra were measured over an experimental field of bushel baskets set on the ice surface of Lake Mendota, and also over the natural ice surface. Comparison of the spectra showed the effects of turbulence generated by the field as a whole and by the spacing of the baskets.

The experimental field of bushel baskets and a small artificial forest were used in studies of wind profile modification. Determinations were made of the effect of obstacle albedo and solar heating on momentum transfer and of the momentum budget over the artificial forest.

Characteristic equations of katabatic flow for height-dependent eddy diffusivity were derived. The mathematical problem was found to be similar to that of spiral-flow in the planetary boundary layer of a barotropic atmosphere. Possible model solutions were discussed.

UNCLASSIFIED

1. Turbulent Boundary Layer
   von Karman's constant
2. Micrometeorology
   Surface roughness
   Temperature spectra
   Wind profile modification
3. Katabatic Flow Theory

Contract DA-36-039-AMC-00878

UNCLASSIFIED

AD _____ Accession Nr _____

University of Wisconsin, Madison
STUDIES OF THE EFFECTS OF VARIATIONS IN BOUNDARY CONDITIONS ON THE ATMOSPHERIC BOUNDARY LAYER
by H. H. Lettau and others. Annual Report (1 Oct 62 to 30 Sep 63). Pub. Nov 63, ERDAA Technical Program, DA Task 1-A-0-11001-B-021-08. 157 p. incl. illus. tables. Unclassified report.

Data from two classical flat plate boundary layer experiments were used to determine values of Karman's constant through the approach of a limiting wall condition for an explicit function described by flow structure. The constant was found to vary with Reynolds numbers.

A theoretical model of the atmospheric boundary layer was used to make a survey of the aerodynamic roughness of natural surfaces of the northern hemisphere and to compute the distribution and seasonal variations of geostrophic drag coefficients and energy dissipation.

Temperature spectra were measured over an experimental field of bushel baskets set on the ice surface of Lake Mendota, and also over the natural ice surface. Comparison of the spectra showed the effects of turbulence generated by the field as a whole and by the spacing of the baskets.

The experimental field of bushel baskets and a small artificial forest were used in studies of wind profile modification. Determinations were made of the effect of obstacle albedo and solar heating on momentum transfer and of the momentum budget over the artificial forest.

Characteristic equations of katabatic flow for height-dependent eddy diffusivity were derived. The mathematical problem was found to be similar to that of spiral-flow in the planetary boundary layer of a barotropic atmosphere. Possible model solutions were discussed.

UNCLASSIFIED

1. Turbulent Boundary Layer
   von Karman's constant
2. Micrometeorology
   Surface roughness
   Temperature spectra
   Wind profile modification
3. Katabatic Flow Theory

Contract DA-36-039-AMC-00878

UNCLASSIFIED